論文 / 著書情報
Article / Book Information

題目(和文)	
Title(English)	Genomes and Single-Cell Phenotypes at Life ’ s Temperature Extremes: A Case Study of Methanogenic Archaea
著者(和文)	PRONDZINSKYAlannah Paulina
Author(English)	Alannah Paulina Prondzinsky
出典(和文)	学位:博士(理学), 学位授与機関:東京工業大学, 報告番号:甲第12326号, 授与年月日:2023年3月26日, 学位の種別:課程博士, 審査員:豊田 栄,大河内 美奈,山田 桂太,関根 康人,MC GLYNN SHAWN ERIN
Citation(English)	Degree:Doctor (Science), Conferring organization: Tokyo Institute of Technology, Report number:甲第12326号, Conferred date:2023/3/26, Degree Type:Course doctor, Examiner:,,,,
学位種別(和文)	博士論文
Type(English)	Doctoral Thesis

TOKYO INSTITUTE OF TECHNOLOGY

Genomes and Single-Cell Phenotypes at Life's Temperature Extremes: A Case Study of Methanogenic Archaea

Alannah Paulina Prondzinsky

Thesis submitted in partial fullfillment
of the requirements for the degree of
Doctor of Science
(Chemical Science and Engineering)

School of Materials and Chemical Technology

東京工業大学
Tokyo Institute of Technology

EARTH-LIFE SCIENCE INSTITUTE
TOKYO INSTITUTE OF TECHNOLOGY

December 2022

ABSTRACT

Methanogenic archaea produce methane during growth across a wide temperature range from -2.5 °C to 122 °C. Here, genomic adaptations and physiological responses of methanogens to varying growth temperatures were investigated. Through a comparative genomics approach, the large conserved genomic core of methanogens was identified. With increasing growth temperatures, genomes were found to become smaller and thermophilic species branched closer to the root of the archaeal tree. Conservation of the core persisted across a large phylogenetic distance.

Single-cell variability in carbon and nitrogen uptake was investigated using nanoSIMS, revealing population heterogeneity across temperatures, as well as within multicellular aggregates. Finally, the underlying metabolic modes of individual cells were investigated using metabolic modeling approaches, with a newly established core model for methylotrophic methanogenesis.

SUMMARY

Methane producing archaea, methanogens, are anaerobic microorganisms whose physiology is found in wide ranges of pH, salinity, pressure, and temperature. Detailed studies of the organisms' adaptive features to their diverse habitats can help us understand their contributions to global methane cycling today, as well as their role throughout Earth history. Here, the adaptive features observable at the genome level or through different single-cell observable growth phenotypes were investigated.

Chapter 1 gives a brief introduction to methanogenesis and its impact on the global carbon cycle on Earth today, as well as its biogeochemical role through Earth's history.

In **Chapter 2**, differences in genome function and composition between psychrotolerant and thermotolerant methanogens were observed across 86 cultured species using comparative genomics approaches: the conserved genomic core of methanogens makes up around one third of a genome on average, and the shared genome content of two species decreases with increasing phylogenetic distance. Throughout the core- and pangenomes, charged amino acids, leucine, and isoleucine content increase with temperature, while polar uncharged amino acids are more abundant at lower temperatures. Thermotolerant methanogens are enriched in metal and other transporters, and psychrotolerant methanogens are enriched in proteins related to structure and motility. Overall, physiology seems to shape genome content more than phylogenetic relatedness in the methanogens.

Chapter 3 focuses on physiological responses to temperature at the single cell level. Using stable isotope probing in combination with high resolution spatial mass spectrometry, physiological responses were assessed for two psychrotolerant, two mesophilic, and two thermotolerant methylotrophic species grown in pure cultures. The species were chosen based on their common carbon substrate, methanol, and their growth temperature ranges: methylotrophic methanogenesis spans from – 2.5 °C to 70 °C and the organisms analyzed here were grown either at 4 °C, 37 °C, or 55 °C for interspecies comparisons. Additionally, the psychrotolerant species *Methanococcoides burtonii* was grown at its optimal growth temperature (23 °C) and the mesophile *Methanosarcina acetivorans* was grown at its temperature limits of 15 °C and 45 °C,

for intraspecies comparisons. Growth is slow at lower temperatures, and slow growth is often associated with stressful or limiting growth conditions. However, when considering single cell phenotypic heterogeneity, carbon uptake heterogeneity is high in cold growth and nitrogen uptake heterogeneity increases with temperature. Increases in heterogeneity have been attributed to stressful growth conditions, but the results show that while low temperatures slow down growth, they do not necessarily induce cellular stress responses.

Spatial heterogeneity was also assessed for cells of M. *burtonii* at 4 °C and 23 °C, which occur in microcolonies. As in free-living cells, carbon heterogeneity is higher at the lower temperature, and nitrogen heterogeneity is higher at the higher growth temperature. Spatial heterogeneity was observed in the cold condition, with cells on the outside of the aggregates incorporating more substrate than the inner cells.

To my knowledge this is the first investigation of phenotypic heterogeneity in archaea, and the first of any organism which documents the effects of temperature on single cell variations. The causes of single-cell variability in isogenic populations are not yet clear, though authors have attributed this heterogeneity to stochastic gene expression, asymmetric cell division, or cellular interactions.

Chapter 4 introduces the use of metabolic modeling to study the different metabolic modes responsible for the observed phenotypes of *M. burtonii*, giving an insight into metabolic flux variations and differences, in an attempt to explain the causes of phenotypic heterogeneity. At first, a core metabolic model for methylotrophic methanogens was created in a top-down approach from an existing genome scale model, by maximizing random gene deletions while maintaining sufficient biomass and methane output fluxes, the number of genes was reduced from 807 to 339. Flux boundaries in the core model were then modified based on media composition and observed cell growth. These modifications did not affect the simulated growth of the model, showing that growth was not limited by media composition. Finally, flux balance analyses were conducted to sample for the observed single cell uptake rates of methanol and ammonia at 4 °C and 23 °C. The flux simulation for the phenotype with the mean carbon and nitrogen assimilation rates at 23 °C was found to be overall similar to carbon limited phenotypes of both temperatures, with methanogenesis fluxes remaining high.

In this thesis adaptive mechanisms of methanogens to varying growth temperatures

were studied from three standpoints: first, genomes of all available methanogens were compared showing compositional, functional, and structural differences. Second, single cell phenotypes and population heterogeneity were assessed for selected methylotrophic species. Increases in carbon heterogeneity at low temperatures and nitrogen heterogeneity at high temperatures, as well as an increase in spatial heterogeneity at low temperatures were observed. Finally, the use of metabolic models to explain the underlying metabolic modes of single cells was proposed, using a core methylotroph model. Genome comparisons of all cultured methanogens and single cell analyses of phylogenetically diverse methylotrophs showed that microorganisms' physiologies rather than phylogenies play an important role in temperature adaptation.

ACKNOWLEDGEMENTS

This thesis would not have been possible without the support of various people that I was lucky to cross paths with in the past years: major thanks go to my supervisors: Dr. Shawn McGlynn, associate professor at the Earth-Life Science Institute, for introducing me to the world of methanogens and giving me the opportunity to conduct this research, and Dr. Sakae Toyoda, associate professor in the department of Chemical Science and Engineering, for his guidance over the last 4.5 years.

The breadth of this thesis was only possible through the fruitful interactions with many researchers: for Chapter 2, I express my gratitude to Professor Hiroyuki Ogata and his laboratory members at the Bioinformatics Research Center at Kyoto University, where I was warmly welcomed and learned a lot about computational tools in biology. For Chapter 3, my thanks go to Dr. Yunbin Guan, director at the Center for Microanalysis at Caltech, who coordinated all of the NanoSIMS analyses with me across timezones. For Chapter 4, I am thankful for Dr. Takeyuki Tamura, associate professor at the Bioinformatics Research Center at Kyoto University, who helped with finding the metabolic core of methylotrophic methanogens.

The work presented in this thesis was conducted at the Earth-Life Science Institute, where I had the chance to meet many excellent scientists and was also supported with settling into life and the laboratory environment in Japan. Special thanks go to Harumi Tanaka, Reiko Nagano and Kanako Yagame who have made life at ELSI more enjoyable and efficient. I am also thankful to the Earth-Life Science Institute for the financial support through Research Assistantships for the entirety of my time there and acknowledge support from the JST SPRING Grant, number JPMSJSP2106, for the second half of the doctoral program.

Looking back on the past years, moral support is at least equally as important as scientific support. I am grateful for Fatima Li Hau, her friendship, the numerous tea breaks with talks about research and life, and her support and cheers over the last months and years. During my graduate studies in Germany I was fortunate to cross paths with Mareike Bach and Alexandra Belitz, from whom I have learned a lot inside and outside of the lab and who have remained a great source of comfort and feedback

over the past years. Sawako Nii has helped me turn Tokyo into a home and has made life here more enjoyable. Serhat Sevgen‘s and Ellen Costa-Almeida’s passion for astrobiology has motivated and inspired me over the last three years – I am looking forward to seeing where the LUNATICS will go.

My biggest thanks go to my family: my parents Gabi Fleischmann and Klaus Prondzinsky, my siblings Tammy and Timothy, and my grandparents Walter and Ingrid, whose support I have felt continuously since starting my university education almost a decade ago. *Danke, dass ihr trotz mehr als 9000 km Entfernung und zu jeder Tages- und Nachtzeit ein offenes Ohr für mich hattet, und mir durch eure teils amüsanten Anekdoten neue Perspektiven auf meine Forschungsvorhaben geliefert habt.*

Dankeschön!

"Extinction is the rule. Survival is the exception"

- Carl Sagan

TABLE OF CONTENTS

LIST OF ABBREVIATIONS

Abbreviations

Acetyl-CoA	Acetyl Coenzyme A
ATP	Adenosine Triphosphate
ABC transporters	ATP-Binding Cassette Transporters
AceP	gene for acetate reversible transport via proton symport
ACKr	Acetate Kinase
BOF	Biomass Objective Function
CoA	Coenzyme A
COBRA	Constrained Based Reconstruciton and Analysis
COG	Clusters of Orthologous Groups
CoM	Coenzyme M
DAPI	4',6-diamidino-2-phenylindole
DIC	Dissolved Inorganic Carbon
DPANN	Diapherotrites, Aenigmarchaeeota, Nanohalarchaeota, Nanoarchaeota
DTI	Differentiation Tendency Index
DTL	Duplication-Transfer-Loss
ECOD	Evolutionary Classification of Protein Domains
F420	Coenzyme $F_4$20
F4D	$F_4$20 Dehydrogenase
FBA	Flux Balance Analysis
FISH	Fluorescence In Situ Hybridization
FMFD	Formylmethanofuran Dehydrogenase
GC content	Guanine-Cytosine content
GEM	Genome Scale Metabolic Model
GTDB	Genome Taxonomy Database
H_4-MPT	Tetrahydromethanopterin
HC	Heterogeneity Coefficient

HDR	Heterodisulfide Reductase
HGT	Horizontal Gene Transfer
ITO	Indium Tin Oxide
KEGG	Kyoto Encyclopedia of Genes and Genomes
KO	KEGG Orthology
LACA	Last Archaeal Common Ancestor
MAR	Microautoradiography
MCMMT	Methanol:Coenzyme M Methyltransferase
Mcr	Methyl-Coenzyme M Reductase
MFR	Methanofuran
Mtr	Tetrahydromethanopterin-Coenzyme M Methyltransferase
MTSPCMMT	Methyl-H4SPT:Coenzyme M Methyltransferase
NanoSIMS	Nanoscale Secondary Ion Mass Spectrometry
NBRC	Biological Resource Center, National Institute of Technology and Evaluation
NCBI	National Center for Biotechnology In-formation
OG	Orthogroup
OGT	Optimal Growth Temperature
PTAr	Phosphotransacetylase
RNF	Methanophenazine Reductase
RSD	Relative Standard Deviation
SC-SIP	Single Cell Stable Isotope Probing
TB	Toluidine Blue
TEMPURA	Growth TEMPeratures of Usual and RAre Prokaryotes database

CHAPTER ONE
Introduction

1.1 Methanogenesis

1.1.1 Studies on Methanogenesis

While the first observations of the process of methanogenesis date back to as early as 1776 (Wolfe, 1993), the identification of the first methane producing organism was only confirmed more than 150 years later by Stephenson & Stickland (1933). The authors described a microorganism with capabilities to produce methane via the oxidation of hydrogen and reduction of carbon dioxide, carbon monoxide, formic acid, formaldehyde, or methanol. Following their work, the studies of methanogens progressed throughout the 20th century: Schnellen (1947) reported the first organisms in pure culture as well as the stoichiometry for methanogenesis from methanol and shortly after isotope studies confirmed the utilization of carbon from CO_2 for methane production (Stadtman & Barker, 1949). At the same time Buswell & Sollo (1948) started investigations into microbial methane production from acetate.

The following decades were marked by new isolation techniques (Hungate, 1950), the first isolations of rumen organisms (Smith & Hungate (1958)) and the discoveries of enzymes and cofactors involved in the pathway (Wolin et al., 1964; Wood et al., 1966; Wolfe & McBride, 1971; Van Beelen et al., 1984). Coenzyme M was confirmed as a marker for methanogenesis (Balch & Wolfe, 1979) and the methyl-coenzyme M reductase (Mcr) resolved into its alpha, beta and gamma subunits (Gunsalus & Wolfe, 1980). Later the structures of methanopterin and methanofuran (Van Beelen et al., 1984; Leigh et al., 1984), as well as the crystal structure of Mcr (Ermler et al., 1997) were discovered. In addition to expanding knowledge of the biochemistry of methanogenesis as well as enzymes and compounds involved, the late 20th century was marked by the discovery of more methanogenic species (Kurr et al., 1991; Franzmann et al., 1992, 1997; Kotelnikova et al., 1998; Jeanthon et al., 1999), methane oxidizing methanotrophs (Hanson & Hanson, 1996; Boetius et al., 2000), as well as the reordering of the tree of life (Woese, 1987).

At the same time anaerobic methane oxidation was proposed to be conducted by methanogens coupled to sulfate reducing bacteria (Hoehler et al., 1994), which was later confirmed to be carried out by archaeal methanotrophs through reversed methanogensis (Hallam et al., 2004).

With an increase in known methanogenic diversity, Bapteste et al. (2005) proposed to split the methanogens into two monophyletic groups: Class I methanogens including the *Methanobacteriales*, *Methanococcales* and *Methanopyrales* and a Class II methanogens including the *Methanomicrobiales*, *Methanosarcinales* and *Methanocellales*. As taxonomy and phylogeny were elaborated, geochemical analyses dated early methanogenic activity to 3.46 Gya (Ueno et al., 2006), and computational models that investigate the relationship of atmospheric oxygen increases and marine anaerobic methane oxidation (Catling et al., 2007) opened up debates about the role of methane metabolisms in the biogeochemical evolution of early Earth.

Sequencing data and metagenomic assemblies lead to the discovery of more alkane utilizing archaea and putative metabolic pathways: Raghoebarsing et al. (2006) and Haroon et al. (2013) identified organisms that couple the oxidation of methane to denitrification, Evans et al. (2015) detected methanogenesis markers in the *Bathyarchaeota* phylum and Laso-Pérez et al. (2016) discovered a butane oxidizing archaeon in the *Ca. Syntropharchaeum* genus. The discovery of hydrogenotrophs within the *Vestraetearchaeota* phylum (Berghuis et al., 2019) and gene evolution studies (Williams et al., 2017; Wolfe & Fournier, 2018; Hua et al., 2019; Wang et al., 2021b) further refined our understanding of the evolutionary history of methanogenesis and other alkane metabolisms, which are still the focus of research efforts today (Garcia et al., 2022).

1.1.2 Methanogenesis Pathways

The metabolism of methanogenic archaea is primarily based on the generation of methane from CO_2, methyl group containing compounds, or acetate (Figure 1.1): hydrogenotrophic methanogens reduce CO_2 to CH_4 with H_2 as the electron donor. Aceticlastic methanogens split acetate, oxidizing the carboxyl-group to CO_2 and reducing the methyl group to CH_4. In methylotrophic methanogenesis the methyl groups from four compounds of methanol or methylamines are transferred to a corri-

noid protein and subsequently to Coenzyme M (CoM). Methyl-CoM then enters the methanogenesis pathway and three methyl-CoMs are reduced to CH_4, with the electrons required for this reduction obtained from the fourth methyl group being oxidized to CO_2 (Thauer, 1998; Liu & Whitman, 2008, overview in Table 1.1).

Besides the well described major pathways, more unconventional pathways for methanogenesis have also been discovered (Kurth et al., 2020): alternate electron donors in hydrogenotrophs include formate, carbon monoxide, ethanol, propanol or 2-butanol. Some methanogens can perform hydrogen dependent methylotrophic methanogenesis, but not hydrogenotrophic or methylotrophic methanogenesis on their own (Söllinger & Ulrich, 2019). Methylotrophic methanogenesis has been observed with the conversion of methylated sulfur compounds (methanethiol, dimethyl sulfide, methylmercaptopropionate), methoxylated aromatic compounds (2-methoxybenzoate), tertiary amines (choline, betaine), dimethylethanolamine or tetramethylammonium (Kurth et al., 2020). In aceticlastic methanogenesis, iron redox cycling can also accelerate methane production through a membrane bound multiheme c-type cytochrome that feeds into the electron transport chain (Wang et al., 2020).

Table 1.1
Major pathways for methanogenesis

substrate	net stoichiometry
CO_2	$CO_2 + 4\,H_2 \longrightarrow CH_4 + 2\,H_2O$
CO	$4\,CO + 2\,H_2O \longrightarrow CH_4 + 3\,CO_2$
$HCOO^-$	$4\,HCOO^- + 4\,H^+ \longrightarrow CH_4 + 2\,H_2O + 3\,CO_2$
CH_3COOH	$CH_3COOH \longrightarrow CH_4 + CO_2$
CH_3OH	$4\,CH_3OH \longrightarrow 3\,CH_4 + CO_2 + 2\,H_2O$
CH_3NH_2	$4\,CH_3NH_2 + 2\,H_2O \longrightarrow 3\,CH_4 + CO_2 + 4\,NH_3$
$(CH_3)_2NH$	$2\,(CH_3)_2NH + 2\,H_2O \longrightarrow 3\,CH_4 + CO_2 + 2\,NH_3$
$(CH_3)_3N$	$4\,(CH_3)_3N + 6\,H_2O \longrightarrow 9\,CH_4 + 3\,CO_2 + 4\,NH_3$

Modified from Liu et al. 2018

After the phylogenetic placement of the methanogens (Woese et al., 1978) and the recognition of them being cosmopolitan organisms, thriving in a variety of environments (Jones et al., 1987; Lyu et al., 2018), an increasing number of studies shifted the focus on their adaptive mechanisms to those environments (Morozova & Wagner, 2007; Ni & Boone, 1998), as well as the use of methanogens as model archaea for physiological studies (Leigh et al., 2011).

1.1.3 Methanogenesis on Earth today: global biogeochemical cycles and varying temperature environments

On Earth today, methanogens can be found in a variety of anaerobic environments including wetlands (Torres-Alvarado et al., 2005), hydrothermal systems (Jones et al., 1989), sediments (Boyd et al., 2010), industrial sewage digesters (Ferry et al., 1974), landfills (Fielding et al., 1988), as well as rumens and intestines of mammals, including ourselves (Lovley et al., 1984). Methane is a potent greenhouse gas with more than half of estimated annual methane emissions being anthropogenically induced and more than a quarter of total emissions originating from agriculture and waste treatment, or biologically produced methane (Jackson et al., 2020, Figure 1.2). Major natural, terrestrial methane sources in the global cycle are microorganisms in

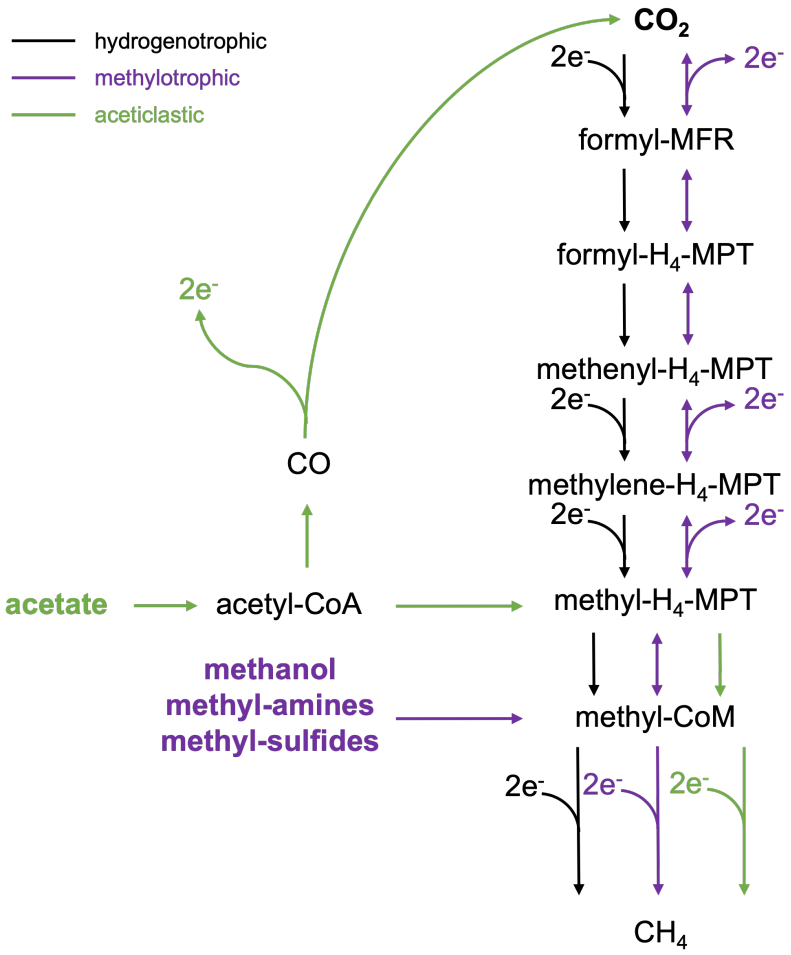

Figure 1.1 Major methanogenesis pathways. Substrates in bold. CoA - coenzyme A, CoM - coenzyme M, MFR - methanofuran, H_4-MPT - tetrahydromethanopterin. Figure adapted from Galagan et al. (2002).

.

the rice rhizosphere, pectin degradation in leaves and plant decay, anaerobic decomposition of wetwood in trees, and intestinal systems of ruminants and termites. In the ocean, major sources constitute fecal pellet disaggregation, mud volcanoes, microbial activity in deep sediments, serpentinization at mid ocean ridges, and hydrate dissociation. Sinks are the anaerobic oxidation of methane near the sediment surface, aerobic methane utilizing communities, oxidation in anoxic water columns, and emissions to the atmosphere. In non-aquatic systems, methane is consumed by anaerobic oxidation and methanotrophs in sediments and the upper soil, and small quantities can escape to the stratosphere (Conrad, 2009; Reeburgh, 2007).

In aquatic systems, methane emissions are higher in those which are anthropogenically impacted compared to natural environments, feeding into the positive feedback loop of global change (Rosentreter et al., 2021). Especially those emissions from waste water treatment, excessively farmed animals' rumens, biomass burning, landfills, constructed wetlands, and rice paddies are anthropogenically induced sources of methane that feed into the global climate crisis (Cavicchioli et al., 2019).

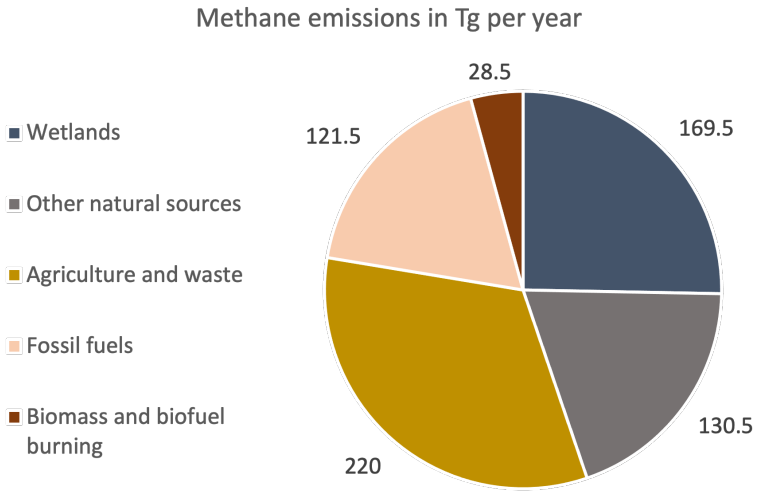

Figure 1.2 Methane emissions estimated for the year 2017 based on Jackson et al. (2020).

.

Besides their environmental impact, methanogens are of interest to scientific studies due to their industrial applications in industrial waste treatments (Lyu et al., 2018) and the wide range of environments they inhabit: methanogens grow in temperatures from -2.5 °C to 122 °C, pH 3 to 10.2, salinities up to 6 M and pressures up to 75

MPa (Takai et al., 2008; Franzmann et al., 1992; Hoehler et al., 2010). These ranges prompt methanogens to be classified as (multi-)extremophiles, often inhabiting environments with low biological diversity due to multiple environmental stress factors. Halophilic methanogens are found in environments such as sedimentary rocks, deep sea anoxic brine lakes, hypersaline microbial mats, and soda lakes, which are also extremely alkaline (McGenity & Sorokin, 2010). Psychrotolerant methanogens are found in polar subglacial (Franzmann et al., 1992) and marine environments (Wagner & Liebner, 2010; Vishnivetskaya et al., 2018), the latter of which are also often high in salinity, while thermotolerant methanogens are found in hot springs (Ward et al., 1985) or hydrothermal vent systems (Kurr et al., 1991), which are often located at great depths in the ocean where pressure is high. The ability of methanogens to thrive in diverse environments, including those that could potentially be seen as analogues for past terrestrial and current extraterrestrial environments, makes them the target of studies in the field of astrobiology (Reid et al., 2006; Taubner et al., 2015).

1.1.4 Methanogenesis throughout Earth's history and in the context of astrobiology

Carl Woese suggested methanogens to be some of the most primitive organisms: in an early atmosphere primarily composed of carbon dioxide, water, nitrogen and hydrogen, methanogens could have possibly been living on CO_2 and H_2, in connection with a primitive photosynthesis cycle (Woese, 1977). Later Kral et al. (1998) also suggested for the methanogenic lifestyle to have appeared on early Earth, where CO_2 would have been an abundant electron acceptor and H_2 a readily available electron donor. This reaction could have allowed for the accumulation of CH_4 in early Earth's atmosphere, with a subsequently increased hydrogen escape to space, a process which may have helped oxidize early Earth (Catling et al., 2001, Figure 1.3). The earliest evidence for biological methane formation dates back to 3.46 Gyr (Ueno et al., 2006), however the extent to which methanogenesis has shaped early Earth since the first appearance of the metabolism is still debated (Olson et al., 2016).

Ueno et al. (2006) date methanogenesis back to more than 3.46 Gya using isotopic carbon signatures, while Wolfe & Fournier (2018) use molecular clock analyses to estimate the origin of methanogenesis at 3.94 Gya ±228Myr, with a split of

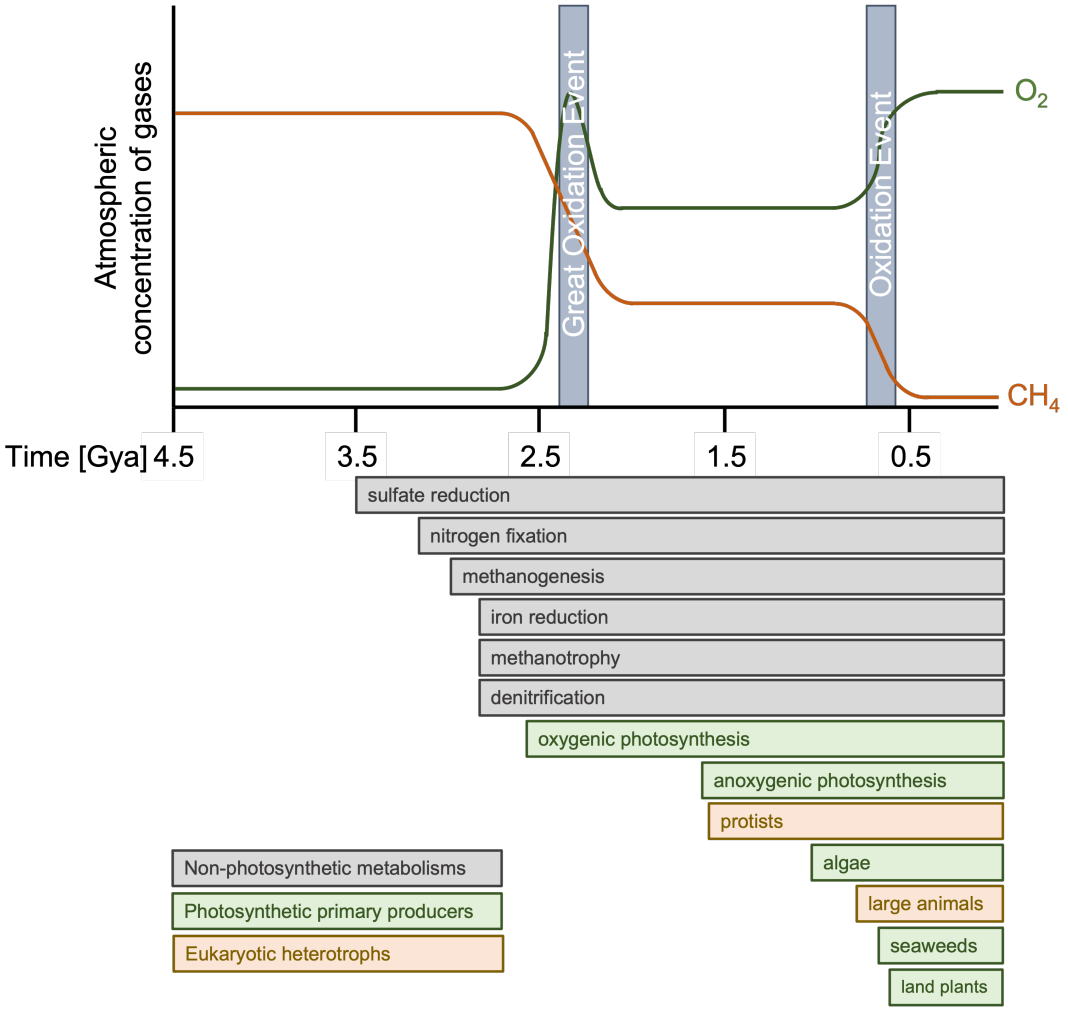

Figure 1.3 Timeline of Earth's history with atmospheric oxygen and methane concentrations and supported appearances of biological processes. Adapted from Olson et al. (2018) and Lepot (2020)

.

Methanosarcinales and *Methanomicrobiales* at 3.10 Gya ±195 Myr.

Within the methanogens, some studies suggest the most ancestral pathway to be hydrogenotrophic, citing the presence in the last common ancestor of deeply rooted clades such as *Vestraetarchaeota* and *Euryarchaeota* as well as the TACK superphylum (Berghuis et al., 2019). Others put the origins at hydrothermal vent systems with hydrogen dependent methylotrophs and a later evolution of tetrahydromethanopterin-coenzyme M methyltransferase (Mtr) that could have allowed for methanogenesis from CO_2 (Hua et al., 2019; Wang et al., 2021b). With the basal placement of hydrogenotrophy or methylotrophy still being debated, aceticlastic methanogenesis is believed to have been acquired through horizontal gene transfer within the last 475 million years (Fournier & Gogarten, 2008).

The ancestry of methanogenesis within the archaea strongly depends on the placement of Diapherotrites, Aenigmarchaeeota, Nanohalarchaeota, and Nanoarchaeota (DPANN), which remains to be determined: since DPANN lack the Mcr complex, placing them at the base of the archaeal tree would imply a non-methanogenic last archaeal common ancestor (LACA). However if they evolved later (as their fast evolutionary rates could falsely indicate a more basal placement), methanogenesis could indeed be an ancestral trait in the archaea (Dombrowski et al., 2020; Martinez-Gutierrez & Aylward, 2021; Garcia et al., 2022), with the *mcr* complex having evolved vertically in methanogens and methanotrophs as suggested by Hua et al. (2019). Williams et al. (2017) propose the LACA to be an anaerobe that fixes CO_2 to acetyl coenzyme A (acetyl-coA) via the Wood-Ljungdahl pathway, generating acetate and adenosine triphosphate (ATP) by using acetyl-coA synthetase, with a proposed optimal growth temperature around 75 °C. Furthermore, they predict a genome size of LACA of at least 1090 genes and independent adaptations to mesophily from a thermophilic ancestor in archaeal clades.

Understanding the history of methanogenesis on Earth can help us understand our own planet's biological evolution and the possibilities of life elsewhere. Methane has been found on every planet in our solar system as well as the dwarf planets Pluto, Makemake, and Eris, and Saturn's moons Titan, Europa, and Enceladus, where possible extraterrestrial habitats might be present in the cold subsurface oceans, or near hydrothermal systems (Jebbar et al., 2020). Past studies have tried to expose methanogens to extraterrestrial conditions, succeeding in proving the viability of organisms under Enceladus-like conditions (Taubner et al., 2018) and in simulated Martian environments (Reid et al., 2006; Kendrick & Kral, 2006; Mickol & Kral, 2017). Understanding the physical limits of life in these analogous conditions can be used to guide the design of future space exploration missions (Cavicchioli, 2002; Taubner et al., 2015).

1.2 Extreme Environments

1.2.1 What makes an environment "extreme"?

Earth today is home to a great diversity of life in different niches, from rich and diverse ecosystems to extreme environments, which are hostile for higher life and many microbial species. Throughout its history, Earth has not always been a hospitable environment, and it is these more extreme environments, that (partly) resemble the conditions of early Earth. Understanding the microbial diversity and adaptive features of organisms in extreme environments today can help us gain insights into what forms of life and what physiologies may have been possible on early Earth or elsewhere today.

Extreme environments are characterized by abiotic factors that largely limit life, such as temperature, pH, salinity, pressure, and radiation (Rothschild & Mancinelli, 2001). Examples of such environments include polar regions (low temperature), the deep sea (low temperature and high pressure), hydrothermal systems (high temperature and high pressure), terrestrial hot springs and geysers (high temperature and low pH), salt lakes (high salinity and high pH), and glaciers (low temperature), many of which present more than one extreme factor (Schröder et al., 2020). As described above, methanogens can be found in many of these environments (McGenity & Sorokin, 2010; Wagner & Liebner, 2010; Vishnivetskaya et al., 2018; Ward et al., 1985; Kurr et al., 1991; Hoehler et al., 2010). Clear definitions of what exactly makes an environment extreme, however, are missing and often the focus is anthropocentric, where any environment hostile to human survival is considered as extreme. Thus some environments with high biological diversity, such as aquatic habitats below 5 °C, are referred to as extreme, though they exhibit high biodiversity (Cavicchioli et al., 2011). However, only few of the organisms in these habitats have the capabilities to also thrive at the other end of the temperature scale, including methanogens.

1.2.2 Microbes in extreme temperatures

Microbial growth occupies a total temperature range of almost 150 °C. The most psychrophilic organism, *Planococcus faecalis*, is a bacterium first isolated from stool of Antarctic penguins that has observable growth down to - 20 °C (Kim et al.,

2015). The most thermophilic organisms, *Methanopyrus kandleri*, is a methanogenic archaeon first isolated from a hydrothermal vent system, with observable growth up to 122 °C (Kurr et al., 1991; Takai et al., 2008).

Psychrotolerant organisms are found in the oceans, soils and sediments, air, fresh water, and man made ecosystems (De Maayer et al., 2014), thermotolerant organisms are found in volcanic and geothermal systems, solar-heated systems (soil and sediments), biological self-heated systems (coal refuse piles), and anthropogenically created systems, such as industrial digesters (Zeikus, 1979; Cheng et al., 2007).

These organisms have adaptive mechanisms at the proteome, biochemical, and physiological levels allowing them to inhabit their temperature niches: their proteomes are compositionally different with respect to amino acids (Gromiha et al., 1999; Feller, 2010; Metpally & Reddy, 2009; Saunders et al., 2003) and different functional genes, such as cold shock proteins (Kuhn, 2012), cryoprotectants (Fuller, 2004; Storey & Storey, 1991), and heat shock proteins (Trent et al., 1994). Organisms at the lower end of the temperature scale present flexible enzymes (De Maayer et al., 2014), while their high temperature counterparts are characterized by thermostable enzymes (Ward & Moo-Young, 1988). Additionally, the differential expression of genes is observed both across species in transcriptional regulators, as well as within individual species if grown at different temperatures in various functional genes (Goodchild et al., 2004; Campanaro et al., 2011; Wang et al., 2015). These previous studies have investigated temperature adaptations across phylogenies and physiologies, leaving open questions regarding the effects of these two factors on the observed differences across temperature regimes.

1.3 Thesis Outline

1.3.1 Temperature adaptations - genomic and phenotypic approaches

Here the genomic and physiological temperature adaptation mechanisms of species sharing the methanogenic metabolism are investigated. Methanogens are used as the model organism since they span almost the entire microbial temperature growth range, from -2.5 °C to 122 °C (Takai et al., 2008; Franzmann et al., 1992). Many methanogens are extremophiles, thriving in high temperatures (Kurr et al., 1991), low

temperatures (Franzmann et al., 1992), high alkalinity, and/or high salinity (Sorokin et al., 2015). This allows for the comparison of organisms sharing the same physiology in different environments.

Chapter 2 gives an introduction to the phylogeny and distribution of methanogenesis in the archaea. A genome comparison for all methanogenic archaea was conducted, resulting in the identification of the conserved methanogenic core genome, and the variable pan-genome. Here function, composition, structure, and evolutionary histories were compared between two distinct temperature groups.

Chapter 3 is a study about the quantification of single cell variation under different temperatures. Here selected species were grown between 4 °C and 55 °C and their uptake of carbon and nitrogen measured at the single cell level. Different growth temperatures result in different distributions of growth rates for individual cells, and differences in the rates of carbon and nitrogen uptake.

Chapter 4 combines the single cell data obtained in Chapter 3 with metabolic modeling methods. This allows for the identification of possible metabolic modes responsible for the observed single cell variations and differences in substrate uptake.

1.3.2 Target organisms

The organisms studied in this thesis can be divided into two groups. The first group consists of 86 archaeal species containing the Mcr alpha, beta and gamma (McrABG) subunits (as described in Chapter 2). Studying these organisms across the full temperature range allows us to genomically resolve adaptations to their respective growth temperatures. The second group is a subset of seven methylotrophic species grown in pure cultures (as described in Chapter 3). These species are grown at varying temperatures, representing psychrotolerant (4 °C and 15 °C), mesophilic (23 °C and 37 °C), and thermotolerant (45 °C and 55 °C) growth conditions. By studying the single cell behavior within each species and across the temperatures, population dynamics and phenotypic adaptations to temperature are identified. Finally, one of these species, the psychrotolerant *Methanococcoides burtonii*, is the focus for metabolic modeling in Chapter 4, where genome composition and phenotypic heterogeneity are linked. This organism was chosen because extensive proteomics data for the relevant growth temperatures is available. Here metabolic models and flux balance analyses

are being used to explain the metabolic modes underlying single cell phenotypes as observed in Chapter 3.

CHAPTER TWO
Genome Study of Alkane Utilizing Archaea - Temperature Specific Features of Methanogens

2.1 Introduction - Methanogen Genome Comparison

2.1.1 Understanding the evolution of methanogenesis

Methane producing archaea have traditionally been classified into the orders *Methanobacteriales*, *Methanococcales*, *Methanomicrobiales*, *Methanosarcinales* and *Methanopyrales* (Liu & Whitman, 2008). However, the past decade has seen the discovery of alkane utilizing organisms outside those clades (Laso-Pérez et al., 2016; Berghuis et al., 2019), which open up new debates about the evolutionary history of the methanogenic metabolism.

While many research efforts focus on the origin of the physiology (as described in Chapter 1), the way in which methanogens shaped biogeochemical environments and gave way to other organisms is also of interest in the study of biological evolution: An early appearance of methanogenesis could have paved the way for other metabolisms on early Earth, most imminently methanotrophy (Figure 1.3), with both processes stabilizing global temperatures (Sauterey et al., 2020).

However, later these microbes may have also had some detrimental effects on other life, with Rothman et al. (2014) suggesting that the aceticlastic *Methanosarcina* were responsible for the end-Permian extinction event about 0.25 Gya, where anaerobic methane oxidation potentially increased sulfide which accumulated in the atmosphere as hydrogen sulfide, causing extinctions on land.

Wolfe & Fournier (2018) suggest that methanogens of the order *Methanomicrobiales* most likely transferred structural maintenance of chromosomes (SMC) complex genes to Cyanobacteria in a single evolutionary event. Furthermore Martijn et al. (2020) found that *Hickarchaeia*, intermediates between the methanogens and halophiles, had lost a large number of genes including methanogenesis and those for the Wood Ljungdahl pathway before gaining genes involved in aerobic respiration, salt adaptation, and UV resistance. The authors conclude that a gradual gene gain

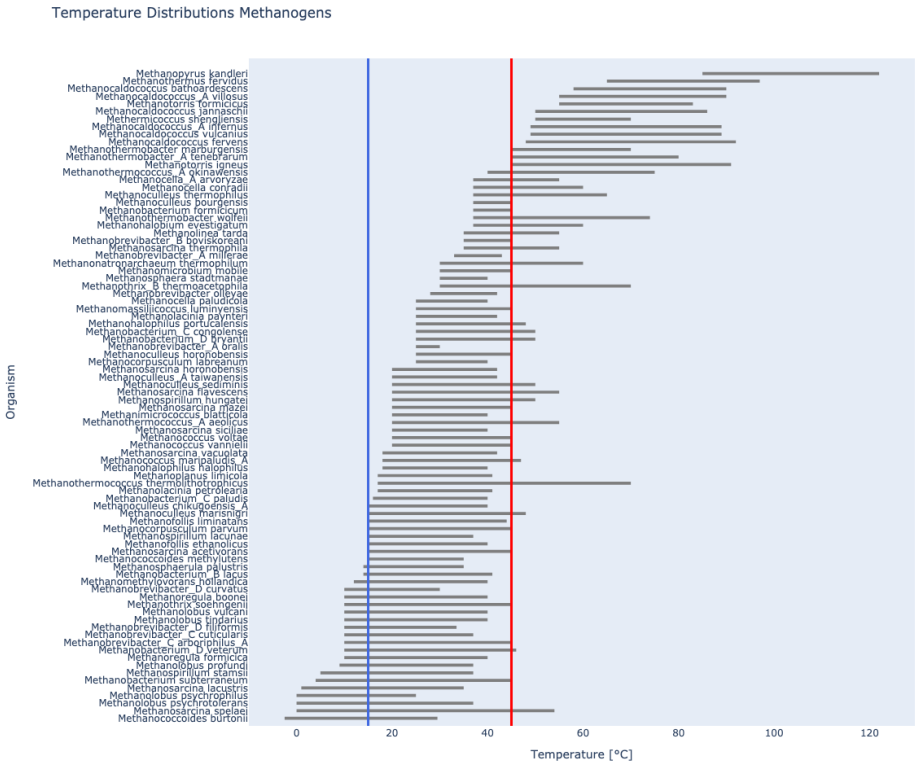

Figure 2.1 Distributions of known growth temperatures for methanogenic archaea. Lines indicate thresholds for psychrotolerant (blue) and thermotolerant (red) groupings used here.

.

and loss rather than a single massive gene transfer event shaped the methanogen to halophile transition.

The evolutionary history of methanogens and their contributions to early biogeochemical cycles are complex. Understanding the adaptive features that these organisms possess to inhabit their ecological niches today, can help us better understand their evolutionary history and the phylogenetic divergences that followed.

2.1.2 Genomes across temperatures

Microbes in extreme environments show adaptive features in their genomes and proteomes. With increasing temperatures, amino acid biases relate back to a decreasing trend in polar residues, increasing trends in the number of charged residues, ion pairs, and side chain contributions to the exposed surface, and the apolar fraction of the buried surface. With decreasing temperatures, higher flexibility with reduced hydrophobic cores, less charged surfaces, and more glycine residues are observed

(Feller, 2010; Suhre & Claverie, 2003). In terms of specific amino acid substitutions or enrichments, it has been shown that thermophilic organisms show a higher relative abundance of glutamic acid, lysine, tyrosine, valine, and isoleucine, and a lower relative abundance of glutamine, histidine, asparagine, alanine, and cysteine, as well as an overall lower GC content in their genomes (Farias & Bonato, 2003; Suhre & Claverie, 2003). Besides single amino acid biases, Farias & Bonato (2003) suggest that the ratio of (glutamic acid + lysine)/(glutamine + histidine) can be used as an indicator for hyperthermophily.

While the majority of studies to date have focused on trends in thermotolerant organisms, it has been shown that in psychrotolerant organisms amino acid substitutions increase protein flexibility (especially in coil regions) and specific activity, decrease thermostability, and that proteomes are less hydrophilic, less basic, less charged, and contain less aromatic amino acids. At the same time they contain more small and neutral amino acids, with overrepresentations of alanine, aspartic acid, glutamine, methionine, serine, and threonine and underrepresentations of arginine, proline, glutamic acid, and leucine, when compared to mesophilic counterparts (Metpally & Reddy, 2009; De Maayer et al., 2014; Saunders et al., 2003). Reductions in arginine and proline content increase flexibility and cause an enhanced degree of complementarity between the catalytic site and substrate, which results in reduced activation energies and increased substrate turnover rates at cold temperatures. The clustering of glycine at the enzyme catalytic site increases local mobility and an increased lysine to arginine ratio lowers hydrogen bonding and salt bridge formation (De Maayer et al., 2014). Furthermore De Maayer et al. (2014) show that some psychrophiles have high GC regions, but at the same time the overall genomic GC content should not be used as an indicator for thermal classes.

Those trends have been observed when comparing psychrotolerant or thermotolerant organisms to their mesophilic counterparts, however Yang et al. (2015) suggest that the trends of amino acid substitutions are not (always) opposite when directly comparing psychrotolerant and thermotolerant groups.

Using the methanogenic genus *Methanococcus*, Klipcan et al. (2006) showed that amino acid biases are affected mostly by optimal growth temperature and not by phylogenetic distance. In another study comprising of methanogenic organsisms,

Saunders et al. (2003) examine nine genomes with optimal growth temperatures (OGTs) between 15 °C and 98 °C, confirming that in cold-tolerant archaea proteins have more noncharged amino acids (glutamine and threonine) and a lower content of hydrophobic amino acids (leucine), with an almost linear trend in the content of glutamine, threonine, and leucine over the complete range of OGTs.

Amino acid substitutions have effects on the folding and unfolding dynamics of proteins at the structural level. Feller (2018) finds that hyperthermophilic proteins unfold slower and fold faster, and psychrophilic proteins unfold faster and fold slower compared to mesophilic proteins. The authors identify the slow unfolding in hyperthermophilic proteins as the main kinetic contribution to high protein stability, whereas fast folding in hyperthermophile proteins would increases the probability of misfolding events and aggregation of misfolded species.

Besides temperature, some studies also report low hydrophobicity and more acidity with an increase of alanine, asparagine, glutamic acid, and glycine, a decrease of cysteine, lower propensities for helix formation and higher propensities for coil structures in halophilic organisms (Wang et al., 2021b; Paul et al., 2008), as which some methanogenic archaea may also be classified (McGenity & Sorokin, 2010). Van De Vossenberg et al. (1998) attribute the structurally different cell membrane of archaea (when compared to bacteria) to the extreme environments they inhabit: membrane lipids are more resistant to high salinities and temperature extremes, and make the membrane more impermeable to ions and protons.

The majority of studies investigating temperature adaptations at the amino acid level focus on either the comparison of organisms at one extreme temperature to mesophilic counterparts or are restricted to a low number of genomes. Here genome scale adaptations throughout the total temperature range for methanogenesis, including all organisms with known growth temperatures, were investigated, further expanding on previous studies and excluding the effects that varying physiologies could have on genome compositions.

2.2 Methodology - Methanogen Genome Comparison

2.2.1 Methanogen database construction

A database with protein sequences and genome information (assembly level, checkM score, genome size, protein count) for methanogenic archaea was created from information and sequences available through the Genome Taxonomy Database (Parks et al., 2022, GTDB release 95). Organisms were identified as alkane utilizers if they contained alpha, beta and gamma subunits of the methyl-coenzyme M reductase (Mcr) enzyme. Mcr catalyzes the final step in methanogenesis by reducing methyl-coenzyme M to methane, and is a functional marker for both methanogenesis and anaerobic methane oxidation (Friedrich, 2005). Annotree v1.2.0 (Mendler et al., 2019) with the underlying KEGG UniRef100 database (Kanehisa et al., 2007) was used to query the *mcr* alpha (K00399), beta (K00401) and gamma (K00402) subunits against all archaeal species. The search resulted in a total of 290 genome hits across six archaeal phyla: Halobacteriota (156), Methanobacteriota (94), Thermoplasmatota (27), Thermoproteota (10), Asgardarchaeota (2), and Hadarchaeota (1). Protein sequences for representative strains of all 290 species were downloaded from the GTDB data repository. In previous taxonomic descriptions, methanogens were separated into Class I (Methanobacteriota) and Class II (Halobacteriota) within the Euryarchaeota phylum (Brochier-Armanet et al., 2011), however here their taxonomy was described using that of GTDB release 95. Though most methanogens also share the 5-methyltetrahydrofolate-homocysteine methyltransferase (*mtr*) gene complex, some of the basal species contain substrate specific methyltransferases and lack *mtr* genes (Borrel et al., 2019), thus only *mcr* was used for the identification of species of interest here.

In addition to genome information, temperature data was accessed through the Database of Growth TEMPeratures of Usual and RAre Prokaryotes (Sato et al., 2020, TEMPURA) and growth substrate information was retrieved from the phymet2 database (Michał et al., 2018). Temperature data was available for 86 out of 290 species, substrate data for 112. This data compilation is available in Supplementary Table S1. There is no universal definition for growth temperatures to classify organisms into psychrotolerant and thermotolerant groups. Here, these temperature groups

were defined based on the overall distribution of growth temperatures for methanogenesis (Figure 2.1). Organisms were classified into psychrotolerant organisms with a minimum growth temperature $\leq$ 15 °C and with no growth observed above 45 °C. Thermotolerant organisms have a maximum growth temperature $\geq$ 45 °C and no growth observed below 15 °C. Organisms spanning $\leq$ 15 °C to $\geq$ 45 °C were considered to be mesophilic. This classification resulted in 21 psychrotolerant, 41 thermotolerant and 24 mesophilic species.

2.2.2 Genome comparisons

OrthoFinder (Emms & Kelly, 2015, 2019) was used for core- and pangenome analyses. The program was run on 86 methanogenic species with temperature data and for further analyses the results were split into three orthogroup (OG) categories: (1) unique OGs - orthogroups found in only one species, (2) shared OGs - orthogroups found in at least two but less than 82 species and (3) extended core OGs - orthogroups found in 82 or more species. Here the extended core (OGs present in more than 95% of species (82 species)) instead of the true core (OGs present in all 86 species) was used to account for the possible false negatives in not 100% complete genomes after Charlebois & Doolittle (2004).

2.2.3 Tree generation

For the archaeal tree with clades containing organisms with *mcrABG*, clades were mapped on the the archaeal tree using the annotree tree of life version 1.2.0 based on GTDB release 95 and KEGG UniRef 100 as described above, which uses 122 archaeal marker genes to infer the phylogeny. Species and gene trees generated by OrthoFinder (Emms & Kelly, 2017, 2018) were used for downstream analyses. Trees were visualized using the interactive tree of life online tool (Letunic & Bork, 2021).

2.2.4 Functional annotation with eggnogmapper

Functional annotations of all genes in all OGs were done using eggnogmapper version 5.0 with default parameters (Huerta-Cepas et al., 2017). A general functional overview of the core- and pangenomes was created using cluster of orthologous genes

(COG) categories from the eggnogmapper output. KEGG KO numbers were used to compare pathways present in thermotolerant and psychrotolerant organisms and to identify those unique to either temperature group, using the KEGG pathway reconstruction tool (Kanehisa et al., 2007).

2.2.5 Protein Homologies with ECOD

Protein homologies were compared using the Evolutionary Classification of Protein Domains (ECOD) database (Cheng et al., 2014). Using the mapping of x groups, the ECOD homology level with the second lowest level of similarity (mapping of x groups onto all archaeal proteins using Hidden Markov Models provided by L. Longo, Earth-Life Science Institute), x groups and architectures for all protein sequences in the analysis were retrieved. X groups were then translated back to architectures (secondary structures and geometric shape), and architecture compositional differences between the different orthogroups and temperature classes identified.

2.2.6 Amino acid composition

Amino acid compositions were analyzed by counting amino acids in the protein sequence files for each orthogroup and temperature group, as well as for each species individually. The relative abundance of each amino acid in the proteome was used to calculate the compositional differences between psychrotolerant and thermotolerant proteomes. In a next step, amino acid compositions were used to calculate average amino acid residue properties using the quantitative amino acid properties from Gromiha et al. (1999).

2.2.7 Gene duplications, transfers and losses

As one of its output files, OrthoFinder provides a species tree with gene duplication event numbers at each terminal branch, which was used to get a first overview of duplication events in every species. Count (Csűrös, 2010), a software for evolutionary analyses of phylogenetic profiles, was then used to estimate gene gain and loss events using Wagner parsimony, which allows for both forward and backward changes (gain and loss). Rate models were optimized using the gain-loss-duplication model (Csűrös & Miklós, 2009) with the Poisson family size distribution at the root.

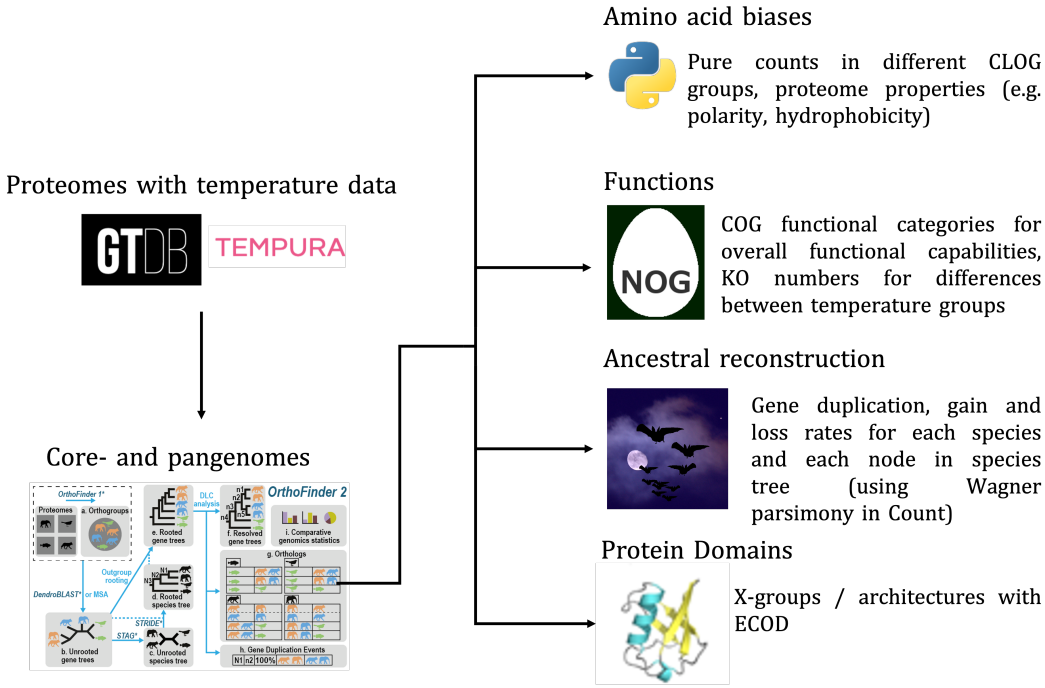

Figure 2.2 Overview of analyses with 86 methanogen genomes: database creation, orthology inference, amino acid compositions, functional annotation, gene evolution analyses and protein domain analyses.

.

Lineage-specific variations were left unspecified, and all other parameters were kept at default (rate variations across families with 1:1:1:1 gamma categories for edge length, loss, gain, and duplication rates, and a maximum of 100 optimization rounds with a convergence threshold of 0.1). An overview of all main methodologies can be seen in Figure 2.2.

2.2.8 Statistics

Pearson correlation p-values were calculated for amino acid counts as well as residue properties for each species using the statistical functions module in python's scipy package (Seabold & Perktold, 2010). They were tested for statistical significance with the Benjamini Hochberg correction using the fdr_correction function with method='indep' in the mne module in python (Genovese et al., 2002). These tests were performed to test for statistically significant trends with temperature in amino acid composition and amino acid residue properties.

2.2.9 Comparative genome core analyses for prokaryotes

For comparison to other microbes, genera with temperature data for at least five of their member species were selected from the TEMPURA database (Sato et al., 2020) and five species selected randomly for core genome analyses using Proteinortho (Lechner et al., 2011), run with the default parameters. The number of species was kept constant to account for the reduction of the core size with the addition of species (Charlebois & Doolittle, 2004) and in order to keep the analyses comparable. Fourteen genera in total were used for this analysis with eight thermotolerant (*Pyrococcus*, *Pyrobaculum*, *Thermococcus*, *Methanocaldococcus*, *Acidianus*, *Thermotoga*, *Caldicellulosiruptor* and *Fervidobacterium*), four mesophilic (*Acholeplasma*, *Bacteroides*, *Eubacterium* and *Methanosarcina*) and two psychrotolerant (*Cryobacterium* and *Paraglaciecola*) groups, including two methanogenic genera.

2.3 Results and Discussion - Methanogen Genome Comparison

2.3.1 Phylogeny, subtrate utilization and growth temperature distributions of methanogenesis

290 archaeal genomes contain the *mcr* alpha, beta, and gamma subunits, out of which 255 are considered to have a high enough quality for analyses herein (checkM score $\geq$ 90).

Those genomes range in size from 1.112 Mbp (WYZ-LMO11 sp004348015 of the *Methanomethyliaceae* family) to 5.752 Mbp (*Methanosarcina acetivorans*) and span five phyla, 17 classes, 21 orders, 38 families and 99 genera, which highlights a continued taxonomic expansion of known methanogens (Liu & Whitman, 2008; Borrel et al., 2013, 2019; Shao et al., 2022, Figure 2.3). A list of these genomes with information on their size, quality, and, where available, growth temperature ranges, isolation environments, and growth substrates of species is available in Supplementary Table S1.

Among those 255 archaeal genomes substrate data from cultivation studies is available for 112 (Michał et al., 2018, Figure 2.4). Eighty-three species have capabilities for hydrogenotrophic methanogenesis, with 72 being strict hydrogenotrophs unable to use other methanogenesis pathways. Hydrogenotrophic organisms growing at

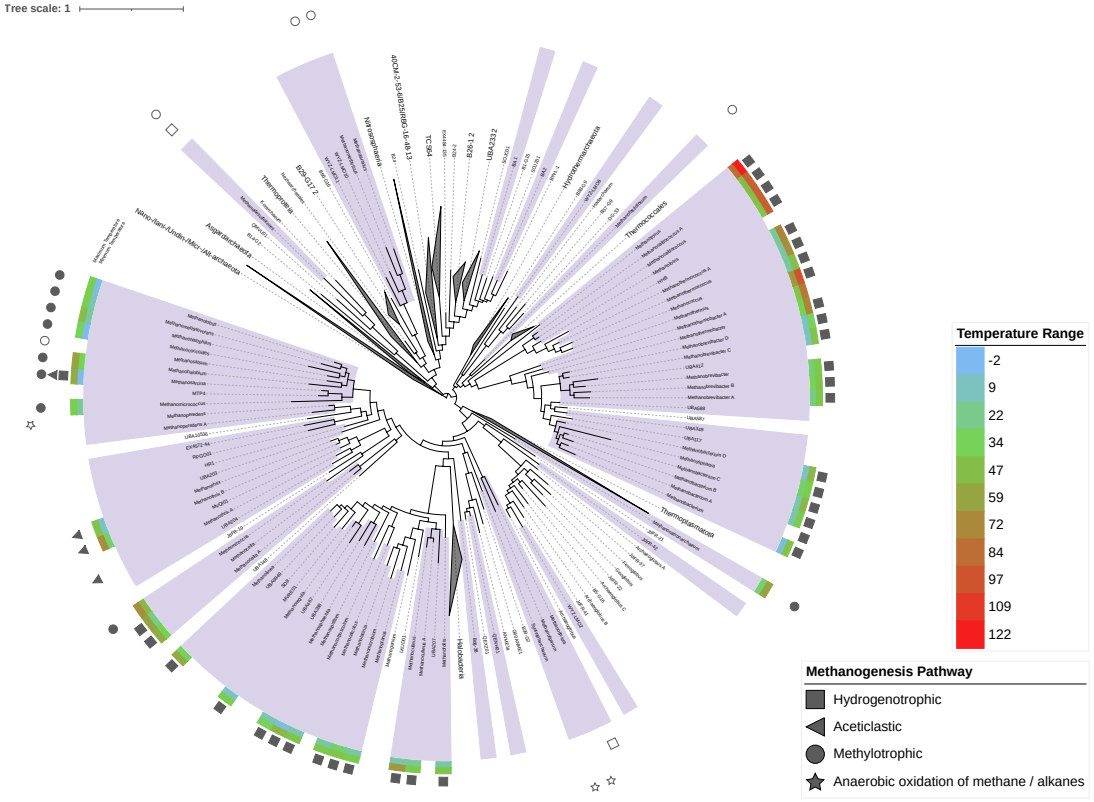

Figure 2.3 Overview of methanogenic archaea within the archaeal tree at the genus level. Branches of mcrABG containing genera with genomes of checkM scores $\geq$90 are marked in purple. Colors indicate minimum and maximum growth temperatures, shapes indicate confirmed substrates used within the genus. Unfilled shapes denote putative substrates that were inferred for uncultured species.

.

temperatures as low as 5 °C to 37 °C include members of the order *Methanomicrobia*, whereas those growing up to 40 °C to 122 °C include *Methanopyri*, *Methanobacteria* and *Methanococci*. With the exception of *Methermicoccus shengliensis* (methylotroph) and *Methanothrix B thermoacetophila* (aceticlast), all methanogens with maximum growth temperatures $\geq$ 65°C are hydrogenotrophic. Thirty species are methylotrophic methanogens with a majority being psychrotolerant (*Methanosarcinales*) and 20 of them being strict methylotrophs. 17 are aceticlastic, mostly psychrotolerant species (*Methanotrichales*), with seven strict aceticlasts. The genus *Methanosarcina* contains five species capable of all three methanogenic pathways: *M. vacuolata*, *M. mazei*, *M. spelaei*, *M. flavescens*, and *M. thermophila*. Other substrates for growth include butanol, 2-butanol, isobutanol, propanol, 2-propanol, carbon monoxide, cyclopentanol, dimethyl sulfide, ethanol, and formate though the capabilities of individual species to use these substrates are not yet well described (Michał

et al., 2018).

The *Methanomicrobia*, *Methanococci*, *Methanocellia*, and *Methanobacteria* genera are strictly hydrogenotrophic, *Methanotrichales* strictly aceticlastic and all genera in the the *Methanosarcinaceae* family besides *Methanosarcina* are strictly methylotrophic, while some species within *Methanosarcina* are capable of all three methanogenic pathways (Figure 2.4).

In addition to cultured organisms, some metagenome assembled genomes and uncultured organisms imply methylotrophic methanogenesis in the *Methanomethylicaceae*, *Methanosalsum* and *Methanofastidiosum* genera, though organisms from the latter presumably only grow on methylated thiols (Vanwonterghem et al., 2016; Sorokin et al., 2015). Hydrogenotrophic methanogenesis is infered for the genus *Methanolliviera* (Borrel et al., 2019), hydrogenotrophic and methylotrophic methanogenesis for the *Methanodesulfokores* (McKay et al., 2019), reverse methanogenesis coupled to nitrate reduction for the *Methanoperedens* (Arshad et al., 2015), the anaerobic oxidation of butane for the *Syntropharchaeum* (Laso-Pérez et al., 2016), and an uncharacterized methanogenesis pathway linked to short chain alkane/fatty acid oxidation for *Methanoliparium* (Borrel et al., 2019).

86 species have temperature data available (Figure 2.4). The lowest reported growth temperature is - 2.5 °C for *Methanococcoides burtonii*, while the highest is 122 °C reported for *Methanopyrus kandleri*. The highest range of temperatures is reported for *Methanothermococcus thermolithotrophicus* with growth between 17 °C and 70 °C. Out of the 86 species, 41 were classified as thermotolerant (max. growth temperature $\geq$ 45°C) and 21 as psychrotolerant (min. growth temperature $\leq$ 15°C), while organisms fulfilling both requirements were not included in either temperature group. An overview of growth temperature ranges can be found in Figure 2.1 and Figure 2.4. The mean genome size of psychrotolerant organisms at 2.853 Mbp is 30% bigger than that of thermotolerant organisms at 2.122 Mbp (Figure 2.8a, a trend that is not unique to methanogens and has been observed throughout the bacteria and archaea (Sato et al., 2020). This figure is also redrawn using minimum and maximum growth temperatures in Appendix Figure A.1). Similarly cold-loving organisms possess 30% more protein coding genes with 2748 compared to 2096 in thermotolerant organisms.

Thermotolerant organisms are associated with the shortest branches to the root

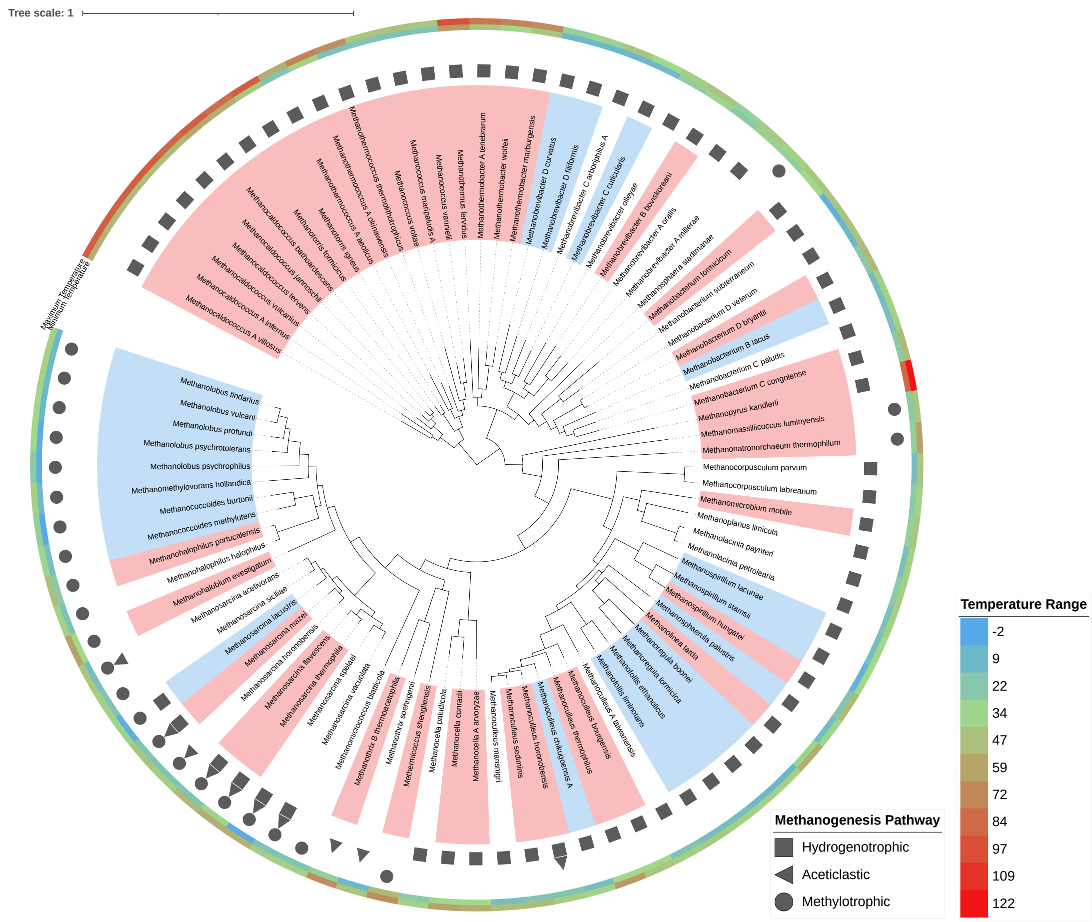

Figure 2.4 Species included in the analyses. Colored rings show minimum and maximum growth temperatures, shapes indicate methanogenesis substrates for each species. Branch coloring indicates temperature group classification (red - thermotolerant, blue - psychrotolerant). Uncolored branches are not classified into either group.

.

of the archaeal species tree, though there is no significant correlation with temperature and a large spread for mesophilic organisms (Figure 2.5, this figure is also redrawn using minimum and maximum growth temperatures in Appendix Figure A.2). This follows the initial observation of Woese (1987), who found that hyperthermophilic archaea were basal in the tree of life. In the case of the methanogens, the combined observation of short branch lengths and small genomes (Figure 2.8a) may run counter to a thermo-reduction hypothesis of genome evolution (Forterre, 1995).

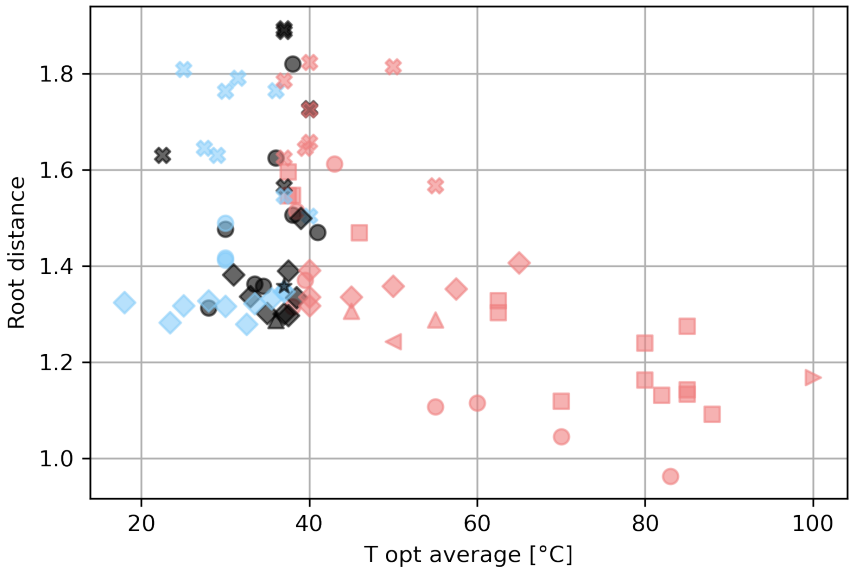

Figure 2.5 Branch lengths from the root of the archaeal tree with temmperature. Colors indicate temperature groups: blue - psychrotolerant, red - thermotolerant, black - no group/mesosphilic. Shapes indicate class level phylogenies: circle- *Methanobacteria*, upward triangle - *Methanocellia*, square - *Methanococci*, x - *Methanomicrobia*, left point triangle - *Methanonatronarchaeia*, right point triangle - *Methanopyri*, diamond - *Methanosarcinia*, star - *Thermoplasmata*.

.

2.3.2 Core- and Pan-genomes

A total of 211650 genes from 86 organisms were grouped into 10131 orthogroups, out of which 791 orthogroups containing 2329 genes are unique to one species. The core includes 330 orthogroups, which are shared by all 86 species, while 552 orthogroups belong to the extended core, which is shared by more than 95% of species and is used to account for partially incomplete genomes. The remaining 8788 orthogroups belong to the shared fraction of the pan-genome, shared by at least two but less than 95% of organisms in the analysis (core- and pan-genome sizes for each genome are shown in Figure 2.6a, the distribution of the number of orthogroup sizes in Figure 2.6b).

Within the temperature groups, the mean size of the genomic core is 30% in psychrotolerant and 35% in thermotolerant organisms. This fraction is large, considering that organisms span three different phyla and comparable core fractions can be found at the genus level in other organisms (e.g. *Comamonas* (Wu et al. (2018)) or

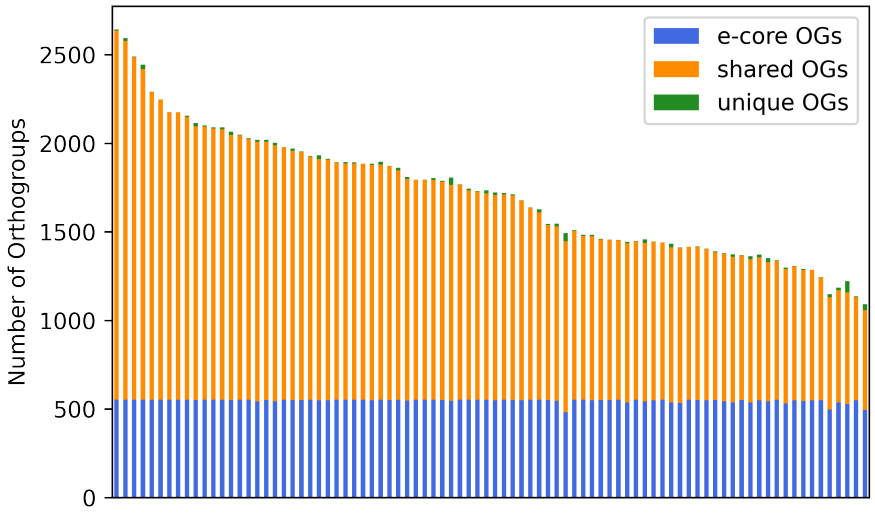

(a) core (present in all organisms), unique (present in only one organism) and shared (shared by at least two but not all organisms) CLOG distrubtion. Each bar represents one species in the analysis.

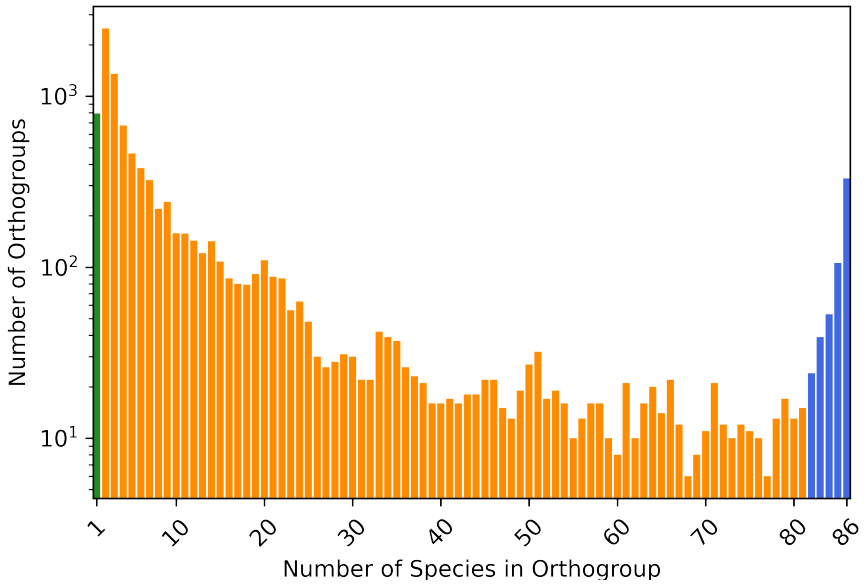

(b) distribution of CLOGs shared by x organisms, color legend same as in (a).

Figure 2.6 core and pangenome structures within the methanogens

.

Streptococcus (Barajas et al. (2019)).

The addition of more genomes into core comparison analyses will reduce the core size (Charlebois & Doolittle, 2004). When including genomes which contain *mcrABG* and have a checkM score ≥ 90 , the extended core contains 403 orthogroups, which is a 27% reduction in comparison to the core size observed when including only the 86 cultivated members. This set includes 255 genomes from methanogens, methanotrophs, and other alkane activating archaea: it appears to be the common core for alkane metabolizing archaea (all OGs from this analysis can be found in Supplementary Table 2).

In a previous analysis including two hydrogenotrophic species from the *Methanothermobacter* genus (Kaster et al., 2011), orthogroups shared between the two genomes were largely related to CO_2 reduction and energy conservation, CO_2 reduction to methane with H_2, as well as the translocation of metals and ions other than sodium. Between those two species from the same genus, 85% and 91% of genomic content was shared respectively. In another study, Borton et al. (2018) showed that across eleven genomes within the genus *Methanohalophilus* which included metagenome assembled genomes, the core accounted for only 42.5 - 49.4% of the total genome size, which may be attributed to the inclusion of MAGs that tend to have lower completeness and quality scores, with most core genes accounting for housekeeping and methylotrophic methanogenesis related functions. Similarly Poehlein et al. (2018) compared species from the *Methanobrevibacter* (16 species) and *Methanosphaera* (3 species) genera, identifying core genomes ranging from 22.57% to 34.51% and 64.29% to 69.99%, respectively. The authors indicate that within the *Methanobrevibacter*, clades may be separated based on functional capabilities surrounding nitrogen fixation and acetate assimiliation in one, and abilities to use ethanol and methanol in another clade. These studies show that the relative size of the genomic core is dependent on the number of species included in an analysis, further supporting Charlebois & Doolittle (2004). Lyu et al. (2018) showed genome content differences in Class I and Class II methanogens, with the latter having better oxidative adaptation abilities. Similar to their analyses the organisms here also span across phylogenies.

To account for the bias of clade sizes, the number of orthogroups shared be-

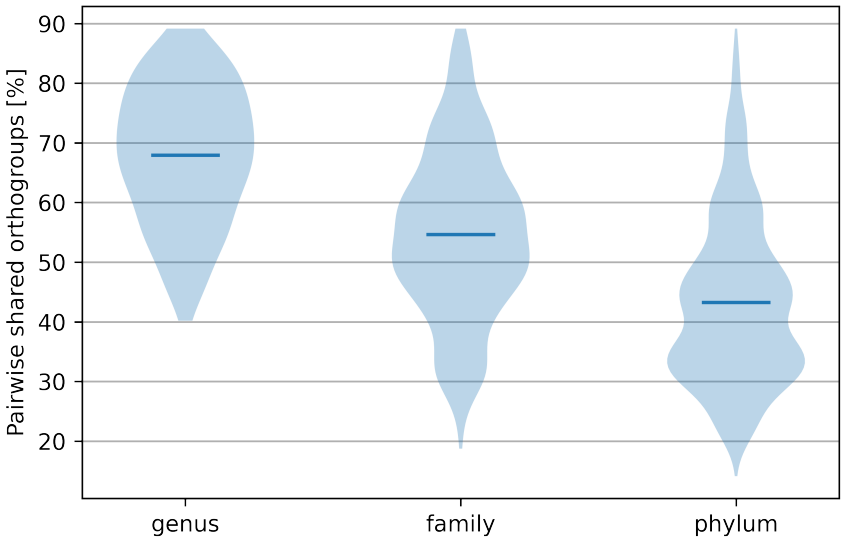

Figure 2.7 Pairwise shared Orthogroup percentages throughout phylogenetic levels. Species - species within genera, genus - genus within families, family - family within phyla. Only Clades with more than one member are shown here.

.

tween two species at the genus, family and phylum level were also compared across the phylogenetic diversity of methanogens. Excluding those clades with only one species member, comparisons include 180 pairwise comparisons in 23 genera, 884 in twelve families and 3640 in two phyla. The fraction of shared OGs decreases with increasing phylogenetic distance. Across methanogens, on average 67.95% of OGs are shared between two species within a genus, 54.66% of OGs are shared between two genera in a family and 43.27% of OGs are shared between two families in a phylum (Figure 2.7).

2.3.3 Prokaryote genome size and content with temperature

To investigate if large core sizes are observed across a wide range of organisms, five species each from a total of 14 bacterial and archaeal genera were analyzed to investigate their core size distributions with temperature. Core fraction size is inversely proportional to growth temperature, and the two methanogenic genera included in these analyses (*Methanocaldococcus* and *Methanosarcina*, both containing more than five species) group with other genera of similar growth temperature ranges (Figure 2.8b, species resolved figures can be found in Appendix Figure A.4).

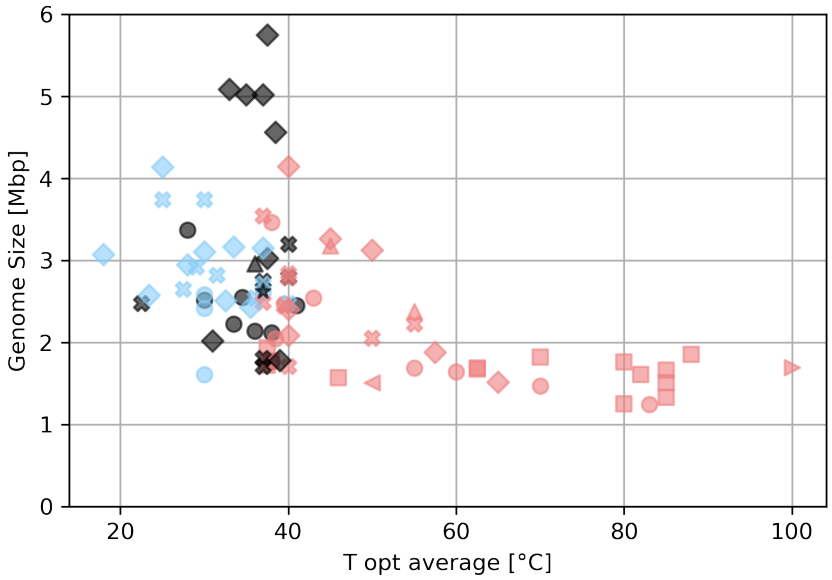

(a) Genome size variations with optimal growth temperatures of an organism. Colors indicate temperature groups: blue - psychrotolerant, red - thermotolerant, black - no group/mesosphilic. Shapes indicate class level phylogenies: circle- *Methanobacteria*, upward triangle - *Methanocellia*, square - *Methanococci*, x - *Methanomicrobia*, left point triangle - *Methanonatronarchaeia*, right point triangle - *Methanopyri*, diamond - *Methanosarcinia*, star - *Thermoplasmata*.

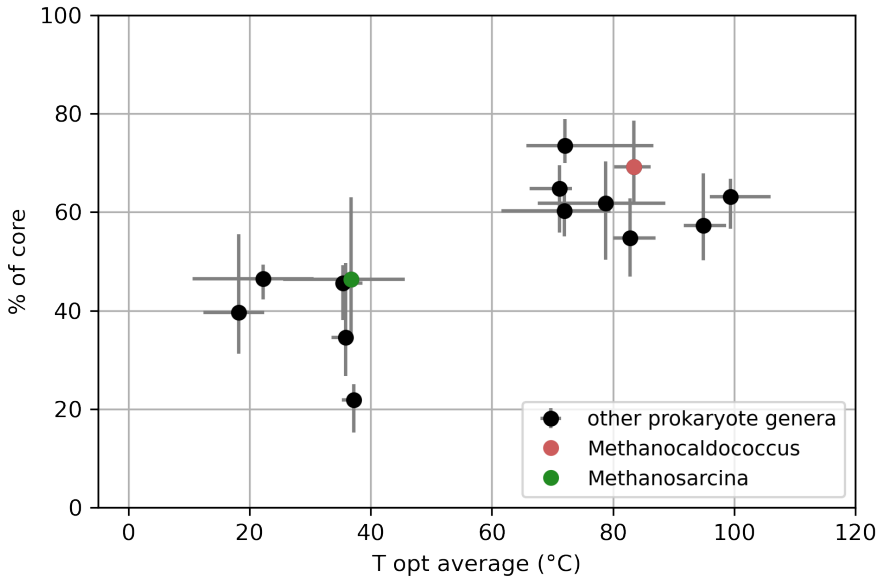

(b) Core sizes of archaeal and bacterial genera with varying growth temperatures. Error bars indicate ranges of optimal growth temperatures of the organisms studied in each genus.

Figure 2.8 Relationships between optimal growth temperatures and genome size and core fraction. 2.8a shows 86 methanogens from this analysis only, 2.8b shows 14 bacterial and archaeal genera with methanogenic genera colored.

.

2.3.4 Protein domain variations with temperature

Protein architectures were analyzed for each OG grouping, however 30% of psychrotolerant whole proteomes and 27% of thermotolerant whole proteomes did not have architecture hits. This fraction increases in the unique OGs to almost 75% for psychrotolerant and 69% for thermotolerant species. Appendix Figure A.5 shows the differences in known architectures between the temperature groups, excluding the unknown fractions. The differences in architectures are most pronounced in the unique OGs, however these are also the lowest in number and should not be used to make generalizations about structural differences. The shared OGs show some differences in architectures (a + b three layers and beta sandwiches are more abundant in psychrotolerant species, a/b three-layered sandwiches in thermotolerant species) and the core seems to be structurally conserved, with a/b three-layered sandwiches being only slightly more abundant in psychrotolerant species.

2.3.5 Amino acid variations

Using the methanogenic genus *Methanococcus*, it has previously been shown that amino acid biases are affected mostly by optimal growth temperature and not by phylogenetic distance (Klipcan et al., 2006). While it has also been suggested that compositional biases in amino acid content biases are not observable at the whole genome level (Feller, 2010), compositional shifts when comparing methanogens at both the whole proteome and conserved extended core levels are obseerved here (Figure A2 in the Appendix). Out of 20 amino acids, 14 show significant correlations with the optimum growth temperature of organisms, with slightly more pronounced differences in the shared proteome compared to the extended core (Figure 2.9, extremotolerant to mesophile comparisons including those of unique OGs are depicted in Appendix Figure A.6). Polar uncharged amino acids are increased in the psychrotolerant species, while lysine, glutamic acid, leucine, and isoleucine are increased in thermotolerant species. The results support the observations of a past genome-centric methanogen study by Saunders et al. (2003), who compared all at the time available methanogen species (n=9), showing an almost linear trend in the content of glutamine, threonine and leucine over the range of studied growth temperatures (15 °C to 98 °C),

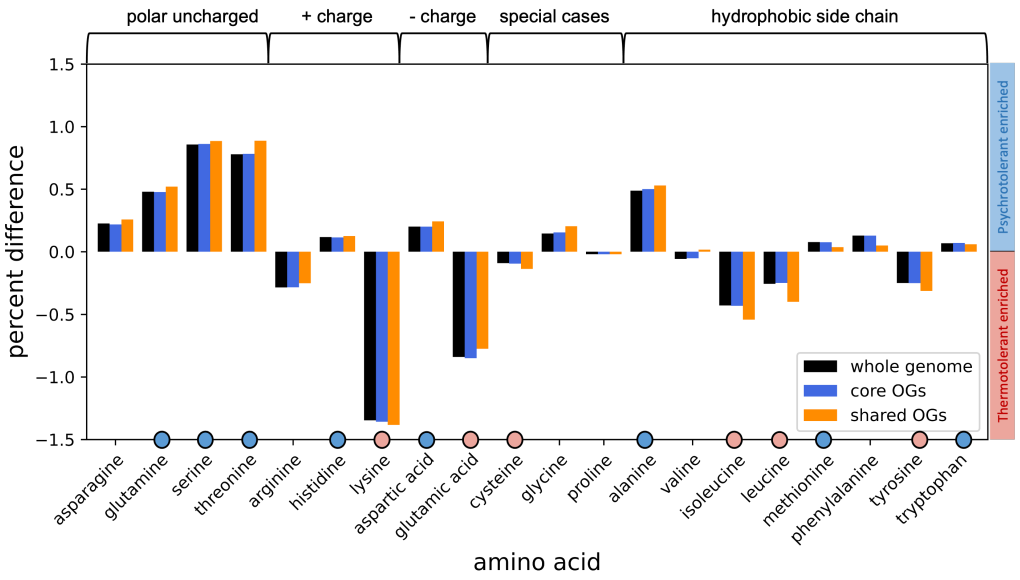

Figure 2.9 Amino acid compositional differences between temperature groups. Positive percentage indicates amino acid enriched in psycrhrotolerant species, negative percentage indicates amino acid enriched in thermotolerant species. Percentages were obtained by averaging the relative amino acid abundance over the whole genome / core OGs / shared OGs of each temperature group and subtracting the thermotolerant mean from the psychrotolerant mean. Circles denote amino acids that have significant correlation (Benjamini Hochberg correction on pearson p-values to test for significance) with temperature, across the whole range of temperatures (amino acid abundance vs. T opt avg). Colors indicate (blue) negative correlation with increasing temperature and (red) positive correlation with increasing temperature.

.

with glutamine and threonine being more abundant and leucine being less abundant in cold-tolerant methanogens.

The amino acid composition of a proteome has a direct impact on its structural and energetic features: we find that the proportion of charged amino acids and hydrophobicity have positive correlations with optimum growth temperature, while amino acid properties associated with structural complexity such as turn and coil tendencies, have negative correlations with the optimum growth temperature of an organism (Figure 2.10, Table 2.1). Some of these properties have been described for thermophilic enzymes in Ando et al. (2021), where the authors propose mechanisms that increase the stability of those enzymes, including entropic stabilization (Sawle & Ghosh, 2011). Interestingly, although enrichment in specific charged amino acids is observed in Figure 6, the charge state of the amino acids across the whole pro-

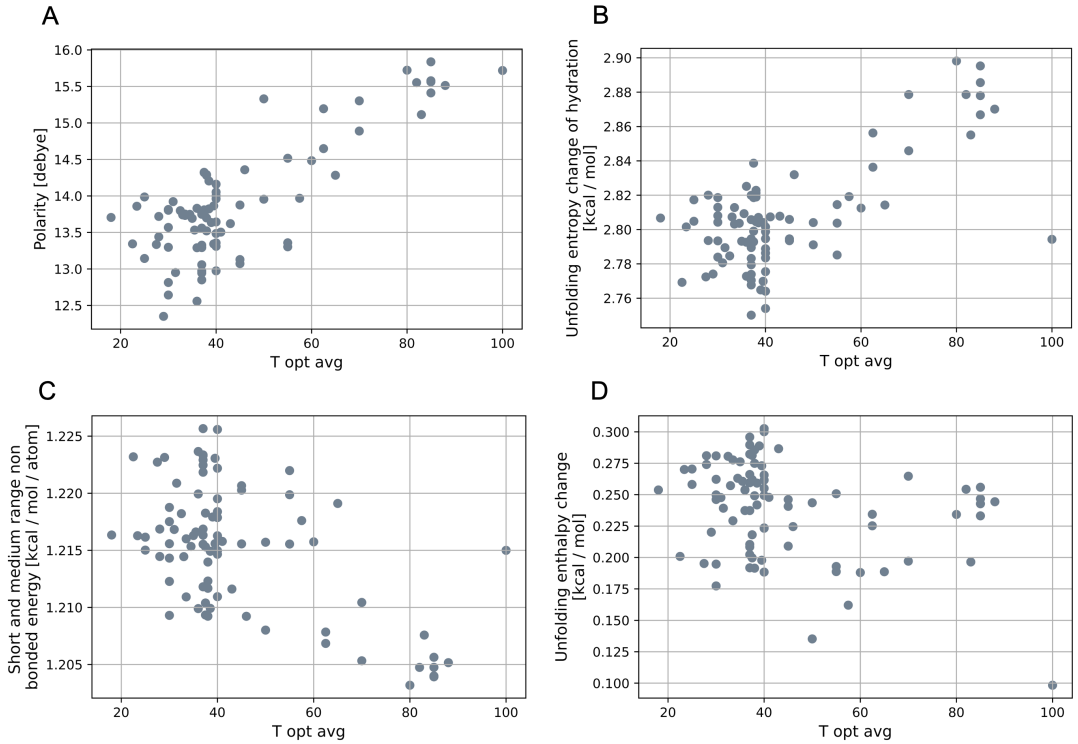

Figure 2.10 Selected amino acid residue properties in relation to optimal growth temperature [°C]. Polarity (A) and unfolding entropy change of hydration (B) have positive correlations with temperature, short and medium range non bonded energy (C) and unfolding enthalpy change have negative correlations with growth temperature.

.

teomes of hyperthermophilic methanogens may be closer to zero compared to their mesophilic relatives, since the average amino acid isoelectric point is closer to neutral water at higher temperatures (Figure S6, recall that neutral pH changes from 7 at 25 °C to 6.1 at 100 °C (Amend & Shock, 2001)). One important and interesting outlier in this study is *M. kandleri*, which grows at the highest temperature of the methanogens at 122 °C. Surprisingly, this organism exhibits many properties more similar to mesophilic organisms. This observation raises questions about the mechanisms of thermal adaptability and the use of amino acid profiles to predict growth temperature. For example, some studies propose the use of certain amino acid ratios (e.g. charged vs. polar amino acids) to predict optimal growth temperatures of (un)cultured organisms (Hua et al., 2019), but *M. kandleri* seems to challenge our ability to make generalizations.

Table 2.1
Amino acid residue properties trend with temperature

Increase with temperature	Decrease with temperature
isoelectric point (0.812)	coil tendencies (-0.677)
polarity (0.808)	turn tendencies (-0.617)
refractive index (0.737)	short and medium range non bonded energy (-0.567)
thermodynamic transfer hydrophobicity (0.715)	combined surrounding hydrophobicity globular and memmbrane (-0.356)
unfolding entropy change of hydration (0.690)	total non bonded energy (-0.350)
unfolding hydration heat capacity change (0.686)	unfolding enthalpy change (-0.318)
helical contact area (0.675)	unfolding enthalpy change of hydration (-0.311)
average medium contacts (0.637)	buriedness (-0.264)
solvent accessible surface area denatured protein (0.622)	compressibility (-0.251)
flexibility (0.579)	chromatographic index (-0.225)
solvent accessible reduction ratio (0.561)	unfolding Gibbs free energy change (-0.218)
bulkiness (0.560)	long range non bonded energy (-0.058)
volume (0.535)	
molecular weight (0.528)	
solvent accessible surface area native protein (0.523)	
unfolding entropy change (0.339)	
shape (0.241)	

Amino acid residue properties with significant correlation to temperature. Pearson correlation coefficient for each property in parentheses. Scatterplots showing the data are available in the appendix (REFERENCE).

Most related studies have focused on the comparison of one extremotolerant temperature group to their mesophilic counterparts, e.g. showing that amino acid substitutions in psychrotolerant organisms increase protein flexibility and specific activity and decrease thermostability (Metpally & Reddy, 2009; De Maayer et al., 2014). Interestingly, amino acid compositional trends were found not to be correlated between psychrotolerant and thermotolerant species at the family level in a previous study by Yang et al. (2015). Here organisms spanning almost the full temperature range for microbial growth were compared and with the exception of valine, all amino acids that are more abundant in one temperature group are less abundant in the other. The results suggest that perhaps for the methanogens, a shared biochemical repertoire underlies coordinated amino acid changes across the growth temperature range.

Though this work is restricted to changes associated with temperature, protein compositional differences are also associated with other environmental variables such as temperature, pH, oxidation state, (Dick & Shock, 2011), and salinity (Dick et al., 2020), showing that the composition of protein groups can hold clues to the environments that they are found in. More work is needed to build an integrative picture of how multiple variables affect the amino acid composition of the proteome.

2.3.6 Functional variations

Between the temperature groups, functional variations as observed by COG categories show similar trends: the methanogen extended core consists mostly of genes related to biosynthesis (57%) and coenzyme transport and metabolism (13%). Eleven percent of genes have unknown functions and the remaining 19% are functionally related to lipid biosynthesis, ion transport, secondary metabolites, intracellular transports, motility, cell wall and membrane biogenesis, cell cycle control, or carbohydrate transport (Figure 2.11a). In both temperature groups functional genes related to cell wall and envelope biogenesis, signal transduction mechanisms, and those without assignment or unknown functionalities show a relative increase through the shared and unique fractions, while those related to biosynthesis and coenzyme transport and metabolism show a relative decrease (Figure 2.11 b and c).

KO numbers of all genes with functional assignments were mapped onto the KEGG pathway map to identify pathways shared between the temperature groups and

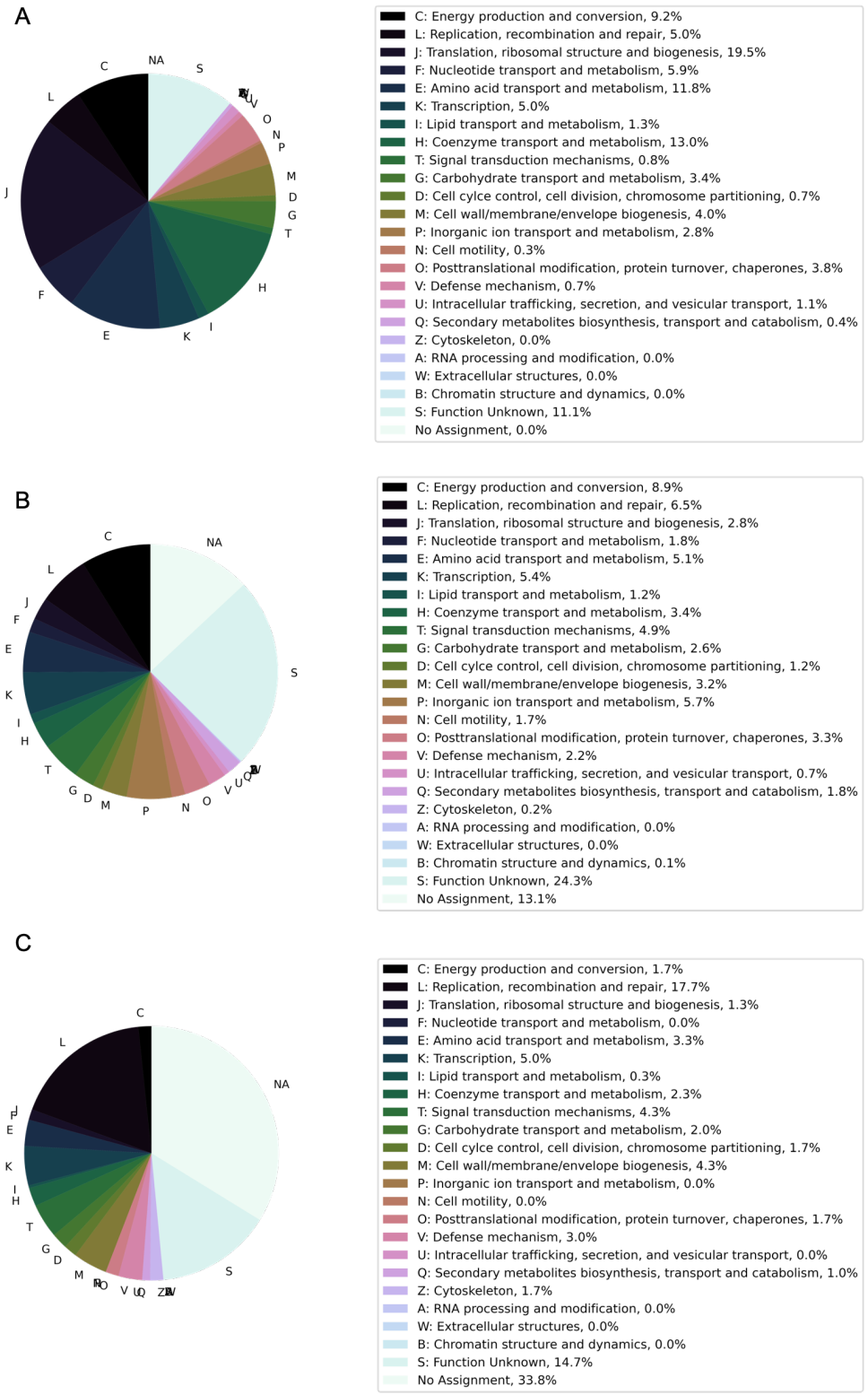

Figure 2.11 Functional composition of the extended core (A), shared (B) and unique (C) orthogroups for all methanogens.

.

those unique to each group. There are no thermotolerant or psychrotolerant specific cores, that is OGs which are shared exclusively and by all members of a temperature group. There are however genes present in one temperature group (though not in all of its member species), which are not present in any species of the other. Thermotolerant organisms are found with (metal) transporter genes and transcriptional regulators and contain the DNA repair gene rad51 and reverse gyrase, while psychrotolerant organisms have genes related to membrane and salt transport, membrane fusion, signaling and motility, chaperones, and the DNA repair gene recN (Table 2.2). Since these genes are not conserved in the temperature groups, they might be related to environmental factors other than temperature, such as high metal concentrations at hydrothermal vent systems, requiring additional metal transporter genes in the thermotolerant organisms being found there, or high salinity in cold environments requiring additional membrane proteins and salt transporters in psychrotolerant organisms. It has been suggested that reverse gyrase may be the only hyperthermophile specific protein (Forterre, 2002; Catchpole & Forterre, 2019), while chaperones and genes involved in membrane and cell wall biogenesis have been reported in psychrotolerant species (Wang et al., 2008). This analysis suggests that thermal adaptation may be largely accomplished by mechanisms other than the use of specific genes - perhaps as previously detailed by amino acid substitution patterns.

Similarly, substrate specific functions unique to hydrogenotrophic, methylotrophic and aceticlastic methanogens were identified: methylotrophs contain specific methyltransferases as has previously been reported (Burke et al., 1998; Söllinger & Ulrich, 2019; Borrel et al., 2019). Hydrogenotrophs contain (de)hydrogenases and aceticlastic methanogens have no unique genes related to methane metabolism (comprehensive list in Supplementary Table S3). The lack of aceticlast specific functional genes could indicate the general ability of hydrogenotrophic methanogens to perform the aceticlastic pathway, which has been observed in the hydrogenotroph *Methanococcus maripaludis* (Vo et al., 2020).

Table 2.2
genes / functions specific to the temperature groups

psychrotolerant specific	thermotolerant specific
bmpABC: basic membrane proteins	afuAB: iron transporters
metN: D-methionine transport system	mtnABC: manganese transporter
ytrF: acetoin utilization transporter	mtsA: iron/manganese/copper transporter
SLC7A4: cationic amino acid transporter / glycoprotein associated	psaA, scaA, sloC: zinc / manganese transporters
SLC10A7: sodium bile salt cotransporter	ABC.MN.A, ABC.MN.P, ABC.MN.S: manganese / iron transporters
wzxC: lipopolysaccharide transporter	SLC24A3: Na^+ / Ca_2^+ - K^+ exchanger
blpB: membrane fusion protein	SLC39A9: metal ion transporter
mshQ: MSHA pilus biogenesis protein	SLC42A: Rh ammonium transporter
rscC: capsule synthesis	FieF: ferrous iron efflux pump
wprA: cell wall associated protease	zipB, TC.BAT1, opuD, betLST, chaA, chrA, phaA: electrochemical potential driven transporters
chpA: chemosensory pili system protein	selB: selenocysteine specific elongation factor
rfpC: cell-to-cell signaling	cpaA, tadVZ, cpaE: tight adherence export apparatus
K20974: swarming activity and biofilm formation	etaA: exfoliative toxin A/B
htpG: molecular chaperone	parB family transcriptional regulator
vsrA: DNA mismatch endonuclease	topG, rgy: reverse gyrase
redN: DNA repair	rad51: DNA repair

Thermotolerant and psychrotolerant specific genes and their functions.

2.3.7 Ancestral Reconstruction

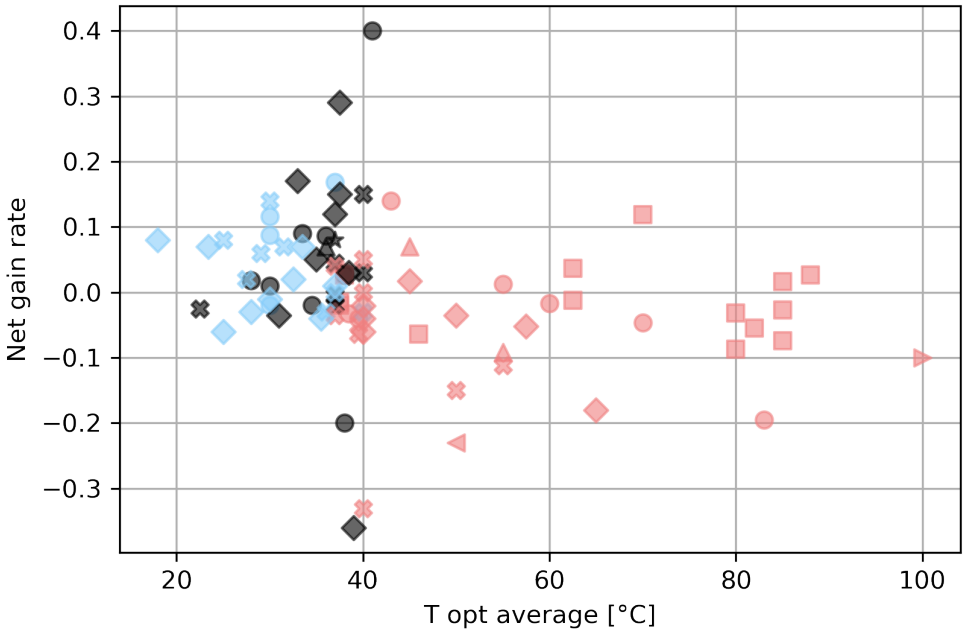

Figure 2.12 Net gain rate (gene gain rate + gene duplication rate - gene loss rate as infered by Count) for each organism with the optimal growth temperature. Colors indicate temperature groups used in this study: blue - psychrotolerant, red - thermotolerant, black - no group/mesosphilic. Shapes indicate class level phylogenies: circle- *Methanobacteria*, upward triangle - *Methanocellia*, square - *Methanococci*, x - *Methanomicrobia*, left point triangle - *Methanonatronarchaeia*, right point triangle - *Methanopyri*, diamond - *Methanosarcinia*, star - *Thermoplasmata*.

.

The species tree of the 86 species was used to investigate a possible phylogenetic relationship between gene gain-loss-duplication events with temperature. Although the thermotolerant organisms have smaller genomes, correlations between temperature and gain-loss-duplication were not observed. Figure 2.12 shows the net gene gain rate, calculated by adding gain and duplication rates and subtracting the loss rate (individual rates are shown in Appendix Figure A.3). This observation leaves open questions as to how the temperature:genome size relationship (Figure 2.8a) came to be.

Thomas et al. (2021) showed that in comparison with 21 other *Methanosarcinales*, the genome of the rumen dwelling and mesophilic methanogen *Methanosarcina blatticola* shows the biggest genome reduction, with the loss of

almost all genes involved in the H4MPT (tetrahydromethanopterin) methyl branch of the Wood-Ljungdahl pathway. In line with this, this analysis shows that *Methanosarcina blatticola* has the highest reduction with a net gain rate of - 0.36, while other *Methanosarcinales* show both net gains and losses. This clade specific variance within the *Methanosarcinales* suggests that gene gain-loss-duplication rates are not solely governed by the phylogenetic placement of organisms, and it may be that this type of variability is part of what clouds our ability to observe a temperature gain-loss-duplication rate relationship.

2.4 Conclusion

Considering the core- and pangenome, the core of methanogenic archaea is conserved with respect to functions and domains, while the pangenome shows differences in amino acid biases mainly in the unique fraction and protein domain differences.

Here the differences in genome size, evolution, functions and composition across the genomes of physiologically similar organisms spanning a wide growth temperature range were shown. Differences in amino acid composition can be found at the whole genome level as well as in the functionally constant extended core. Thermotolerant methanogens have smaller, reduced genomes with an increase in charged amino acids and functional genes related to ion transport, which are not found in their psychrotolerant counterparts. The latter have larger genomes with an increase in polar uncharged amino acids and additional functional genes related to cell structure and mobility. To fully understand the adaptive mechanisms of life to extreme temperatures, future work may target the functionally uncharacterized proteins unique to temperature groups.

The organisms in the core genome analysis span three phyla but share a large extended core, suggesting that physiological similarity has a stronger effect on temperature adaptation than phylogenetic distance in the methanogens. Core size decreases with increased phylogenetic distance between the methanogenic archaea; it will be interesting to explore this trend across the tree of life.

The expansion of our knowledge of alkane utilizing archaea, their phylogenies, metabolisms and genomic features has widened our understanding of archaeal

evolutionary history in the past decade (Berghuis et al., 2019; Laso-Pérez et al., 2016; Wolfe & Fournier, 2018; Hua et al., 2019; Wang et al., 2021b; Dombrowski et al., 2020; Martinez-Gutierrez & Aylward, 2021; Garcia et al., 2022; Williams et al., 2017). Further studies focusing on their genome evolution and characteristics can help us narrow down the first appearances of methanogens and methanotrophs in Earth's history.

Results of this paper are partially published as Prondzinsky et al. (2022), which is attached as Supplementary File 1.

CHAPTER THREE
Temperature Dependent Phenotypic Heterogeneity

3.1 Introduction - Temperature Resolved Phenotypic Heterogeneity

3.1.1 Phenotypic heterogeneity

Individual cells in a genetically homogeneous population do not necessarily exhibit the same traits, or phenotype. This phenomenon is referred to as phenotypic heterogeneity and is defined as the "phenotypic diversity that occurs independently of genetic or environmental variation and thus manifests between genetically identical individuals that live in the same microenvironment" (Ackermann, 2015). The diversity within one genotype can be beneficial in multiple ways: the genotype may survive in fluctuating environments ("bet-hedging"), interactions of phenotypically diverse cells can result in new functionality, and the division of labor among cells can enhance growth (Ackermann, 2013, 2015).

The causes for this phenomenon are not yet understood, but many hypotheses as to what can cause single cells to deviate from the population mean have been established. Takhaveev & Heinemann (2018) suggest three different factors that need to be considered to understand phenotypic heterogeneity - ecological factors, such as the growth matrix or cellular interactions, inherent dynamics, such as cell ageing and the cell cycle, and molecular noise, like differential gene expression. Phenotypic heterogeneity can be further categorized into spatial resource heterogeneity and temporal resource heterogeneity (D'Souza, 2020). Spatial resource heterogeneity can appear due to the spatial variation of nutrient availability and the spatial distribution and growth patterns of the cells, while temporal resource heterogeneity appears due to temporal changes in nutrient availability or community composition.

Goldschmidt et al. (2021) bring forward possible causes for nongenetic heterogeneity, which are based on the initial positioning of cells rather than environmental or genetic heterogeneity. The authors introduce neighborhood effects (non-uniform distributions of cells), stochastic phenotypic heterogeneity and demographic effects (cell age or history) as possible underlying causes for non-genetic heterogeneity. It has

also been noted that cellular metabolism is inherently stochastic. Metabolic stochasticity could allow for the adoption of a wide spectrum of metabolic states within a population and could be a generic source of cellular heterogeneity, while also limiting optimal growth and efficient biosynthesis (Kiviet et al., 2014).

Striednig & Hilbi (2022) give a recent overview on the proposed causes of phenotypic heterogeneity. They include stochastic or responsive gene expression, the level of heterogeneity being driven by the cell cycle, cellular age, cell to cell interactions (either through direct contact or signalling molecules), or environmental factors. However, current analytical methods do not allow us to directly assess which of these potential causes are certain, a concept which will further be explored in Chapter 4.

Previous studies have focused on the quantification of phenotypic heterogeneity (Zimmermann et al., 2015; Schreiber et al., 2016; Calabrese et al., 2019) as well as the effects of environmental factors such as substrate availability on metabolic rates within genotypically homogeneous populations (Zimmermann et al., 2015). These studies show that substrate limitation and the induced stress increase phenotypic heterogeneity within a community (Schreiber et al., 2016; Zimmermann et al., 2018; Sheik et al., 2016; Hermelink et al., 2009; Berthelot et al., 2019).

Past studies on phenotypic heterogeneity have focused exclusively on bacteria and the effect substrate limitation on single cell variation. Here the effects of temperature on phenotypic heterogeneity in methanogenic archaea are investigated using species that share the methylotrophic pathway of methanogenesis, but capable of growing at a wide temperature range.

3.1.2 Single-cell stable isotope probing techniques to quantify phenotypic heterogeneity

Recent works on phenotypic heterogeneity rely mainly on single-cell stable isotope probing (SC-SIP) to investigate single cell phenotypic heterogeneity, to identify metabolisms in complex environments without prior in-depth knowledge about them, and to confirm that cells are active (Alcolombri et al., 2022). Musat et al. (2012) review microautoradiography (MAR), raman microspectroscopy and SIMS in combination with SIP and cell identification methods. The authors review the use of NanoSIMS to elucidate on host-symbiont relationships and suggest a combined

approach using NanoSIMS and epifluorescence microscopy or flow cytometry to visualize or concentrate cells prior to SIMS analyses. Alternatively, FISH or catalyzed reporter deposition-FISH were suggested to distinguish between populations of cells. Most of the proposed methods however are destructive and do not allow for further analyses of samples, and cell identification and sample preparation protocols introduce uncertainties with respect to isotope labels being washed out of the samples (Musat et al., 2012; Pett-Ridge & Weber, 2012; Meyer et al., 2021).

The dilution of isotopic signals due to varying pre-treatment protocols remains one of the biggest challenges in SC-SIP. Meyer et al. (2021) study the effects of different fixation, staining, and FISH techniques on ^{13}C, ^{15}N, ^{18}O, ^{2}H and/or ^{34}S NanoSIMS analyses for multiple species, including *Methanosarcina acetivorans*. Different protocols decrease isotope enrichments by as much as 80% depending on taxonomy, growth phase, isotope label and applied protocol (Musat et al., 2014). This leads to the underestimation of microbial metabolic rates when adding unlabeled compounds in treatment protocols, e.g. just drying cells without the use of other chemicals results in lowered observed isotope ratios (94% $\pm$ 1.2% ^{13}C and 89.5% $\pm$ 3.8% ^{15}N of expected values).

To overcome some of those challenges, the combination of real-time imaging techniques with omics and synthetic ecology-based approaches have been proposed to increase the analytical resolution, and to understand heterogeneities on community and single cell levels (D'Souza, 2020). Additionally Alcolombri et al. (2022) suggest non-destructive methods such as femtosecond stimulated Raman spectroscopic imaging and high resolution infrared microspectroscopy, successfully using the method to study phenotypic heterogeneity, symbiosis, and cross-feeding. Simliarly Hermelink et al. (2009) used confocal raman microspectroscopy to study heterogeneity in *Legionella bozemanii*, *Bacillus cereus*, and *Bacillus thuringiensis*, showing inter- and intra-cellular heterogeneities in those lab grown pure cultures.

Single cell studies have only been conducted since the beginning of the century, and the realization of their faults have encouraged novel innovations. Some of the challenges mentioned herein may soon be overcome.

3.1.3 Methylotrophic methanogenesis

Methanogenesis is the process of anaerobic, biological methane formation through methanogenic archaea. In methylotrophic methanogenesis, methylated compounds such as methanol, methyl amines or methyl sulfides, are reduced to form methane (Liu and Whitman 2008). In the first step of the reaction, methyl transferases and corrinoid-containing proteins transfer methyl groups from substrates to coenzyme M (CoM) to form methyl-CoM. The methyl-CoM reductase (Mcr) complex catalyzes the rate limiting and terminal step of methanogenesis by reducing methyl-CoM to methane and the reverse reaction in archaeal methanotrophs (Evans et al., 2019). One quarter of substrates is oxidized to CO_2 to gain electrons for the reduction of the methylated compounds (as denoted in Table 1.1). When using methanol instead of methylamines, methanogens have to transport ammonium across the membrane in addition to methanol, as only methylamines could serve as a substrate for both, carbon and nitrogen.

Methylotrophic methanogens inhabit environments ranging in temperature from - 2.5 °C (Franzmann et al., 1992, *Methanococcoides burtonii*) to 70 °C (Cheng et al., 2007, *Methermicoccus shengliensis*). They can be found in aqueous environments, rumens, soil and industrial sludge and waste water treatment plants (Michał et al., 2018). With the exception of *Methanohalophilus halophilus* and *Methanomicrococcus blatticola*, who grow exclusively on methylamines, all methylotrophic methanogens have the capabilities to use methanol as a substrate for methanogenesis.

3.2 Methodology - Temperature Resolved Phenotypic Heterogeneity

3.2.1 Species used

To investigate the physiological adaptations to different growth temperatures, species for analyses were chosen based on their growth temperature and a common carbon source. As cultivation without pressurized gases was desired for easier culture setups, methanol was chosen as the substrate for methanogenesis. Six species were chosen for interspecies comparison based on their growth temperatures, spanning the entire temperature range for methylotrophic methanogenesis:

1. *Methanococcoides burtonii*, first described in Franzmann et al. (1992), is an obligately methylotrophic, coccoid methanogen isolated from methane saturated waters from the bottom of Ace Lake, Antarctica. The temperature range for its growth is from -2.5 °C to 29 °C, with the optimum at 23 °C.

2. *Methanolobus psychrotolerans*, first described in Chen et al. (2018) was isolated from lake Shira in Siberia. Cells are non-motile, irregular cocci, 0.8 - 1.2 µm in diameter. The growth temperature range is from 0 °C to 37 °C with fastest growth observed between 30 °C to 37 °C.

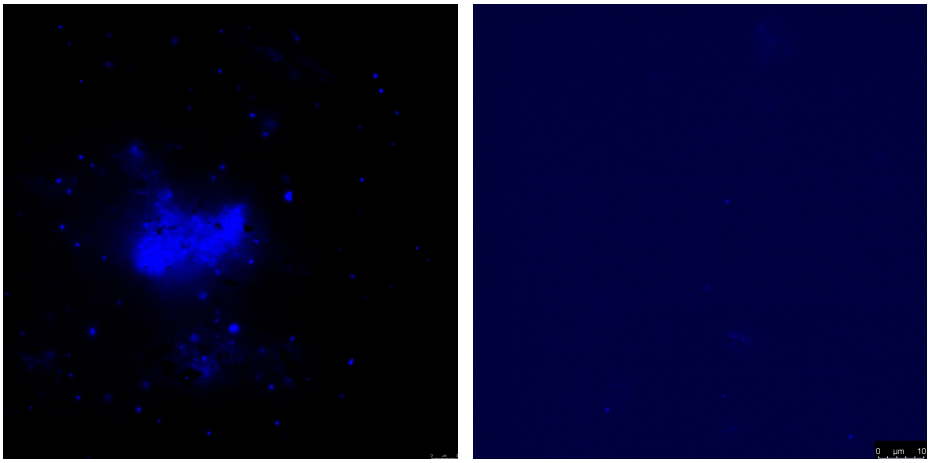

(a) *Methanococcoides burtonii* (b) *Methanolobus psychrotolerans*

Figure 3.1 Psychrotloerant species: Fluorescence microscope picture of DAPI stained cells. Scalebars in bottom right corners.

.

3. *Methanosarcina barkeri*, first officially described in Bryant & Boone (1987), was isolated from a sewage sludge digestor. Cells are non-motile, irregular cocci ranging from 1.5 to 2 µm in both width and length. The growth temperature range is between 25 °C and 50 °C with the optimum at 40 °C to 45 °C, and cells form small aggregates.

4. *Methanosarcina mazei* was first described in Barker (1936) as *Methanococcus mazei*, and later renamed and described in more detail by Mah & Kuhn (1984). This species was isolated from a sewage sludge plant, and its growth temperature range is between 20 °C and 50 °C, with the optimum between 35 °C and 45 °C. Cells are non-motile, irregular cocci, ranging in length and width between 1 and 3 µm.

5. *Methermicoccus shengliensis*, first described in Cheng et al. (2007) was isolated from Shengli oilfield in China. Its temperature range is from 50 °C to 70 °C,

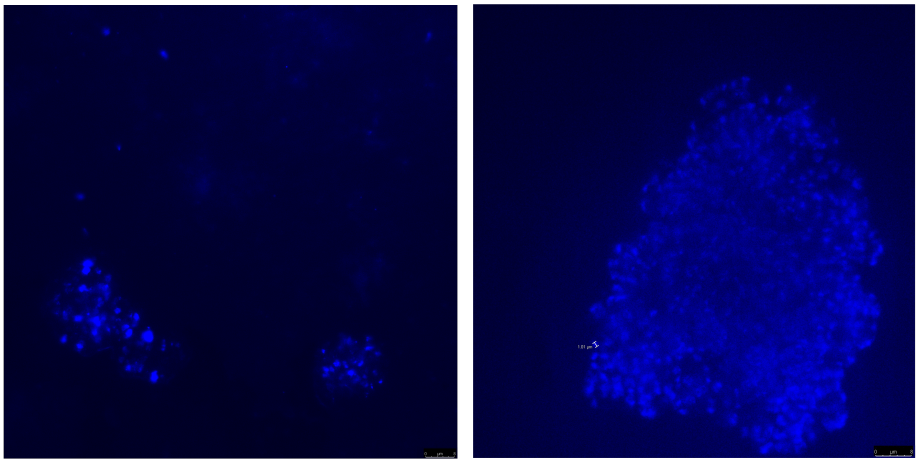

(a) *Methanosarcina barkeri* (b) *Methanosarcina mazei*

Figure 3.2 Mesosphilic species: Fluorescence microscope picture of DAPI stained cell aggregates. Red box is 100 µm x 100µm. Scalebar in bottom right corner.

.

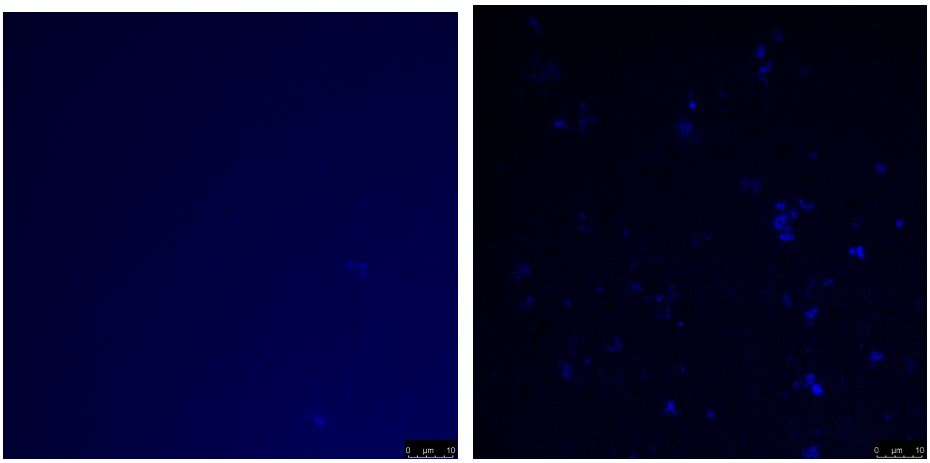

(a) *Methermicoccus shengliensis* (b) *Methanomethylovorans thermophila*

Figure 3.3 Thermotolerant species: Fluorescence microscope picture of DAPI stained cells. Scalebar in bottom right corner.

.

with the maximum observed growth rate at 65°C. Cells are coccoid with 0.7 - 1 µm diameter, typically in clusters of two to four cells with occasional cyst formation.

6. *Methanomethylovorans thermophila*, first described in Jiang et al. (2005), was isolated from an anaerobic reactor fed with methanol. The growth temperature range is from 42 °C to 58 °C, with fastest growth observed at 50 °C. Cells are irrgeular cocci ranging in length and width from 0.7 - 1.5 µm.

In addition to these six species, *Methanosarcina acetivorans* was grown at three different temperatures to compare different growth temperature phenotypes within one species. *M. acetivorans* was first described by Sowers et al. (1984) and

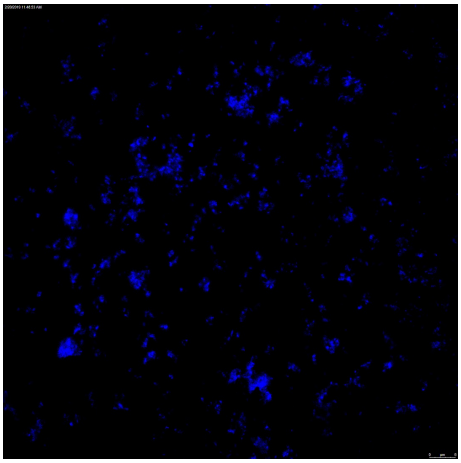

(a) *Methanosarcina acetivorans*

Figure 3.4 *M. acetivorans*: Fluorescence microscope picture of DAPI stained cells. Scalebar in bottom right corner.

isolated from Scripps Canyon near LaJolla, California. The known temperature range is from 10 °C to 50 °C, with fastest growth observed at 40 °C. Cells are non-motile, irregular cocci, ranging in length and width from 1.5 to 2.5 µm.

Species *M. acetivorans, M. barkeri and M. mazei* were reinnoculated from stock cultures available in the laboratories of the Earth-Life Science Institute, Tokyo Institute of Technology, all other species were ordered as pure cultures from the National Biological Resource Center, Chiba, Japan (NBRC strain No. 112514 (*M. psychrotolerans*), 107633 (*M. burtonii*), 112467 (*M. shengliensis*) and 107638 (*M. thermophila*)).

3.2.2 Culture conditions

All species were grown methylotrophically on methanol. Two psychrotolerant strains, *Methanococcoides burtonii* and *Methanolobus psychrotolerans* were grown at 4 °C, three mesophilic strains, *Methanosarcina acetivorans*, *Methanosarcina barkeri* and *Methanosarcina mazei* were grown at 37 °C, and two thermotolerant strains, *Methermicoccus shengliensis* and *Methanomethylovorans thermophila* were grown at 55 °C. For intraspecies comparative analyses *M. burtonii* was additionally grown at 23 °C and *M. acetivorans* was additionally grown at 15 °C and 45 °C.

All psychrotolerant and mesophilic species, as well as *M. thermophila*, were grown in a modified *Methanococcoides* medium (DSMZ medium 141-c, Table 3.1)

Table 3.1
Medium components of modified DSMZ 141-c medium

component	per L
NaCl	18.00 g
$MgSO_4$ - 7 H_2O	3.45 g
MOPS	5.25 g
NH_4Cl	0.25 g
$MgCl_2$ - 6 H_2O	4.00 g
$CaCl_2$ - 2 H_2O	0.14 g
K_2HPO_4	0.14 g
KCl	0.34 g
$Fe(NH_4)_2(SO_4)_2$ - 6 H_2O (0.1percent w/v)	2 ml
bacto yeast extract	0.10 g
Trace element solution	10 ml
resazurin	0.0005 g
vitamin solution	10 ml
methanol	5 ml
Na_2S - 9 H_2O	0.50 g

Note: prepared according to original protocol: salts and yeast extract, iron solution, trace element solution and resazurin mixed and adjusted to pH7, then degassed with 80:20 N2:CO2, autoclaved and vitamins, methanol and sulfide added after. Trace element and vitamin solution details in Appendix Tables B.1 and B.2.

under an 80:20 N_2:CO_2 atmosphere. *M. shengliensis* requires coenzyme M to be provided in the medium and was therefore grown in a modified version of NBRC medium No. 1433 (Table 3.2), also under an 80:20 N_2:CO_2 atmosphere. Media were modified to contain sodium phosphate instead of bicarbonate buffers, minimal amounts of yeast extract, and no cysteine, acetate, or peptone. These modifications were made to minimize alternate carbon sources that may interfer with the isotopic signal in SC-SIP analyses.

Cultures were grown in 100 ml crimped glass vials with 50 ml liquid and 50 ml headspace. They were maintained in their exponential growth phase through a semi-continuous setup by exchanging culture liquid with fresh medium based on observed growth for each species. Growth rates were determined by cell counts in duplicates: 2 x 1 ml of culture were sampled at each timepoint, filtered with 0.2 µm PTFE membrane filters (REF: JGWP02500, Merck Millipore Ltd., Ireland), stained with 4',6-diamidino-2-phenylindole (ProLong Gold antifade reagent with DAPI, Invitrogen, Waltham, MA, USA) and counted with a Leica automated microscope system (Leica DN5500 B microscope with DFC9000 GT camera and HCX PL FLUOTAR

Table 3.2
Medium composition of modified NBRC1433 medium for *Methermicoccus shengliensis*

component	per L
NaCl	20.00 g
MOPS	5.25 g
NH_4Cl	0.54 g
$MgCl_2$ - 6 H_2O	3.05 g
$CaCl_2$ - 2 H_2O	0.147 g
KH_2PO_4	0.136 g
Coenzyme M	0.0014 g
Trace element solution	1 ml
resazurin	0.001 g
vitamin solution	2 ml
methanol	0.8 ml
Na_2S - 9 H_2O	0.30 g

Note: prepared according to original protocol: salts, trace element solution and resazurin mixed and adjusted to pH7, then degassed with 80:20 N2:CO2, autoclaved and vitamins, methanol and sulfide added after Trace element and vitamin solution details in appendix. ….

100x/1.30 Oil objective, Leica, Wetzlar, Germany). Cells in 100 x 100 µm frames were counted and enumerated to 1 ml of cell culture based on the filtration area and, where applicable, dilution rate.

3.2.3 Isotope labeling study design

Stable isotopes of hydrogen, carbon and nitrogen were used to trace uptake rates for each cell according to the schematic in Figure 3.5. A 1% D_2O label was used as a passive bioactivity tracer for incorporation into cellular lipids. A 4% $^{15}NH_4Cl$ label was used to trace the uptake of nitrogen and its incorporation into amino acids. Finally, a 10% $^{13}CH_3OH$ label was used to trace the uptake of carbon and its incorporation into biomass. Labeling strengths were based on previous experiments and incubation times based on Kopf et al. (2015), who showed that with 1% D_2O label 0.2816 doubling times of incubation are needed to observe an uptake signal. Previously, enrichments of as low as 1.7 atm% ^{13}C with 13.6% ^{15}N were also verified as sufficient in SC-SIP experiments (Pett-Ridge & Weber, 2012).

Isotope incubations were conducted in 30ml crimped glass vials. 10ml of double labeled medium (2% ^{2}H, 8% ^{15}N and 20% ^{13}C) and 10ml of active culture in the

exponential growth phase were combined, diluting the label to the desired strengths. Incubations were set up for 0.2816 doubling times for all species in duplicates as in Table 3.3.

Samples for NanoSIMS analyses were taken in duplicates by opening the crimped vials and sampling 2 ml of culture. Cultures were then filtered on 0.2 µm PTFE membrane filters (REF: JGWP02500, Merck Millipore Ltd., Ireland). Filters were washed with 2 x 1ml miliQ water and placed onto 1 cm in diameter ITO covered glass slides with the cell side down and left to dry overnight. After drying, filters were peeled off and glass slides prepared for shipping to the Caltech SIMS facility, where they were stored until analyses.

To avoid contamination and isotope dilution through fixatives (Musat et al., 2012), NanoSIMS samples were not fixed. Additionally, dilution rates were adjusted prior to isotope incubations through microscopy, to not have to concentrate cells with flow cytometry or stain them with DAPI to identify areas of interest. Since all samples were pure cultures of methanogens, methods to distinguish between populations of cells (such as FISH or CARD-FISH) were not needed. Forgoing fixatives poses a tradeoff between cell resolution with NanoSIMS and isotope dilution.

For each vial additional biomass aliquots were taken for future analyses: 3 x 0.9 ml of culture with 0.3 ml 16% methanol free paraformaldehyde were stored at 4 °C and pellets of 6 x 1 ml of culture, centrifuged at 15000g at 4 °C for 15 min, were stored at -80 °C.

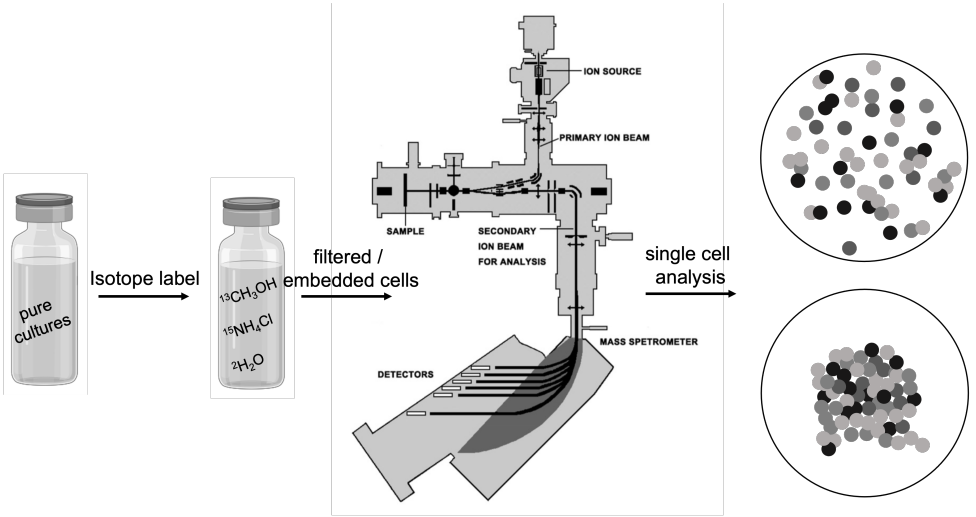

Figure 3.5 Workflow schematic. Only *M. burtonii* aggregates were embedded and analyzed.

Table 3.3
Doubling time based isotope incubation times for each species. **M. barkeri* cells were prepared but not analyzed.

species	temperature [°C]	doubling time [days]	incubation time [h]
psychrotolerant			
Methanococcoides burtonii	4	5.4	36.50
Methanolobus psychrotolerans	4	10.69	72.24
Methanosarcina acetivorans	15	11.36	76.78
mesosphilic			
Methanococcoides burtonii	23	4.44	30.04
Methanosarcina mazei	37	4.11	27.75
Methanosarcina barkeri	37	2.98	20.13*
Methanosarcina acetivorans	37	4.49	30.24
thermotolerant			
Methanosarcina acetivorans	45	5.46	36.90
Methanomethylovorans thermophila	55	0.53	3.57
Methermicoccus shengliensis	55	1.05	7.10

3.2.4 Aggregate embedding

Methanococcoides burtonii was chosen for aggregate analyses, since it is known to form aggregates at 4 °C and 23 °C. *M.burtonii* cultures were incubated with isotope labels as described above. At the time of sampling, crimp vials were opened, and 1 ml of culture was sampled for the embedding procedure, in addition to PFA samples and cell pellets as described above. To 1 ml of sample, 40 µl of 0.1% Toluidine Blue (TB) aqueous solution was added for easier identification of cells. Aggregates were pre-embedded in 2% agar by preparing 1.5 ml Eppendorf tubes with 600 µl of molten agar and adding 70 µl of TB stained culture to the lower part of the agar solution. The agar was then left to solidify at 4 °C for at least 6 h and afterwards cut out of the Eppendorf tube. Due to the TB stain, the part of the agar containing cell aggregates was identifiable, and the agar blocks were cut down to about half of their original sizes. Agar blocks were then embedded in a plastic resin following the Technovit 8100 protocol (Technovit 8100, Kuzler, Wehereim, Germany) with modifications as follows: each agar embedded sample was dehydrated in 1 ml of 99% Ethanol at 4 °C overnight. In the first 20 min of dehydration ethanol was exchanged 4 times at 5 min apart. Afterwards agar blocks were infiltrated in Technovit solution overnight. Following infiltration, 1.5 ml Eppendorf tubes with 600 µl Technovit solution and 20 µl hardener were prepared, vortexed and agar blocks were placed in the tubes and left to solidify at 4 °C overnight. The resins were then cut out of the Eppendorf tubes and the tips further cut down with razorblades to have a small surface area (about 3 mm x 3 mm) for microtome-sliced thin sections. ~3 µm thin sections were then prepared using a microtome (Reichert Jung Ultracut, Vienna, Austria) with glass knives (from Leica glass strips 400 x 25 x 6.44 mm prepared with Leica EM KMR3 knifemaker, Leica, Wetzlar, Germany). Thin sections were placed into 2 µl water droplets on ITO slides (6 sections per slide). Each thin section was mapped for easier aggregate identification under the NanoSIMS: each slice was stained with 1 µl DAPI and mapped using the mosaic picture assembly with the Leica microscope software. Afterwards slides were washed in small petri dishes with miliQ water for 30 min and left to dry. Slides were then prepared for shipment to the Caltech SIMS facility where they were stored until analyses.

As described in the introduction section, the use of DAPI to identify aggregates in thin sections may have a dilution effect on carbon and nitrogen effects (in *M. acetivorans* DAPI affect carbon measurementy by 7.8% $\pm$ 14.5%, and nitrogen measurement by 2.7% $\pm$ 2.1%, (Meyer et al., 2021)).

3.2.5 NanoSIMS analysis settings

Samples were analyzed with a CAMECA NanoSIMS 50L (CAMECA, Gennevilliers, France) located at the Division of Geological and Planetary Sciences at the California Institute of Technology, USA. Before loading, each slide was coated with a gold film, to minimize charging during analysis. Samples from *M. burtonii* at 4 °C and 23 °C were coated with a 50 nm gold film and presputtered for 2.5 min with a 80 pA Cs^+ beam. All remaining samples were coated with a 20 nm gold film and presputtered for 5 min with a 80 pA Cs^+ beam. Random 30 µm x 30 µm areas on each ITO were presputtered according to their gold coating thickness before analyses of 25 µm x 25 µm areas within the presputtered area with a 6 pA primary Cs^+ beam. Six masses were acquired at the same time, as mentioned above (^1H, ^2H, ^{12}C, ^{13}C, $^{12}C^{14}N$ and $^{12}C^{15}N$). One frame for each area was acquired with a count per pixel rate of 10000, resulting in 45 min of analysis for each area. Analytical parameters such as primary beam focus, secondary beam centering, and mass resolution for all ions were verified between each slide. Multiple areas were analyzed to get to several hundreds of cells per condition (one condition = one species at one growth temperature). For embedded cells, mapped areas were identified with the NanoSIMS and 30 x 30 µm areas presputtered with a 80 pA Cs^+ beam for three minutes before analysis with an 8 pA beam. Areas in embedded samples were analyzed in either two or four planes.

3.2.6 NanoSIMS data analysis

NanoSIMS data was analyzed with the MATLAB package look@NanoSIMS (Polerecky et al., 2012, LANS). Raw image files were loaded into the program, plane images autoscaled and checked for noise. For measurements with multiple acquisition planes, planes were aligned using the new, registration based alignment algorithm based on the $^{12}C^{14}N$ plane. For all areas, cells were defined as regions of interest (ROIs) on the $^{12}C^{14}N$ image. Pure masses and mass ratios of $^{12}C^{15}N/^{12}C^{14}N$, $^{13}C/^{12}C$

and $^{2}H/^{1}H$ were then displayed and stored for each ROI. For each round of measurements, ROIs whose ion counts did not reach the measurement-specific threshold were removed from downstream analyses to filter out noise.

Fractional abundances (Equation 3.1) based on isotope ratios R:

$$F = \frac{R}{1+R} \tag{3.1}$$

were used to calculate growth rates based on both carbon and nitrogen for each cell as in Equation 3.2 after Scheller et al. (2016), where t is the incubation time with isotope label in days:

$$\mu = \frac{\ln(1-(\frac{F_{\text{sample}}}{F_{\text{label}}-F_{\text{natural}}})}{t} \tag{3.2}$$

Doubling times (in days) were than calculated from the growth rate μ:

$$d = \frac{\ln(2)}{\mu} \tag{3.3}$$

These estimations can be used as a proxy for carbon and nitrogen based growth. Relative assimilation rates of carbon and nitrogen were calculated based on Stryhanyuk et al. (2018) as in Equation 3.4 below. Stryhanyuk et al. (2018) propose mathematical approaches to enumerate assmiliation rates of single cells from SIP NanoSIMS data, taking into account different sample preparation techniques. The authors propose the use of cell specific masses of atoms to calculate assimilation rates, which is not available here, and thus the relative assimilation rate was calculated instead:

$$K_A = \frac{R_f - R_i}{(R_i+1)\cdot(D_{gs}\cdot(R_f+1)-R_f)} \tag{3.4}$$

where R_f and R_i are final and initial cellular isotope ratios, and D_{gs} is the fraction of heavy over light isotope in the growth medium during incubation.

3.2.7 Statistics

To quantify single cell heterogeneity based on NanoSIMS data, two measures were calculated: the coefficient of variation (CoV, Equation 3.5), also called relative standard deviation (RSD), was used to get insight into how spread out the data is. Previously, this measure was used to assess the levels of heterogeneity with a comparison between batch cultures and chemostat cultures (Zimmermann et al., 2018). Normalizing the standard deviations of assimilation rates with the mean allows for normalization to growth rates. Since growth rates between low and high temperature cultures range from multiple hours to several days, this is an important measure to commensurate calculated assimilation rates and doubling times.

$$CoV = \frac{K_{Astddev}}{K_{Amean}} \tag{3.5}$$

Using the median relative assimilation rate, $\tilde{K}_A$ (calculate based on Equation 3.4) and the total distribution width, DW, the heterogeneity coefficient (HC) was calculated after Calabrese et al. (2019) as in Equation 3.6:

$$HC = \frac{1}{2} \cdot \frac{DW}{\tilde{K}_A} \tag{3.6}$$

Where DW is the difference between maximum and minimum values but can also be given as standard deviation, median absolute deviation, interquantile or interquartile ranges.

To test for statistically significant difference in dispersion coefficients between psychrophile, mesophile, and thermophile temperature groups, the non-parametric Kruskal-Wallis H-test was applied using the critical chi square value at the 5% significance level. Both tests were conducted using the Scientific Python library in Python (Virtanen et al., 2020).

3.3 Results and Discussion - Temperature Resolved Phenotypic Heterogeneity

3.3.1 Growth at different temperatures

Across the tree of life, metabolic rates increase with temperature (Gillooly et al., 2001). At low temperatures, growth is limited by losses of membrane functions

and lower affinity for substrates (Nedwell, 1999) and proteins are more susceptible to denaturation (Privalov, 1990).

At the other end of the temperature scale, organisms are limited by the denaturation of their proteomes (Dill et al., 2011), as well as the melting of their lipids, losses in membrane functions and unfolding of DNA (Lepock et al., 1990).

When comparing different methanogenic species grown with the same growth medium but at different growth temperatures, close to their respective upper or lower limits, cell count based doubling times range from several hours in thermotolerant species to more than ten days in psychrotolerant species (Figure 3.6). When looking at growth rate distributions within individual species, the highest growth temperature does not necessarily correspond to the fastest growth: here *M. acetivorans* was found to have the fastest growth at 37 °C, with slightly slower growth at 45 °C and the slowest growth at its proposed lower temperature limit of 15 °C. Cells here were grown in a methanol containing medium, but similar observations of optimal growth temperatures between 35 °C and 40 °C with a rapid decline in growth above 40 °C and very little growth at 15 °C have been made when the organism is grown on trimethylamine (Sowers et al., 1984). *M. burtonii* shows faster growth at 23 °C than at 4 °C. It has previously been shown that the growth rate declines above 23 °C until the maxium growth temperature of 28 °C is reached (Williams et al., 2017).

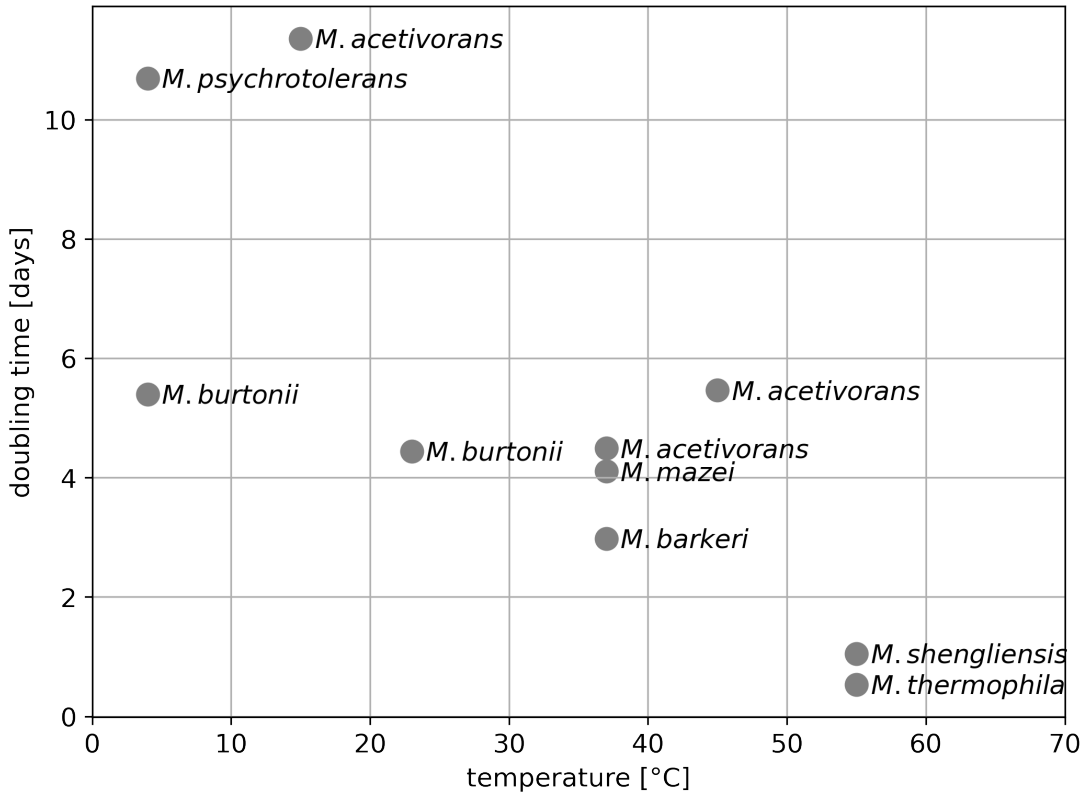

Figure 3.6 doubling times vs. growth temperatures for methylotrophic methanogens grown on methanol. Note that one species (*M. shengliensis*) was grown on a different medium.

.

3.3.2 Single cell carbon and nitrogen incorporation data

For each species at its respective growth temperature, several hundred single cells (Table 3.4) were analyzed using NanoSIMS and ^{1}H, ^{2}H, ^{12}C, ^{13}C, $^{12}C^{14}N$, and $^{12}C^{15}N$ ions were counted. Due to low ^{1}H and ^{2}H ion counts (at most several tens of counts for ^{2}H), only carbon and nitrogen data is presented here. For measurements of *M. acetivorans* at 37 °C, nitrogen isotope ratios were higher than possible (Figure 3.11 with the used labeling strength of 4%, possibly due to insufficient peak separations of $^{11}B^{16}O^{-}$ (mass 26.811) and the $^{12}C^{15}N$ (mass 27.018) ions on the NanoSIMS). Nitrogen measurements for this temperature were thus neglected in downstream analyses. For the remaining species and temperatures, measured ^{13}C methanol and ^{15}N ammonium incorporation data were used as proxies to calculate doubling times for individual cells.

Table 3.4
Mean doubling time estimates

species and growth temperature	cells	count based doubling [days]	C based doubling [days]	N based doubling [days]
psychrotolerant				
M. burtonii 4 °C	375	5.4	7.56	9.67
M. psychrotolerans 4 °C	655	10.69	16.17	16.61
M. acetivorans 15 °C	290	11.36	17.73	19.94
mesosphilic				
M. burtonii 23 °C	436	4.44	6.02	7.70
M. mazei 37 °C	888	4.11	6.20	6.86
M. acetivorans 37 °C	519	4.49	6.36	NA
thermotolerant				
M. acetivorans 45 °C	336	5.46	8.53	8.31
M. thermophila 55 °C	429	0.53	0.75	0.86
M. shengliensis 55 °C	464	1.05	1.61	1.62

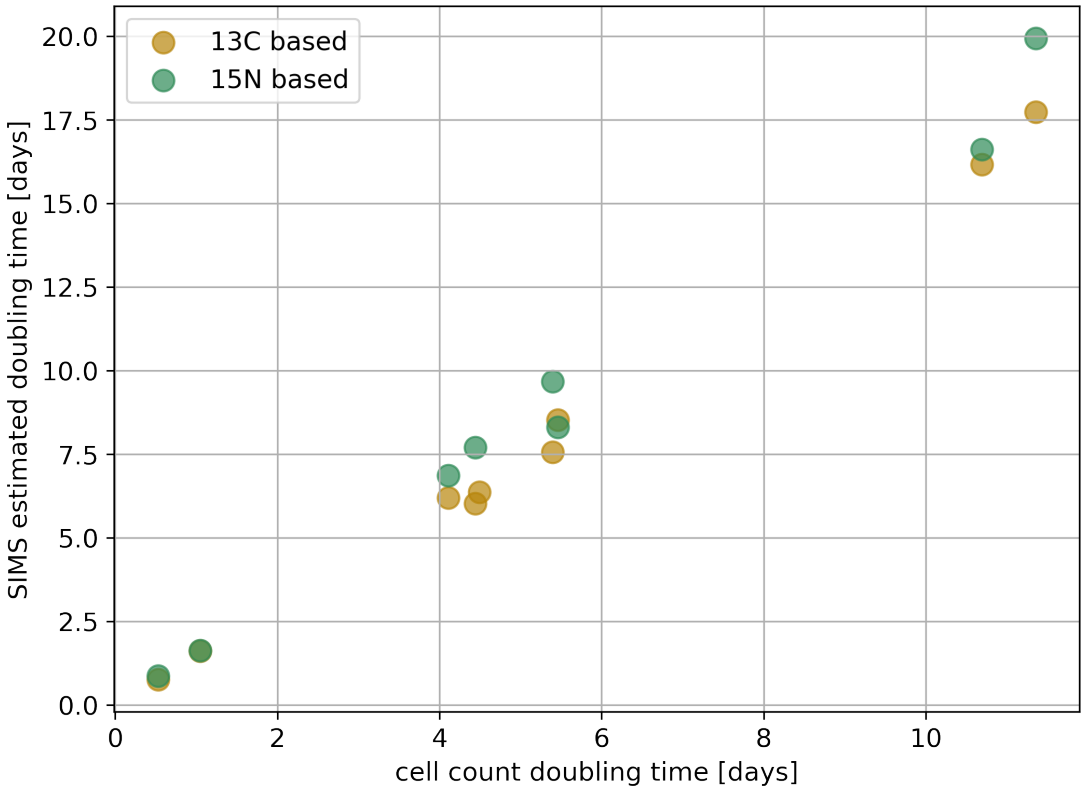

Figure 3.7 SIMS estimated doubling times and cell count doubling times.

.

Mean doubling time estimations are presented in Table 3.4, and in all cases present an offset to cell count doubling time measurements (Figure 3.7), where SIMS doubling times are slower by a factor of 1.51 to 1.8 for nitrogen estimates and 1.36 to 1.56 for carbon estimates (Table 3.4).

In addition to the offset between cell count and isotope data doubling times, an offset between carbon and nitrogen based data was observed: when looking at the distributions of growth rates for each species and condition (Figures 3.8, Figure 3.9, Figure 3.10, and Figure 3.11), in all cases the peak of the carbon distribution is at a faster doubling time than that of the nitrogen distribution. Carbon incorporation variability is higher than that of nitrogen in colder temperatures, and nitrogen incorporation variability is higher than that of carbon in warmer temperatures (Figure 3.12).

The observed carbon-nitrogen offset opens questions about the use of other carbon and nitrogen sources in the medium. In the case of carbon, it has been shown that methylotrophic methanogens in nature produce up to twelve percent of methane from CO_2 (Yin et al., 2019), showing that these organisms grow mixotrophically,

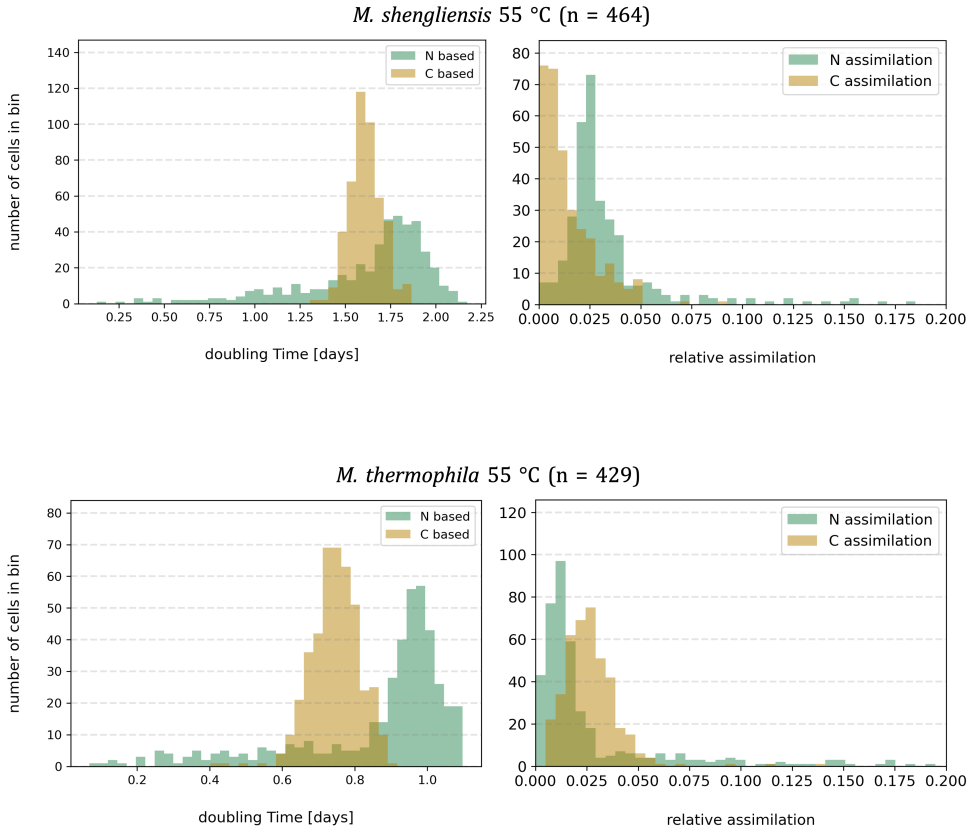

Figure 3.8 SIMS data based doubling time estimates (left) and relative assimilation rates (right) histograms for *M. shengliensis* (top) and *M. thermophila* (bottom), both grown at 55 °C. 19 cells are outside the shown nitrogen assimilation range for *M. shengliensis*, 26 cells are outside the shown nitrogen assimilation range for *M. thermophila*.

.

though they are presumed to be obligate methylotrophs. The authors also confirmed that inorganic carbon was the main carbon source for nucleic acids, further proving DIC as a carbon source for assimilation. Additionally they found that in pure cultures with optimal growth conditions, higher methanogenesis rates decrease the amount of methane produced from CO_2 in obligate methylotrophs, and that without the addition of H_2, up to 3% of methane was produced from CO_2. More methane being formed from CO_2 when the overall kinetics are slow, i.e. at slow growth in lower temperatures, would result in lower incorporation of ^{13}C methanol, however here the opposite is observed: at low temperatures, more ^{13}C from methanol is incorporated into cells than at high temperatures both in the interspecies comparison (Figure 3.12) as well as in the intraspecies *M. acetivorans* comparisons (Figure 3.13). Kenealy & Zeikus (1982) showed that in *M. barkeri* equal amounts of carbon from CO_2 and methanol are

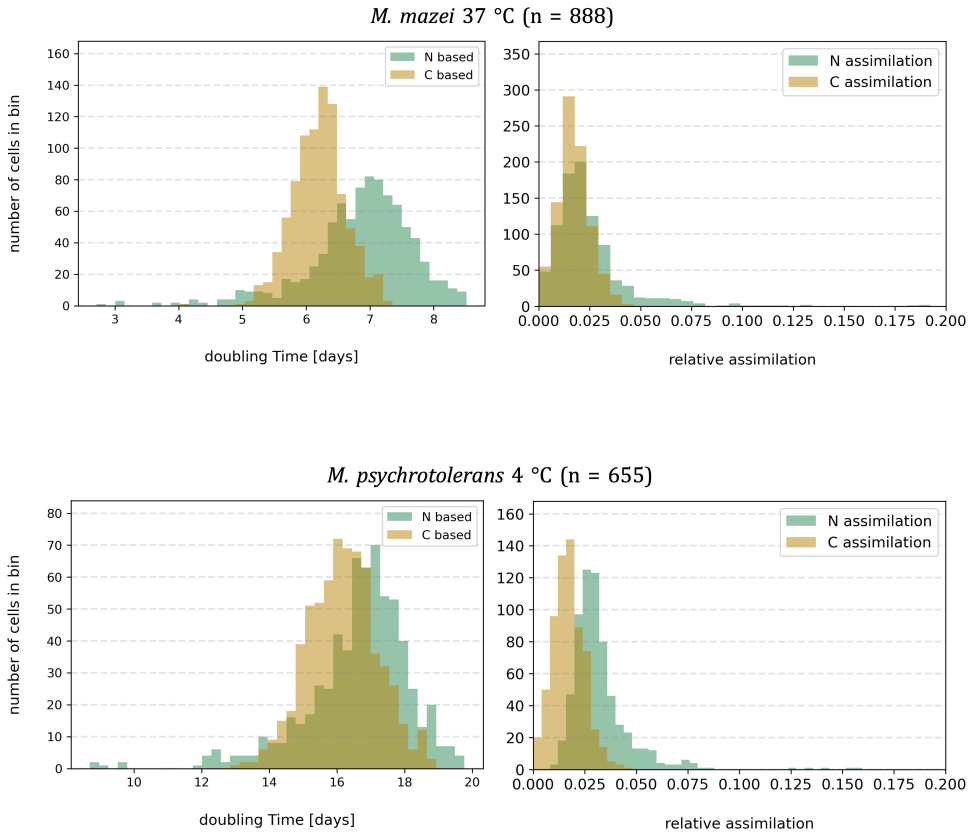

Figure 3.9 SIMS data based doubling time estimates (left) and relative assimilation rates (right) histograms for *M. mazei* (top), grown at 37 °C and *M. psychrotolerans* (bottom), grown at 4 °C. One cell is outside the shown nitrogen assimilation range for *M. mazei*.

.

incorporated into cell components and used for methane production, an even larger amount than was proposed by Yin et al. (2019). Kellermann et al. (2012) also note that in anaerobic methane oxidizers, inorganic carbon is assimilated into lipids, as was shown by ^{13}C methane incubation studies. Though the methyl-coenzyme M reductase step is reverse, the physiologies of ANME and methanogens are similar, and biomass could be made up of more carbon from CO_2 than methanol in methanogens.

For nitrogen, increased incorporation of ^{15}N ammonium is observed at higher temperatures (Figure 3.12). In addition to ammonium, nitrogen sources in the medium are dinitrogen gas and nitrogen in low amounts from yeast extract and decomposing cell material. Some methanogens are known to have nitrogen fixation capabilities. In the species analyzed, the *nifH* nitrogenase gene is found in five out of seven species, not including *M. burtonii* and *M. thermophila*. Nitrogen fixation by methanogens

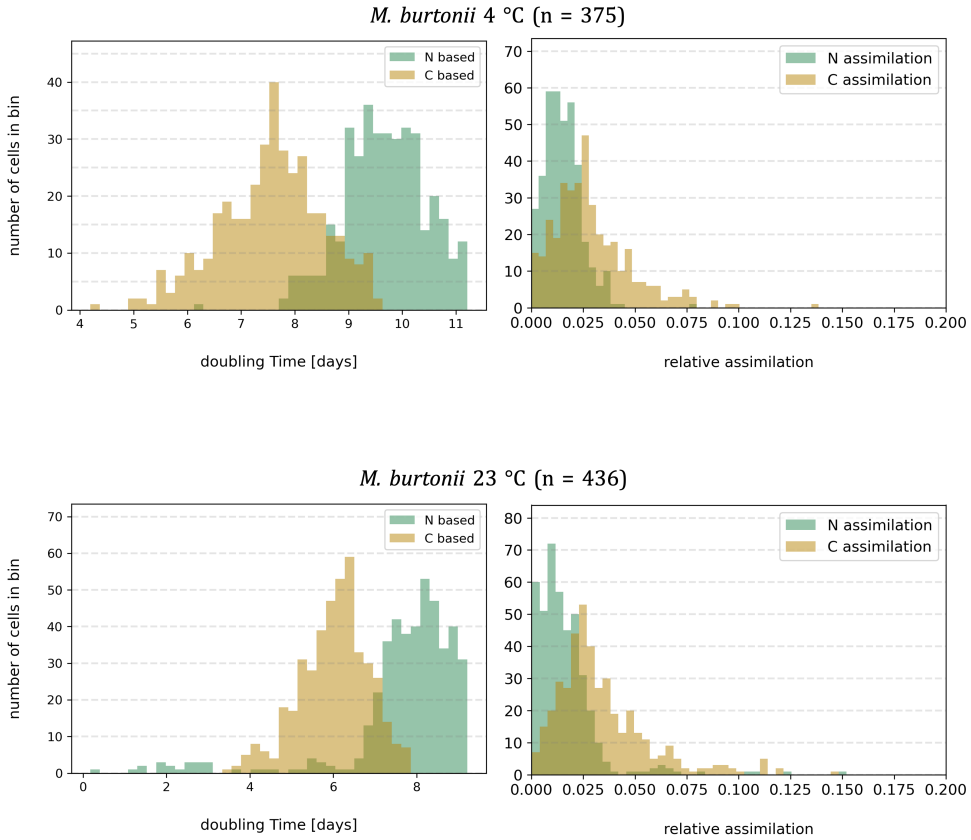

Figure 3.10 SIMS data based doubling time estimates (left) and relative assimilation rates (right) histograms for *M. burtonii*. Top: data for growth at 4 °C, bottom: data for growth at 23 °C. 19 cells are outside the shown nitrogen assimilation range for *M. burtonii* at 23 °C.

.

has been confirmed when N_2 is the only nitrogen source and even in high temperature environments (Mehta & Baross, 2006; Kessler & Leigh, 1999; Nishizawa et al., 2014). An early study has shown that N_2 fixation is more energetically costly than ammonium assimilation in *M. barkeri*, and that molybdenum needs to be supplied in the growth medium as nitrogenases require it as a cofactor (Lobo & Zinder, 1988). Ammonia switch-off describes the shutdown of nitrogen fixation if more favorable nitrogen sources, such as ammonia, are available (Kessler & Leigh, 1999). This leaves open the question if nitrogen fixation can occur even if ammonia is not limited in the growth medium. If this is the case, it could pose an alternative nitrogen source explaining the lower ammonia incorporation rates in cold-grown methanogens containing *nifH*, but not in *M. burtonii*, which does not contain the gene. However, to date no studies have shown that nitrogen and ammonia are simultaneously used by methanogens. Nishizawa et al. (2014) grew a *Methanothermococcus* species with

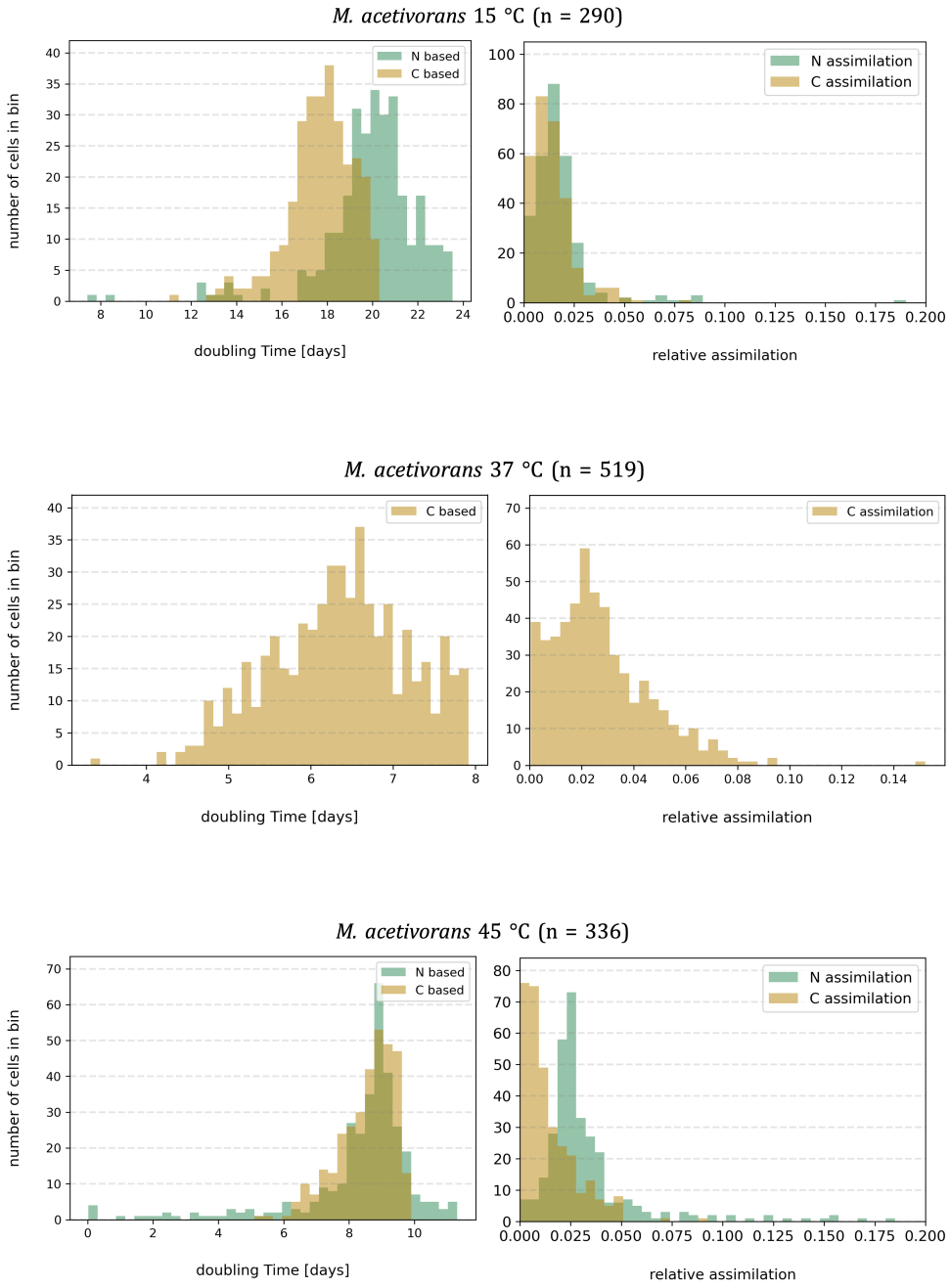

Figure 3.11 SIMS data based doubling time estimates (left) and relative assimilation rates (right) histograms for *M. acetivorans*. Top: data for growth at 15 °C, center: data for growth at 37 °C, bottom: data for growth at 45 °C. Note that nitrogen data from 37 °C analyses are excluded from downstream analyses. One cell is outside the shown nitrogen assimilation range for *M. acetivorans* at 15 °C, 17 cells are outside the shown nitrogen assimilation range for *M. acetivorans* at 45 °C.

.

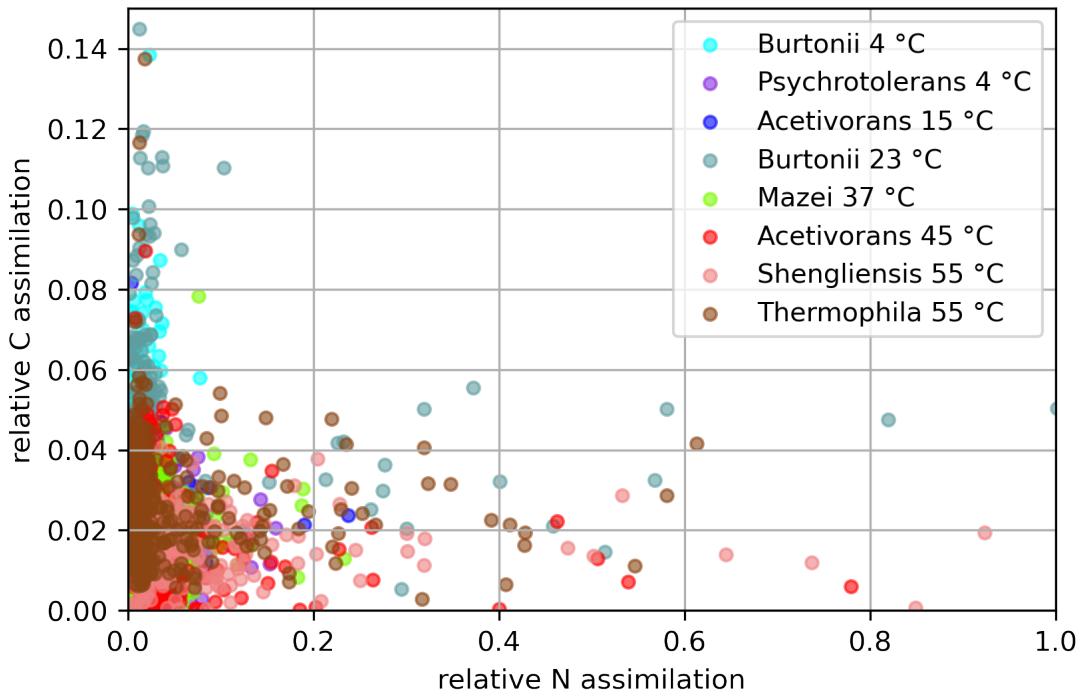

Figure 3.12 Relative carbon and nitrogen assimilation rates for all species.

.

ammonia as the main nitrogen source and in a nitrogen containing atmsophere, stating that both ammonia and dinitrogen can be used as nitrogen sources, however it remains unclear if the organisms do indeed use both.

Observed carbon and nitrogen offsets might partially be explained by the methodologies chosen: different pre-treatments and sample preparation methods lead to variations in isotope signal dilutions observed with the NanoSIMS. It has been shown that only drying cells, without any other fixatives or stains results in reduced isotope signals (94% $\pm$ 1.2% for ^{13}C and 89.5% $\pm$ 3.8% ^{15}N ratios), and that nitrogen signals are inherently lower than carbon signals, which needs to be considered when comparing the two (Musat et al., 2014). Additionally, transmission of either C^- or CN^- ions is reduced if the two are detected simultaneously (Pett-Ridge & Weber, 2012), as is the case here, so this should not affect the ratios of heavy over light isotopes. Care was given when choosing the methodologies to avoid artefacts as much as possible, such as by forgoing fixation. While some influence on the carbon-nitrogen offset through methodologies cannot be completely ruled out, differences in the offset are observed across species and temperatures, though all samples for filtered cells were prepared and measured in the same way. If the offset was entirely methodological, it

would be the same across all analysis conditions, however differences are observed (Figure 3.7), for which the causes need to be identified.

Offsets between carbon and nitrogen uptake rates have previously been described for cyanobacteria in Berthelot et al. (2019). There the offset as observed with NanoSIMS was explained by the metabolic shifts between dark and light growth conditions, as the offset was only observed in surface layer cells. While the light-dark cycle may explain differential carbon and nitrogen uptakes in photoautotrophic organisms, it is not applicable for methanogens, which are not reliant on cyclic external abiotic factors and are grown in constant conditions. A factor that does need to be taken into consideration when hypothesizing about differential uptake rates though, is the cellular composition of different species grown in different (temperature) conditions. Scherer et al. (1983) assessed the Redfield ratios for *M. barkeri, M. bryantii* and *M. arboriphilus* in hydrogenotrophic and methylotrophic growth in batch and semicontinuous cultures. They find that the overall C:H:N:S:P ratio is 37:5:11:1:2 (C:N:P 36.7:10.67:2.3), showing lower carbon and nitrogen requirements per phosphorus than in other organisms (e.g. in plankton the Redfield ratio is C:N:P 106:16:1), as well as differing C:H:N:S:P ratios with different growth substrates. Additionally, they observe interspecies differences in C:N ratios, which are unknown for the organisms in this analysis but might hold clues about the carbon and nitrogen requirements in each growth temperature.

In this experiment, only *M. burtonii* at 23 °C, *M. acetivorans*, and *M. mazei* at 37 °C were grown at their optimal growth temperatures. It is known that while *M. burtonii* shows the fastest growth at 23 °C, this growth temperature causes a heat shock response observable through proteomics (Goodchild et al., 2004). The temperature ranges for optimal growth are narrow for any given organism and heat- or cold- stress responses are observed outside of those (Lange et al., 1997; Goodchild et al., 2004). Additionally, cellular stress may be caused by non-optimal growth substrates (Li et al., 2007). Zimmermann et al. (2018) tested substrate and electron donor limitations effects on phenotypic heterogeneity in green sulfur bacteria (*Chlorobium phaeobacteroides*) using NanoSIMS and found that different limitations induce different heterogeneities: ammonium limitation induces N_2 fixation heterogeneity and electron donor (H_2S) limitation induces N_2 and CO_2 fixation heterogeneity. Since

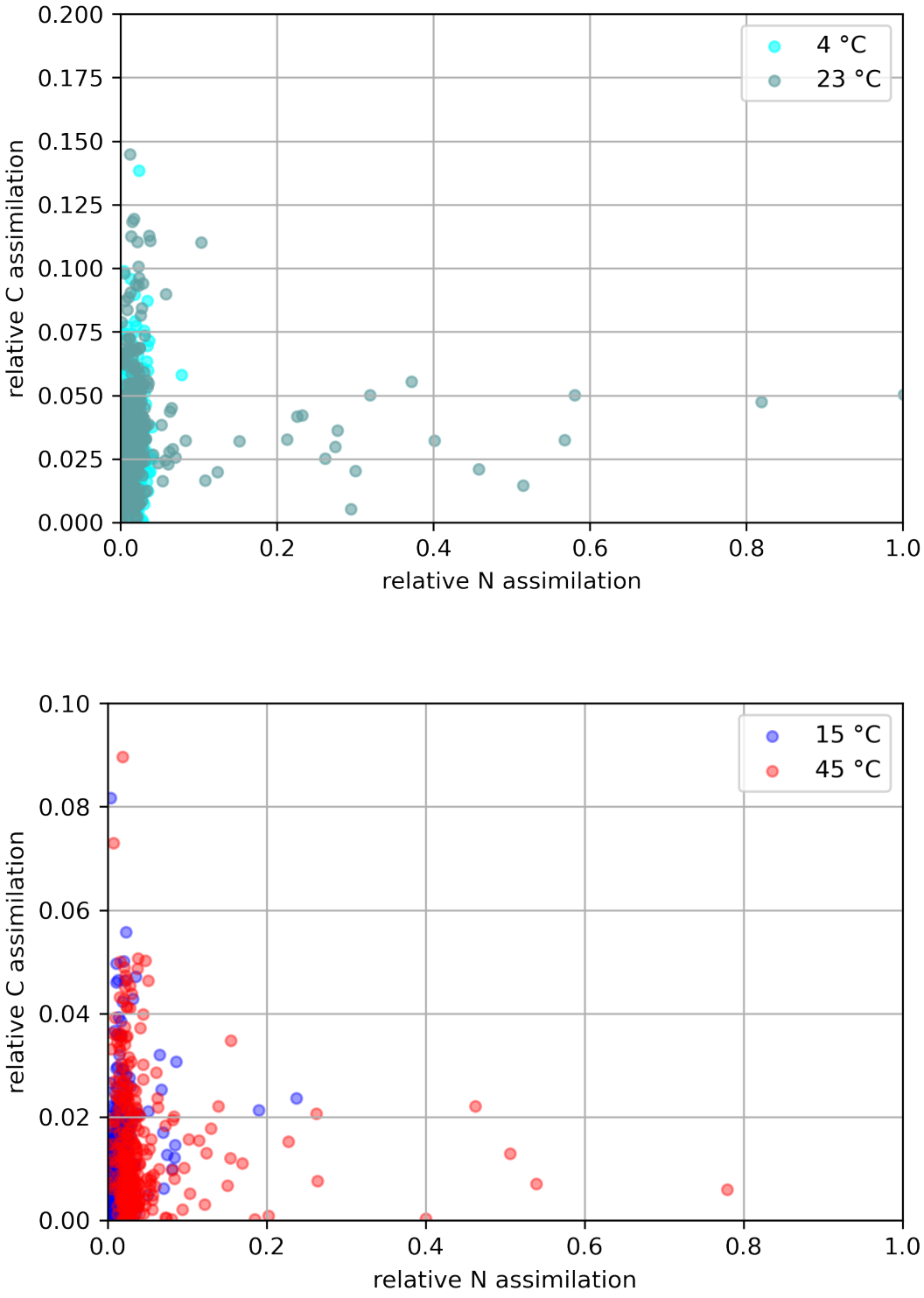

Figure 3.13 Relative carbon and nitrogen assimilation rates for *M. burtonii* grown at 4 °C and 23 °C (top), and *M. acetivorans* grown at 15 °C and 45 °C (bottom).

.

organisms here were only grown on methanol as a substrate, and for some of the species this is proven to not be the optimal, but limiting substrate, part of the observed heterogeneity may not be temperature resolved. Not growing psychrotolerant and thermotolerant organisms at their optimal growth temperatures, but instead colder or warmer, respectively, allows for the comparison of phenotypic heterogeneity in response to cold- and heat- stress, in the cases of *M. psychrotolerans*, *M. acetivorans* and *M. thermophila*.

However, it is important to point out that before SIP incubations, the organisms here were grown at their respective growth temperatures for at least one year. It is possible that the long term adaptation to low or high temperatures may have diminished phenotypic heterogeneity in the cultures. Studies on bacterial growth in rapidly fluctuating nutrient environments have shown that fluctuation induced growth physiologies are different from single shift physiologies: in the single shift physiology cells first grow slower than steady state until they have adapted after several hours, meaning cells adapt in the long term. In fluctuating environments where fluctuations occur over long periods of time, cells repeatedly go through the single shift physiology, however if fluctuations are shorter, growth remains below steady state. This is another way for microbes to deal with fluctuating environments, but at the community level rather than single cell phenotypic heterogeneity (Nguyen et al., 2021). Calabrese et al. (2021) conducted time resolved NanoSIMS SIP to investigate metabolic heterogeneity in *Pseudomonas putida, Pseudomonas stutzeri* and *Thauera aromatica*. The authors found that in substrate limited cultures anabolic heterogeneity is high in the beginning of the incubation, and decreases over time. On the other hand, they observed constant low levels of heterogeneity when enough substrate was supplied to organisms and they were not under any limitation. One possible explanation for their observation is referred to as the metabolic history of cultures: if cultures were previously exposed to low substrate conditions, then initially high levels of heterogeneity are due to a memory effect where cells *remember* limiting conditions and increase their heterogeneity.

This interplay of phenotypic plasticity and phenotypic memory was first described in Jablonka et al. (1995), where the authors attribute medium and long term adaptations of cultures to their phenotypic memory. In future experiments, the expo-

sure of cultures to cold- or heat-shock without prior long term incubations at those temperatures may help our understanding of short-term temperature effects on phenotypic heterogeneity.

3.3.3 Spatial mapping of isotope ratios within aggregates

Planktonic cells of *M. burtonii* were observed to form aggregates after about five days with a 40% inoculation at 4 °C, and after about seven days with a 40% inoculation at 23 °C. Aggregates were embedded in a plastic resin to conserve their structural integrity, sliced into thin sections, and analyzed with the NanoSIMS (Figure 3.14).

A total of 275 cells in two aggregates were analyzed for growth in 4 °C, 318 cells in four aggregates were analyzed for growth in 23 °C. Cells were classified as outer cells if they were directly exposed to the outside of the aggregate. Cells that were not in direct contact with their surroundings and at least 1 µm away from the edge were classified as inner cells. These two groupings of cells were then compared for each temperature condition. This relaxed classification of cells was used to account for low spatial resolution of individual cells inside the aggregates, a possible result of forgoing fixatives.

As with filtered cells, higher carbon than nitrogen based growth rates were observed. In the case of embedded aggregates, this offset can partially be explained by the dilution effect of DAPI stains on carbon and nitrogen isotopes (Meyer et al., 2021).

Relative assimilation rates for carbon and nitrogen overlap in the 4 °C incubation, and nitrogen assimilation rates are lower than carbon assimilation rates in the 23 °C incubation (Figure 3.15).

In the colder grown aggregates, the level of heterogeneity, as indicated by the coefficient of variation, is higher in the outer cells compared to the inner cells. Additionally, the heterogeneity for carbon assimilation is higher than that for nitrogen assimilation, as is also observed in colder grown filtered cells. In warmer grown aggregates, the heterogeneity for nitrogen assimilation is higher than that for carbon assimilation, however only minimal differences in the level of heterogeneity are observed when comparing outer cells to inner cells (Table 3.7).

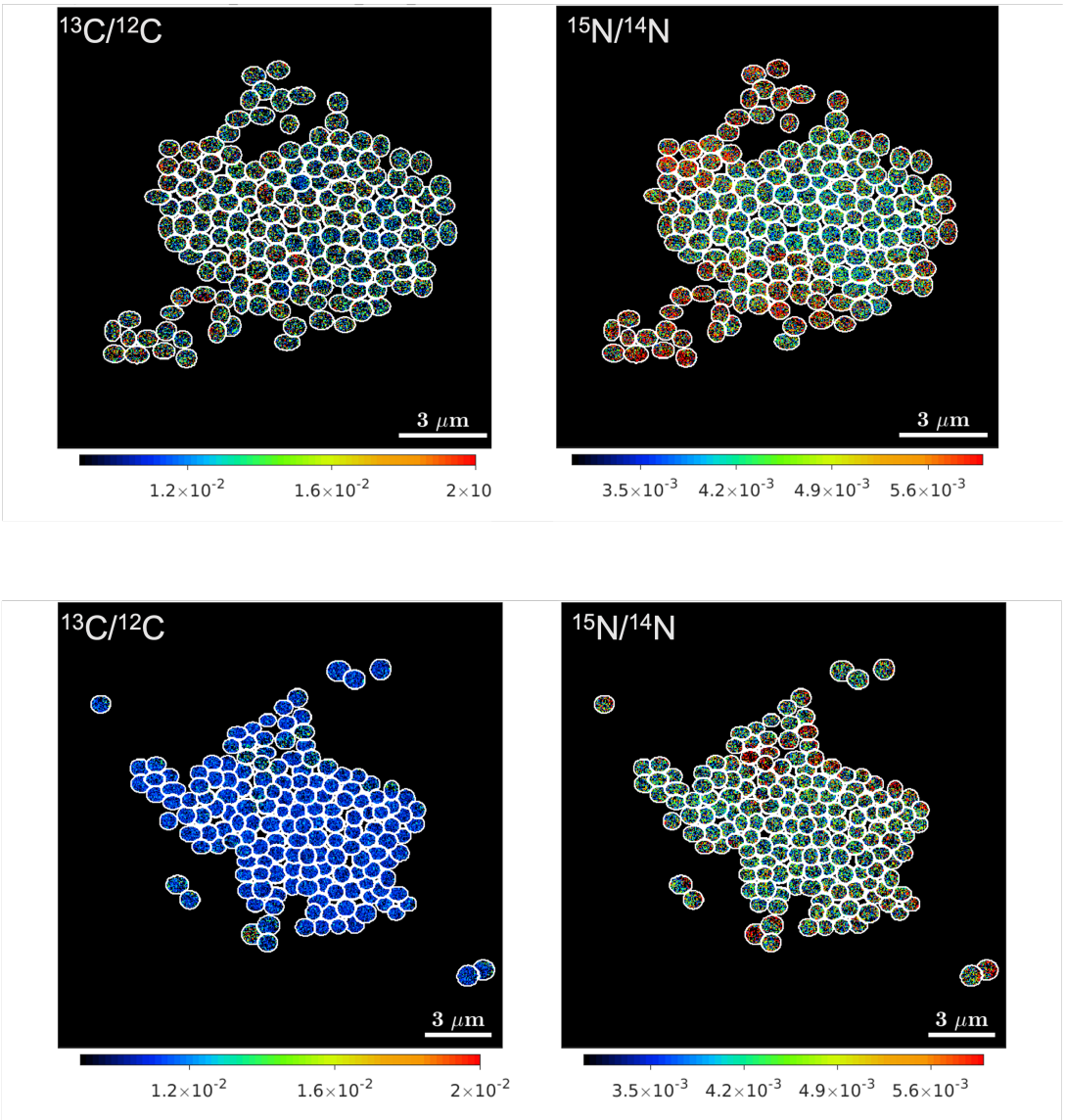

Figure 3.14 Isotope ratio maps of *M. burtonii* cells grown at 4°C (top) and 23 °C (bottom) forming an aggregate. White lines indicate cell outlines, coloring indicates measured nitrogen and carbon ratios according to scale bars.

.

Stressful, nutrient depleted growth conditions lead to collective behaviors, as shown in multicellular clusters of *Vibrio splendidus* by Schwartzman et al. (2022). The authors analyzed cell aggregates about 40 µm in diameter, and distinguished between shell and core phenotypes. They identified a static shell, while the inner, motile core population stores carbon and can readily propagate on substrate once the aggregate is dispersed, allowing for community survival. Here, in the cold-grown aggregates, the outer cells were found to have slightly higher carbon and nitrogen assimilation rates compared to the interior of the aggregates. In the warm-grown aggregates, assimilation rates were marginally higher for interior cells than for outer cells, possibly due to more rapid transport of material from the outer rim of the aggregate to the inside. This behavior could be comparable to the nutrient limited *V. splendidus* aggregates in Schwartzman et al. (2022), where inner cells store substrates in response to limiting conditions, which can be released once growth conditions are more favorable for growth. This would also indicate that *M. burtonii* is indeed more stressed in its heat-shock state at 23 °C compared to the cold adaptation at 4 °C (Goodchild et al., 2004), and could indicate cells storing nutrients in case temperatures rise further and disrupt growth. A similar observation has previously been made for the psychrophile *Clostridium psychrophilum*, incubated between - 15 °C and 10 °C. The organism changes its morphology according to growth temperature and stores carbon once temperatures drop below -10 °C, as if cells are preparing for long term survival (Perfumo et al., 2014).

In a different study Sheik et al. (2016) investigated the spatial heterogeneity in filaments of *Ca. Microthrix parvicella* using NanoSIMS. They showed that the heterogeneity in individual cells allows the filament communities to adapt to fluctuating environments, which are often observed in wastewater treatment plants, where these cells originate. D'Souza (2020) attribute spatial resource heterogeneity to the initial spatial positioning of cells throughout biofilms, when growing on organic matter, and to environmental heterogeneity. Here, *M. burtonii* was grown planktonically in a homogeneous growth medium, yet microbial spatial heterogeneity was observed even without environmental heterogeneity or surface attachment of cells. These previous studies show that spatial heterogeneity, especially of outer and inner cells in aggregates, increases in limiting conditions. Here higher levels of spatial heterogeneity

Table 3.5
Mean doubling time estimates for cells in aggregates

cell group	number of cells	C doubling time [days]	N doubling time [days]
4 °C aggregates			
outer cells	108	8.19	9.39
inner cells	167	8.29	9.75
23 °C aggregates			
outer cells	153	6.68	8.09
inner cells	165	6.67	8.07

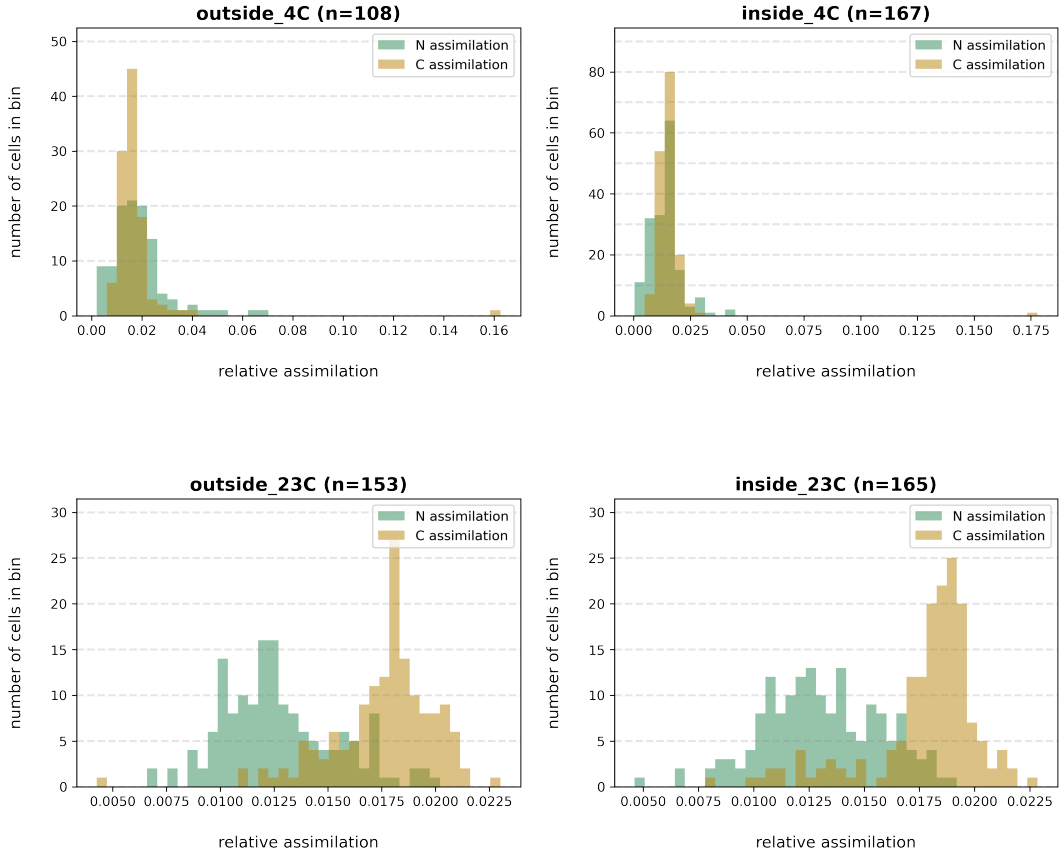

Figure 3.15 assimilation rate distributions for *M. burtonii* aggregates grown at 4 °C (top) and 23 °C (bottom).

.

between outer and inner cells were observed in the 4 °C aggregates, suggesting the lower temperature to be more stressful in terms of population homogeneity.

3.3.4 Quantifying heterogeneity across temperatures

Quantitavely, nitrogen uptake single cell heterogeneity is higher at higher growth temperatures, while carbon uptake single cell heterogeneity is higher at lower

growth temperatures within species, as indicated by the coefficient of variation and heterogeneity coefficients for both carbon and nitrogen for *M. burtonii* and *M. acetivorans* (Figure 3.16 and Figure 3.17, Mean absolute deviations as a third indicator for assimilation rate variations are depicted in Appendix Figure B.2). The heterogeneity coefficient was chosen to quantify heterogeneity, because distributions of assimilation rates and estimated doubling times follow unimodal distributions (Calabrese et al., 2019). Both coefficient of variation and heterogeneity coefficients are statistically different between the psychrotolerant, mesophile and thermotolerant temperature groups, as verified by the Kruskal-Wallis H-test (H values are 0.0889 for carbon coefficients and 5.555 for nitrogen coefficients, for a critical chi square value of 5.981), though here only three temperature groups were compared. The metabolic modes that can explain differential uptake of methanol and ammonia will be explored in Chapter 4.

Within aggregates of *M. burtonii*, coefficients of variation are higher in the colder grown aggregates, and higher in the outer cells therein. Similar to the analyzed filtered cells, within aggregates from the same temperature, carbon variation is higher in colder temperatures and nitrogen variation is higher in warmer temperatures (Table 3.7). In filtered cells of the same species, levels of carbon heterogeneity are more similar between growth temperatures, however levels of nitrogen heterogeneity are higher at the organisms' optimal growth temperature (Table 3.6). Similar to the observations from the cell aggregate data, this raises questions about the relationship of optimal growth temperatures and cellular stress, suggesting that phenotypic heterogeneity is caused by cellular stress rather than non-optimal growth.

In *M. acetivorans* the levels of heterogeneity are the lowest in the organisms' optimal growth temperature, slightly elevated at slow growth in 15 °C and elevated (especially with respect to nitrogen) at 45 °C (Table 3.6). This observation follows that of the interspecies comparisons, where nitrogen heterogeneity increases with temperature. On the other hand, *M. acetivorans* exhibits high levels of heterogeneity at 15 °C as well, suggesting that the driving factor for heterogeneity is indeed stressful or limited growth. Proteomics data elucidating on the effect of temperature on the organism's stress response are not currently available. Assuming that the fastest growth at 37 °C corresponds to the lowest level of cellular stress, and the slowest

Table 3.6
Heterogeneity across species and temperatures, assessed by nitrogen and carbon assimilation rate coefficients of variation (CoV) and heterogeneity coefficients (HC).

species	N CoV	C CoV	N HC	C HC
psychrotolerant				
M. burtonii 4 °C	0.593	0.655	2.705	2.736
M. psychrotolerans 4 °C	0.477	0.439	2.569	1.366
M. acetivorans 15 °C	1.127	0.764	7.775	3.358
mesosphilic				
M. burtonii 23 °C	3.981	0.653	92.234	2.528
M. mazei 37 °C	0.826	0.460	5.719	2.372
M. acetivorans 37 °C	NA	0.692	NA	3.191
thermotolerant				
M. acetivorans 45 °C	7.902	0.925	113.948	4.218
M. thermophila 55 °C	8.317	0.506	483.439	2.707
M. shengliensis 55 °C	5.184	0.411	129.097	1.315

Table 3.7
Heterogeneity within *M. burtonii* aggregates, assessed by nitrogen and carbon assimilation rate coefficients of variation (CoV) and heterogeneity coefficients (HC).

cell group	N CoV	C CoV	N HC	C HC
4 °C aggregates				
outer cells	0.598	0.859	2.004	4.982
inner cells	0.487	0.833	1.506	5.887
23 °C aggregates				
outer cells	0.210	0.140	0.549	0.521
inner cells	0.203	0.142	0.557	0.407

growth at 15 °C corresponds to the highest level of cellular stress, one would assume that the highest levels of heterogeneity would be observed at 15 °C, and not at 45 °C. The observation that heterogeneity is lower at 15 °C than at 45 °C could mean that thermodynamic constraints at low temperature limit growth, and that cells are indeed more stressed at 45 °C, though their growth rate is similar to optimal growth. This could also explain the rapid decline in growth rate above 40 °C for *M. acetivorans* (Sowers et al., 1984).

A less explored possible explanation for phenotypic heterogeneity is polyploidy (Soppa, 2014). Cells have more copies of their genome during fast growth (Malandrin et al., 1999; Hildenbrand et al., 2011), which can be beneficial as it lowers the chances for propagation of mutations, serves a non-genetic purpose as a phos-

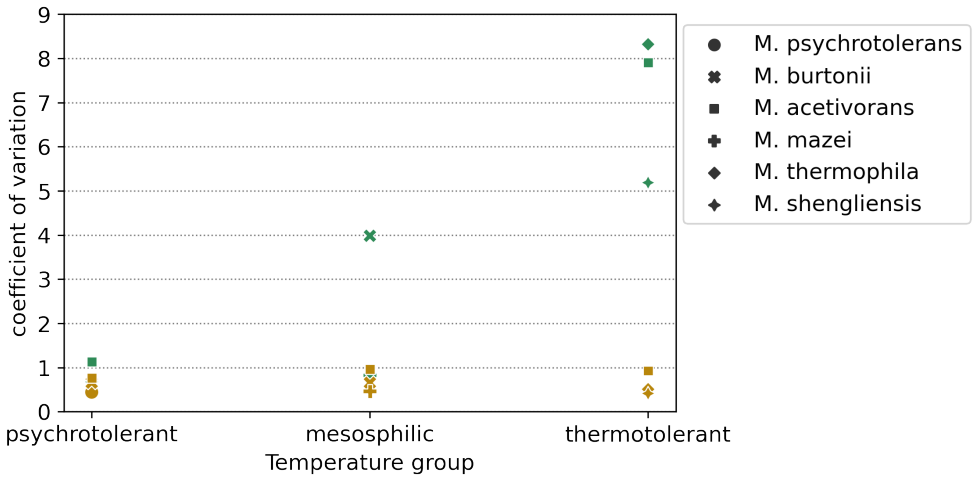

Figure 3.16 Coefficients of variation for nitrogen (green) and carbon (yellow) relative assimilation rates.

.

phorus storage molecule, and increases resistance against DNA double strand breaks, enhancing survival at high temperatures or in desiccation (Soppa, 2014; Van de Peer et al., 2017).

In *Methanocaldococcus jannaschii* polyploidy is assumed to relax control during cell division, enhancing growth (Malandrin et al., 1999), and in *Methanococcus maripaludis* it ensures that copies of essential genes are conserved even if a large part of genome copies undergo mutation (Hildenbrand et al., 2011). In the case of *M. acetivorans*, ploidy changes between fast and slow growth, with 17 genome copies observed at a doubling time of 6 h and only three genome copies at a doubling time of 49 h (Hildenbrand et al., 2011). A lower number of genome copies may lead to higher levels of differential gene expression, which in turn increase phenotypic heterogeneity.

Polyploidy has been confirmed in all methanogens in which it was investigated, except for *Methanothermobacter thermoautotrophicus*, which is diploid and grows in filaments, meaning each cluster of cells contains multiple copies of the genome by default (Majerník et al., 2005; Hildenbrand et al., 2011; Malandrin et al., 1999). The enumeration of genome copy numbers in individual cells in combination with cellular substrate uptake rates could elucidate the effect that polyploidy has on phenotypic heterogeneity.

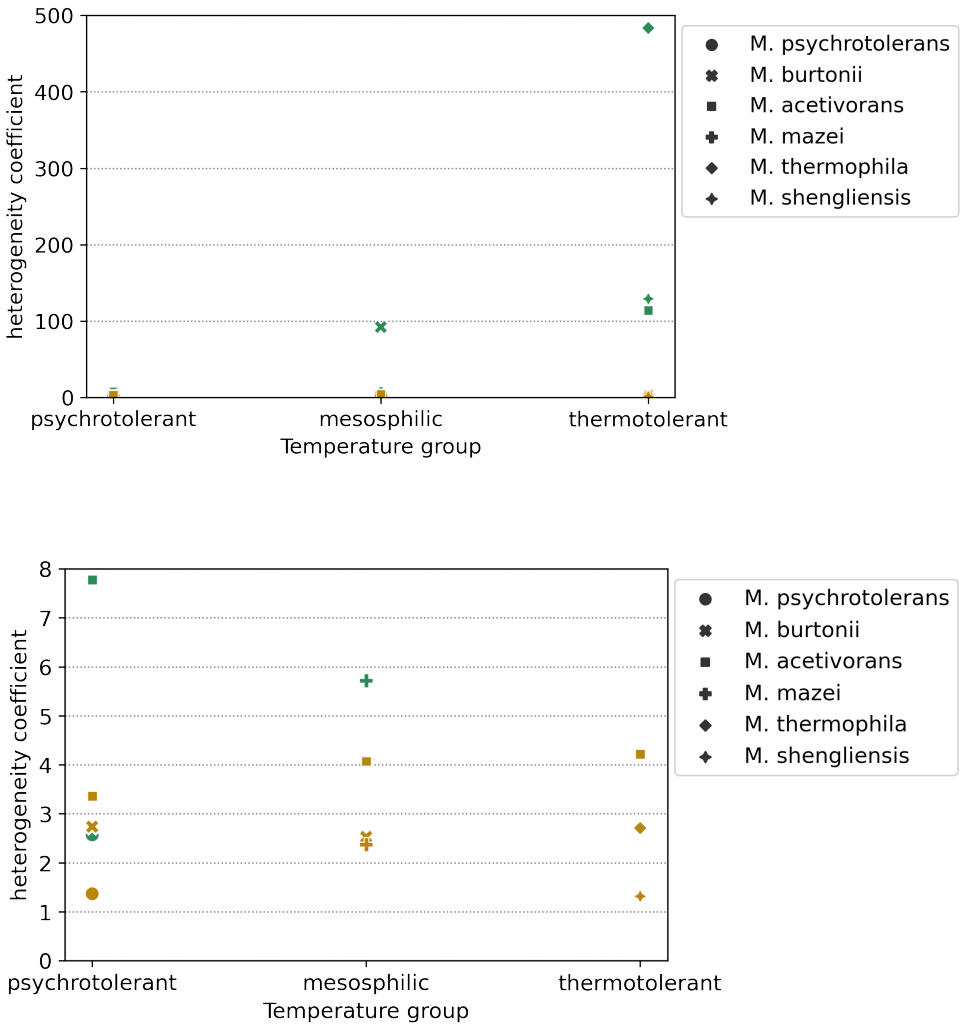

Figure 3.17 Heterogeneity coefficients for carbon (yellow) and nitrogen (green) assimilation rates. All values (top) and subset (bottom) for better visualization.

.

3.3.5 Conclusion

Physiological responses of microorganisms to stressful, limiting, or fluctuating environments are complex. Previous studies focused on the extent of heterogeneity during slow growth in nutrient limiting conditions (Schreiber et al., 2016; Zimmermann et al., 2015, 2018). Here carbon and nitrogen uptake in single cells of methanogens were analyzed to quantify single cell phenotypic heterogeneity in archaea across growth temperatures, and within cell aggregates to characterize spatial differences of this heterogeneity. Though growth at low temperatures is slower, it seems to not always induce cellular stress, at least in terms of heterogeneity. An increase in nitrogen assimilation heterogeneity with temperature is observed across and

within species, regardless of whether higher temperatures correspond to faster growth rates or not.

Overall, there are remaining challenges when evaluating which growth conditions are stressful for methanogens, since the range of growth substrates and temperatures is wide across the physiology. It is known that in *M. burtonii*, fastest growth at higher temperature is associated with heat shock responses, but that organisms are adapted to 4 °C growth (Goodchild et al., 2004). Similarly, *M. acetivorans* expresses chaperones when grown on methanol instead of acetate, and *M. mazei* expresses the same genes when exposed to heat shock (Li et al., 2007). Single cell carbon and nitrogen uptake data support these observations that faster growth does not necessarily indicate optimal growth conditions. More studies comparing various substrates will be needed in the future to define optimal growth conditions for methane producing microorganisms.

When defining *optimal growth conditions*, not only growth rate, but also cellular stress response and population dynamics should be considered, as fastest growth does not always occur at physiologically optimal conditions. Here, long pre-incubation of cultures at their respective temperatures may have diluted heterogeneity as cells adapted to the growth condition. Future experiments may focus on more imminent heat- or cold- shock responses to improve our understanding phenotypic heterogeneity responses to temperature.

The offsets in carbon and nitrogen uptake across cells can not be fully resolved with currently available proteomics or other experimental data. Chapter 4 will give an introduction to a computational approach which can be used to resolve the observed metabolic activities in single cells.

CHAPTER FOUR
Metabolic Models Explain Phenotypic Heterogeneity

4.1 Introduction - Combining Single Cell Uptake Analyses with Metabolic Modeling

4.1.1 Metabolic networks as a link between genotype and phenotype

A metabolic model is a map to an organisms metabolism. Metabolic models are either genome scale models (GEM), which represent an entire genome or core models, which focus on specific subsystems of a metabolism. They use two matrices for the mathematical representation of the reaction network, one associating metabolite to reactions and one associating reactions to enzymes and genes (Wang et al., 2021a).

Metabolic models can be used to predict phenotypes from an organism's genotype and are used for flux predictions, integration of omics and kinetics data, and flux sampling based on given phenotypic states (De Martino et al., 2015). They are also used for the prediction of enzyme functions, pan-reactome analyses, drug targeting in pathogens, metabolic engineering, modelling cellular interactions, and understanding human disease (Gu et al., 2019). Additionally, it has recently been proposed that metabolic models can aid in the isolation of novel organisms by studying their metabolisms prior to designing isolation media (Medina-Chávez & Travisano, 2021).

The process of creating and refining a metabolic model is time consuming and can last from weeks to months depending on the level of manual refinement desired (Thiele & Palsson, 2010). Automated generation methods have been established, however their accuracy even with manual refinement is low (Henry et al., 2010). Working with genome scale models is computationally expensive and can lead to misinterpretations if experimental data is only available for fluxes through the central metabolism (Erdrich et al., 2015). The reduction of genome scale models to core metabolisms or metabolic subsystems of interest have been proposed to overcome computational challenges and get higher resolution data for subsystems of interest (Tamura, 2018; Quek et al., 2014; Zamboni & Sauer, 2009).

Well-refined genome scale metabolic models exist for conventional model organisms such as *E. coli* (Reed & Palsson, 2003; Orth et al., 2010) and yeast (Lu et al., 2019; Sánchez et al., 2017; Österlund et al., 2012). Though in low numbers, metabolic models for archaea do exist, and recent suggestions to use metabolic modeling for the cultivation of more organisms from the domain have led to an increase in the number of established models (Thor et al., 2017; He et al., 2022).

4.1.2 Overview of methanogenic metabolic models

The number of archaeal metabolic models is small compared to their bacterial counterparts, however the majority (nine out of 15) of them are models for methanogenic organisms (Thor et al., 2017). Tsoka et al. (2004) provided the first model for a methanogen, *Methanococcus jannaschii*, based on automated prediction of metabolic pathways. The first large scale, curated model of a methanogen (and archaeon), allowing for genome scale simulations, was established by Feist et al. (2006). The authors curated a model for *Methanosarcina barkeri* and conducted flux balance analyses to investigate the organism's growth on methanol, acetate, H_2/CO_2, and pyruvate. They also defined minimal growth media based on the model conditions for biomass composition. An updated model version was later provided by Gonnerman et al. (2013), refining the existing model with laboratory data and comparing the accuracy of both models for growth on methanol, acetate, and H_2/CO_2.

Following *M. barkeri*, the first automated model for *Methanosarcina acetivorans*, having the largest known genome of methanogens and archaea, included 941 genes, 705 reactions, and 708 metabolites (Satish Kumar et al., 2011). At the same time a manually curated model for *M. acetivorans* was established containing 745 genes, 756 reactions (4% of the reactions are methanogenesis reactions), and 716 metabolites (Benedict et al., 2012). The authors then used this model to study growth and by-products when CO is used as the substrate for methanogenesis. Another updated *M. acetivorans* model is that of Nazem-Bokaee et al. (2016) with 868 genes, 845 reactions, and 718 metabolites. Shortly after, the most current genome scale model for *M. acetivorans* with 807 genes, 829 reactions, and 733 metabolites was established (Peterson et al., 2016). The authors used this model to compare flux differences between growth on acetate or methanol, giving an overview of metabolic subsystems

with significant flux differences between the two growth conditions.

Building on the existing methanogen models, reconstructions for additional species were made: Shoaie et al. (2013) generated metabolic models for three different organisms, including one for *Methanobrevibacter smithii*, to study gut microbiomes. In their analyses, the authors focused on the metabolic contributions of each organism as well as the dynamic interactions between them. Goyal et al. (2014) generated a metabolic model for *Methanococcus maripaludis* to investigate how to maximize CO_2 capture and methane production. Since *M. maripaludis* can fix nitrogen, they also look at flux differences between growth with ammonia and growth with dinitrogen as nitrogen sources, and find that growth is decreased when nitrogen needs to be fixed. Hamilton et al. (2015) established a model for the methanogen *Methanospirillum hungatei*, as well as its syntrophic partner, *Syntrophobacter fumaroxidans*, to study their ATP generation mechanisms as well as the interactions between the two organisms.

Curated models for selected methanogens exist, and can be used as starting points for metabolic reconstructions of different species. Though large parts of the metabolism are shared, attention needs to be given to differences in genes that are present in one, but not the other species. To generate a *methanogen metabolic core model*, it is essential to understand what makes a methanogen a methanogen at the core, and which reactions and pathways are universal to all methanogens. The genome comparison and resulting (extended) core genome from Chapter 2 provided a set of genes that are conserved across the methanogens. Those however also include some genes of unknown functions, and alone cannot be used to construct a metabolic model.

Here a reduced metabolic core model for methylotrophic methanogenesis was established and used to explain the single cell variations observed in *Methanococcoides burtonii* that are described in Chapter 3.

4.1.3 Growth differences of *Methanococcoides burtonii* at 4 °C and 23 °C

Methanococcoides burtonii has been well studied in terms of differential gene expression, structural features, and phenotypes at temperatures ranging from -2 °C to 28 °C: comparing growth at 4 °C and 23 °C, Goodchild et al. (2004) found differential abundances of proteins, with at least a two-fold increase of mcrABG, trimethylamine

methyltransferases, $F_{420}H_2$ dehydrogenase, and Methylcobalamin:CoM methyltransferase at 4 °C, and a decrease of corrinoid proteins at 23 °C. Williams et al. (2010b) studied the organism's cold adaptation using global proteomics at 4 °C and 23 °C . They find a difference in unsaturated (4 °C) and saturated (23 °C) lipids (similar findings reported in Nichols et al. (2004)), a higher abundance of surface layer proteins at 4 °C (many containing domains related to cell adhesion), and small proteins with TRAM domains (which binds tRNA and delivers the RNA-modifying enzymatic domain to their targets) that possibly serve as RNA chaperones instead of cold shock proteins at 4 °C. At 23 °C they report oxidative stress proteins, as well as integral membrane proteins of unknown function.

Campanaro et al. (2011) find that a large number of genes are differentially abundant between 4 °C and 23 °C and that there is a large dynamic range (up to 23.6 fold increase) between the two temperatures. At low temperatures cell surface proteins, tRNA modification, specific RNA binding proteins, ribosomal proteins, and proteins involved in secretion are upregulated. Here ABC transporters for glycine, betaine, and molybdate as well as one system for iron transport are upregulated. At high temperatures proteins involved in methanogenesis and energy generation, the core carbon and nitrogen metabolisms, and specific integral membrane proteins are upregulated. Additionally, Na^+/H^+ antiporters, ABC transporters for phosphate, and a different iron transporter are upregulated.

The most detailed temperature range is reported by Williams et al. (2011), who conducted proteomics studies of *M. burtonii* at -2 °C, 1 °C, 4 °C, 10 °C, 16 °C, 23 °C, and 28 °C. They find that growth and expression patterns at - 2 °C correspond to a cold stress response, between 1 °C and 16 °C organisms are in cold adaptation mode, and at 23 °C and 28 °C organisms show heat stress responses. Though *M. burtonii's* growth rate is lower at 4 °C than at 23 °C, it shows cellular stress responses at its optimal growth temperature when looking at the degree of single cell variation in carbon and nitrogen uptake rates.

Combining metabolic modeling with known expression patterns, this chapter is an introduction to explaining phenotypic heterogeneity through computational approaches. By combining methanol and ammonia uptake rates and sampling through all other metabolic subsystems, flux differences on the whole metabolism level were

identified and compared between temperatures.

4.2 Methodology - Combining Single Cell Uptake Analyses with Metabolic Modeling

4.2.1 Metabolic network construction

Genome scale models exist for *Methanosarcina aceticvorans* and *Methanosarcina barkeri* which are closely related to *Methanococcoides burtonii* and share most core functionalities. Both *M. acetivorans* and *M. burtonii* are marine organisms and use the same energy conservation mechanisms (Li et al., 2006, Rnf instead of Ech). However, *M. burtonii* differs slightly from other *Methanosarcina* species, e.g. it can only use methanol or methylamines for methanogenesis and thus a separate model needed to be generated.

A methylotrophic methanogenesis core model was calculated based on the full GEM for *M. acetivorans*, iST807, established by Peterson et al. (2016), which is provided as a supplementary file. The full model contains 807 genes, 733 intracellular metabolites, and 759 reactions in 30 subsystems and 70 transport and exchange reactions. An algorithm to randomly delete genes while keeping $\geq$ 10% of methane production (reaction name: EX_ch4[e]) and 10% of the biomass objective function (BOF, reaction name: EX_biomass_met[e]), was used (algorithm applied by Associate Professor Takeyuki Tamura, Bioinformatics Center, Institute for Chemical Research, Kyoto University, Software Repository https://github.com/MetNetComp/randomReduction2). Genes were deleted individually, and the number of deleted genes maximized, until no more gene was able to be removed without inhibiting growth or methane production above the set threshold.

As iST807 is based on *M. acetivorans*, but data for *M. burtonii* was used as the input for flux sampling and the growth medium was modified, there were conditions that had to be fulfilled while calculating the core: to ensure methanol is used as a substrate for methylotrophic methanogenesis, methanol uptake was enabled by changing the lower bound of the methanol uptake reaction from 0 to - 1000, where negative flux values denote fluxes into the cell. Because *M. burtonii* is not aceticlastic and lacks relevant genes to metabolize acetate, flux boundaries for reactions

involved in aceticlastic methanogenesis and methanogenesis from CO were set to 0 (these include acetate exchange, acetate kinase, phosphotransacetylase, acetate reversible transport via proton symport). As cysteine was not provided in the medium, its exchange reaction was set to 0, and instead sulfide and ammonia transport reactions were used for sulfur and nitrogen uptake, respectively. All reaction modifications are shown in Table 4.1. Additionally, the ratios of methane production to methanophenazine reductase to Coenzyme F_{420} (F420) dehydrogenase to heterodisulfide reductase (EX_meoh:RNF:F4D:HDR) was chosen to be as close to 4:1:2:3 as possible, which is the theoretical stoichiometry of reactions to generate methane from methanol.

The first minimal solution to match the predicted stoichiometry of the physiology, for which fluxes for the BOF and methane exchange (production) were $\geq$ 10 % of the fluxes from the optimized genome scale iST807, and that fulfilled all of the above conditions, was chosen as the core model. Multiple solutions which achieve these values may exist.

Table 4.1
Changes made to iST807 model before calculating the essential core.

reaction name	reaction number	modification	lower bound [mmol gDW^{-1} h^{-1}]	upper bound [mmol gDW^{-1} h^{-1}]
EX_meoh[e]	791	allow uptake	- 1000	1000
EX_ac[e]	749	no uptake	0	1000
EX_cys-L[e]	768	no uptake as cysteine is not provided in the medium	0	1000
EX_nh4[e]	799	nitrogen source in medium	- 1000	0
EX_h2s	783	sulfur source in medium	- 1000	0
PTAr	624	gene not present in *M. burtonii*	0	0
ACKr	21	gene not present in *M. burtonii*	0	0

4.2.2 Modifications to flux boundaries based on medium composition

The modifications of metabolic models based on media composition has previously been proposed (Marinos et al., 2020). For the generated core model, flux boundaries for exchange reactions were modified based on medium composition and experimental parameters as described in Chapter 3. Flux boundaries were calculated based on the gain in dry weight during isotope incubation times [g], the concentrations of substrates in the growth medium [mmol], incubation volumes [L], and incubation times [days]. First, the gain in cells over the duration of isotope incubations was calculated in Equation 4.1:

$$Z_f = Z_i \cdot 2^{(\mu \cdot t)} \tag{4.1}$$

where Z_i and Z_f are initial and final cell numbers, μ is the growth rate [days], and t is the incubation time [days]. The gain in biomass, gDW, was then calculated using initial and final cell numbers, as well as the estimated weight of one methanogen cell, W [g] (W = $1e-13$ g, gDW = $1.16e-10$ g):

$$gDW = (Z_f - Z_i) \cdot W \tag{4.2}$$

Maximum fluxes were calculated after Equation 4.3, where C is the concentration of substrates [mmol] and V is the incubation volume used [L], assuming the minimum possible gain in dry weight, which corresponds to the maximum fluxes:

$$F = (C \cdot V) \cdot \frac{1}{gDW \cdot t} \tag{4.3}$$

Finally, doubling times per day (DT) were calculated based on the BOF growth output as in Equation 4.4:

$$DT = (\frac{LN(2)}{BOF\,flux}) \cdot 24 \tag{4.4}$$

All analyses with the core model were run using the substrate concentration based uptake fluxes as shown in Table 4.2.

Table 4.2
Calculated flux boundaries for the core metabolic model based on DSMZ141-c medium composition.

DSMZ medium component	concentration [mmol]	reaction name	calculated uptake flux limit [mmol gDW^{-1} h^{-1}]	lower bound [mmol gDW^{-1} h^{-1}]	notes
methanol	123.50	EX_meoh[e]	5838.05	- 1000	calculated flux below default; not adjusted
ammonia	4.67	EX_nh4[e]	220.93	- 220.93	lower bound adjusted
sulfide	2.08	EX_h2s[e]	98.40	- 98.40	lower bound adjusted
potassium	4.56	EX_k[e]	215.58	- 215.58	lower bound adjusted
magnesium	19.67	EX_mg2[e]	930.07	- 930.07	lower bound adjusted
sulfate	13.99	EX_so4[e]	661.66	- 661.66	lower bound adjusted
calcium	0.64	EX_ca2[e]	30.21	- 30.21	lower bound adjusted
phosphate	0.80	EX_pi[e]	37.99	- 37.99	lower bound adjusted

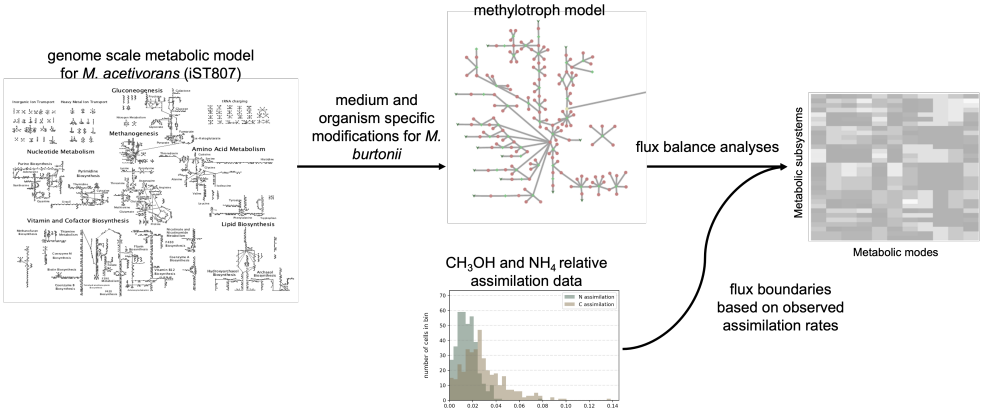

Figure 4.1 Workflow for using metabolic modeling to explain observed single cell phenotypes.

.

4.2.3 Incorporation of NanoSIMS single cell data

Mean single cell carbon and nitrogen relative assimilation rates for each temperature were incorporated into the metabolic model by adjusting methanol and ammonia uptake fluxes, respectively. Mean relative assimilation rates, K_A, were calculated as in Equation 3.4, maximum methanol and ammonia uptake fluxes [mmol gDW^{-1} h^{-1}] as in Equation 4.3, and the incubation time of 0.2816 doubling times taken into consideration to calculate single cell fluxes F_S [mmol gDW^{-1} h^{-1}] as in Equation 4.5:

$$F_S = F \cdot K_A \cdot \frac{1}{0.2816} \tag{4.5}$$

Flux optimizations for biomass were then run using the calculated methanol and ammonia fluxes from Table 4.3.

4.2.4 Model analyses and flux sampling

All metabolic modeling was done using the COBRA Toolbox in MATLAB (Vlassis et al., 2014; Heirendt et al., 2019). Flux balance analyses with the COBRA Toolbox were done using the gurobi solver (Gurobi Optimization, LLC, 2022). An overview of the combination of single cell data and metabolic modeling approaches can be seen in Figure 4.1.

4.3 Results and Discussion - Combining Single Cell Uptake Analyses with Metabolic Modeling

4.3.1 Core metabolic model

A core model was created based on the genome scale metabolic model iST807 of *M. acetivorans* and is provided as supplementary file. The number of reactions was reduced from 759 (iST807) to 446 (core model) and the number of genes from 807 (iST807) to 339 (core model). The biomass exchange flux (growth) decreased from 8.52 mmol gDW^{-1} h^{-1} in the optimized full model for iST807 to 2.79 mmol gDW^{-1} h^{-1} in the core model, methane production increased from 82.86 mmol gDW^{-1} h^{-1} in iST807 to 669.88 mmol gDW^{-1} h^{-1} in the optimized core model.

Acetate has been shown to be synthesized from CO_2 or CH_3OH or both in the physiologically similar *M. barkeri*, and thus transport out of the cell was permitted, but uptake and its use for methanogenesis was not (Kenealy & Zeikus, 1982). PTAr and ACKr were excluded as they are only essential when acetate is used as the substrate for methane production, and AceP was allowed to convert intracellular acetate to extracellular acetate, as this gene is present in *M. burtonii* and PTAr and ACKr are not (Rohlin & Gunsalus, 2010). The core model fulfills all of the desired modifications from the GEM iST807:

- methanol is used as the substrate for methanogenesis;
- acetate uptake is not allowed, but acetate release is;
- L-cysteine uptake is prohibited, as it was not supplied in the growth medium;
- ammonia and sulfate are used as the nitrogen and sulfur sources;
- acetate kinase and phosphotransacetylase are excluded, as these enzymes are not present in *M. burtonii*;
- the flux ratio of methanol uptake to methanophenazine reductase to $F_4$20 dehydrogenase to heterodisulfide reductase in the flux solution optimizing for biomass is -1000:153:516:669, fulfilling 4:0.6:2:3 (closest to estimated 4:1:2:3 ratio);

- the biomass output in the core model was 32.75%, methane production 808.45% from the original GEM.

In the core model flux solution where biomass output is optimized, the nucleotide metabolism metabolic subsystem has the highest production flux (10075.77 mmol gDW^{-1} h^{-1}), followed by methanogenesis (6022.93 mmol gDW^{-1} h^{-1}), transport (2681.18 mmol gDW^{-1} h^{-1}), exchange (2510.56 mmol gDW^{-1} h^{-1}), and the central metabolism (2065.23 mmol gDW^{-1} h^{-1}). H4MPT, MFR, CoM, CoA, and CoB syntheses have the lowest fluxes (0.39, 0.19, 0.13, 0.047, and 0.0088 mmol gDW^{-1} h^{-1}, respectively).

Compared to the GEM iST807, the core has about three times higher absolute fluxes through the methanogenesis subsystem, and around 30% higher fluxes for vitamin and cofactor biosynthesis. In the GEM the central metabolism has three times higher fluxes than in the core (Figure 4.2). The increase in methanogenesis fluxes in the core stems from the default setting of iST807 to use acetate, not methanol, as a substrate for methanogenesis, the impacts of which on the entire metabolism have been discussed by Peterson et al. (2016).

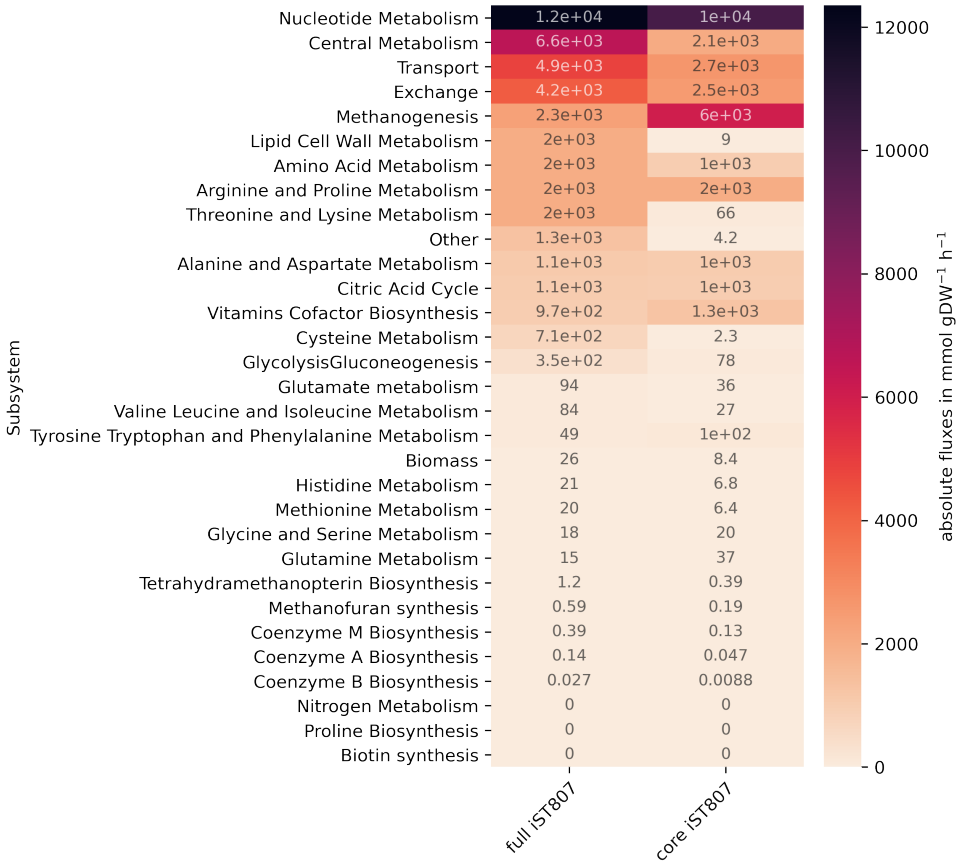

Figure 4.2 Comparison of absolute fluxes through all metabolic subsystems between the GEM iST807 and core model.

.

4.3.2 Flux optimizations for growth, methanol uptake, ammonia uptake, and methane production

To get an insight into the highest theoretically possible fluxes throughout the core model, flux solutions were calculated for maximizations of biomass output, methanol uptake, ammonia uptake, and methane production. Maximization of methanol uptake and methane production both resulted in no biomass production, and fluxes through the vitamin cofactor biosynthesis subsystem were higher than in the other two conditions, where biomass was produced. These simulations without cellular growth but methanogenesis fluxes remaining high, also show higher ATP synthase fluxes (598 and 625 mmol gDW^{-1} h^{-1} for methanol uptake and methane production optimizations compared to 588 mmol gDW^{-1} h^{-1} in both biomass and ammonia uptake maximizations). Fluxes through arginine and proline metabolism and lipid cell wall metabolisms were lower in the biomass optimization solution than in all other so-

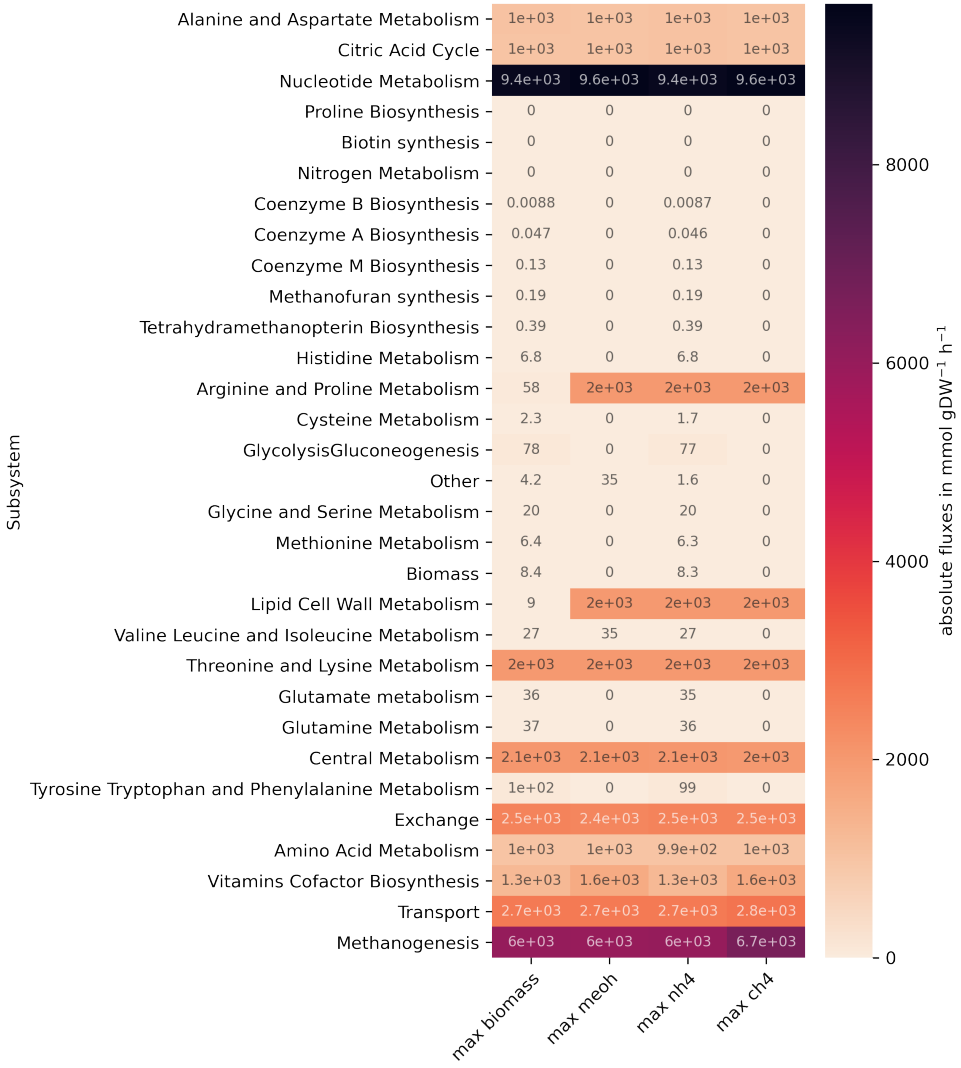

Figure 4.3 Heatmap of total fluxes through all subsystems when simulating maximum growth, maximum methanol uptake, maximum ammonia uptake, and maximum methane production.

.

lutions, even though the maximization of ammonia uptake resulted in similar growth as the biomass optimization (Figure 4.3). Fluxes through all reactions for each optimization run are provided as supplementary material.

4.3.3 Subsystem flux differences for SIMS data

The metabolic modes responsible for the single cell phenotypes observed in Chapter 3 were assessed by optimizing biomass output with flux constraints on methanol and ammonia uptake reactions, calculated from the relative assimilation rates. Five metabolic modes for characterization were chosen for each temperature

condition: one corresponding to mean carbon and nitrogen assimilation, one each for minimum and maximum carbon assimilation with the corresponding nitrogen assimilation value, and one each for minimum and maximum nitrogen assimilation with the corresponding carbon assimilation value. Calculated flux bounds can be found in Table 4.3. To result in biomass production, methanol uptake rates for the minimum carbon incorporation mode for both temperatures had to be adjusted: at 4 °C the methanol flux could not be higher than -660 mmol gDW^{-1} h^{-1}, and at 23 °C the methanol flux could not be higher than -57.7 mmol gDW^{-1} h^{-1} (details on adjustments made can be found in Supplementary Table 1 for this Chapter). This discrepancy between measured uptake rates and feasible model inputs could indicate that when cells are limited by methanol, even with high ammonia availability, they enter a catabolic state that can only be switched back to anabolism once enough methanol becomes available, as broken down cellular components were not measured and can not be assessed through FBA. The computed growth rates in Table 4.3 however show that cells are limited by nitrogen rather than by carbon when it comes to biomass production: in both simulated modes the growth is higher for maximum nitrogen assimilation, not for the maximum carbon assimilation.

It has previously been suggested to link substrate limitations to microbial growth through metabolic modeling, and it has been confirmed that in substrate limiting conditions, rate limiting enzymes control growth (Jin et al., 2022). In the case of temperature, rate limiting enzymes or the overall thermodynamics of reactions could limit growth. To understand the effects of thermodynamics and reaction kinetics, experimental values for melting temperature, heat capacity change, and optimal temperature for each enzyme are needed (Li et al., 2021), data which is not available here. Instead, individual carbon and nitrogen uptake phenotypes from the different growth temperatures were used as flux solutions to solve for. Using the calculated methanol and nitrogen fluxes for the 4 °C and 23 °C mean growth phenotypes (Table 4.3), the resulting calculated doubling times were 16.84 days for 4 °C for and 8.16 days for 23 °C, compared to cell count doubling times of 5.4 days and 4.44 days, respectively.

When looking at the absolute flux distributions through different metabolic subsystems between the temperatures, the fluxes corresponding to data from the mean cell phenotype at 23 °C are similar to those in carbon limited cells (for both temper-

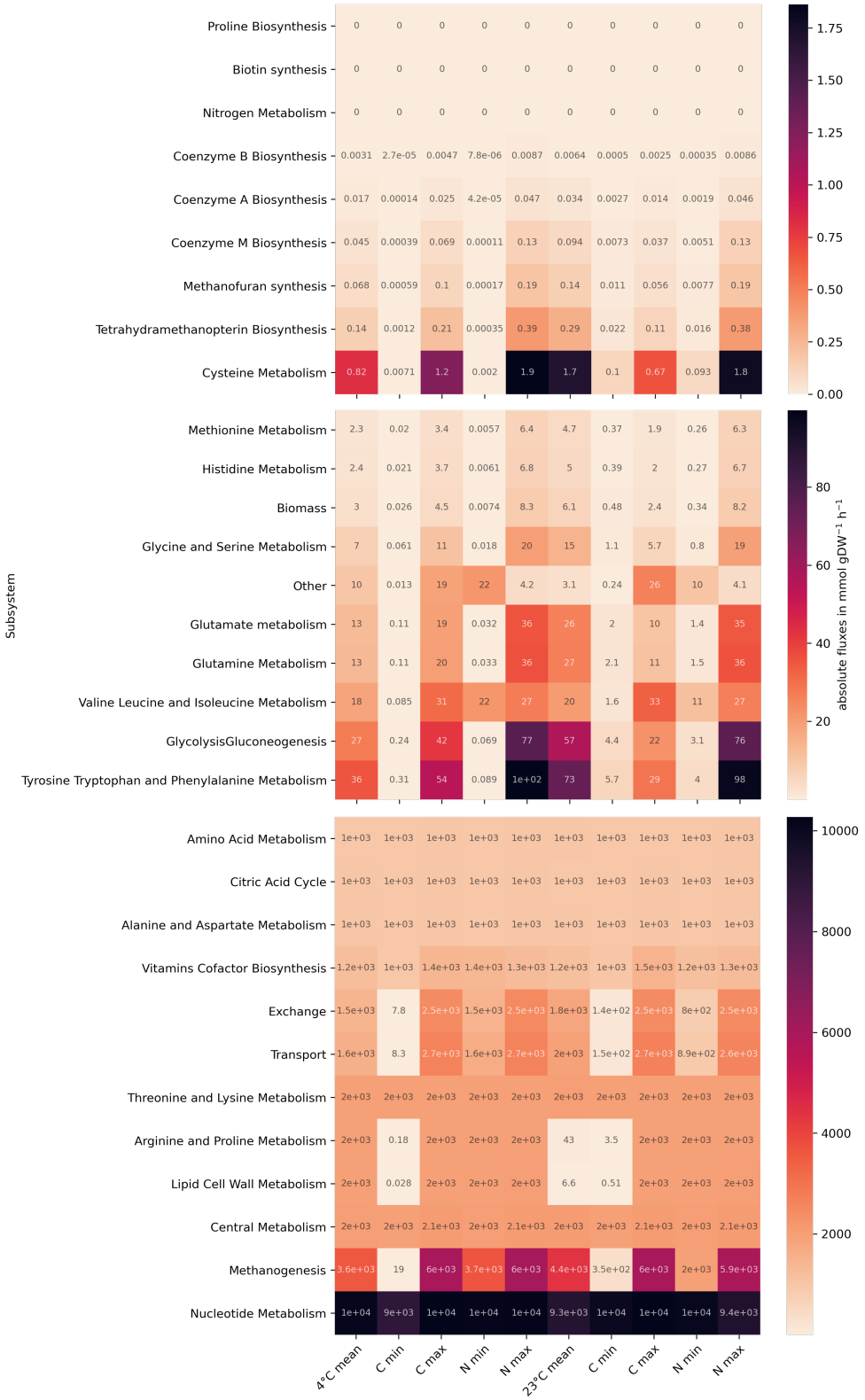

Figure 4.4 Heatmaps of absolute fluxes through all subsystems when solving for SIMS resolved methanol and ammonia uptake rates. Grouped by flux magnitudes from small fluxes (top) to large fluxes (bottom).

.

atures) for the lipid cell wall metabolism and similar to those nitrogen maximizing cells (for both temperatures) for many amino acid metabolisms, while maintaining high methanogenesis fluxes. Subsystems for nucleotide metabolism, cell wall lipid metabolism, and arginine and proline metabolisms show lower overall fluxes in these three growth simulations. However, in the 23 °C mean phenotype setting, methanogenesis remains high, suggesting that carbon is mainly used for methanogenesis instead of biomass incorporation. Additionally, exchange and transport subsystems as well as amino acid metabolisms other than arginine and proline, and H4MPT, MFR, CoA, CoB, and CoM syntheses are higher than in the 4 °C mean cell (Figure 4.4, net fluxes for all simulations can be found in Appendix 5.2). A study on *Arabidopsis thaliana*, where growth under different conditions (including changes in temperature) was simulated, showed that higher temperatures increased fluxes through the TCA cycle and decreased those through phosphoenylpyruvate carboxylase and those under hyperosmotic stress (Williams et al., 2010a). Linking their results with ^{13}C stable isotope studies, the authors found a 3-fold reduction in carbon use efficiency at high temperature. They also suggested the use of constrained based modeling to verify the changes in the central carbon fluxes in stressful conditions and found significant differences in biomass output, glucose consumption, and biomass and protein content at high temperatures. Though these results suggest a decrease in metabolic efficiency in plants at higher temperatures, for the organisms studied here, the increase in methanogenesis fluxes at 23 °C growth simulations is contrary to findings by Goodchild et al. (2004), who found a two-fold increase at 4 °C compared to 23 °C through a proteomics approach. However, later Campanaro et al. (2011) found that methanogenesis genes are upregulated at 23 °C when compared to 4 °C, which if gene regulation is correlated with activity could be verified by flux distributions generated here.

4.3.3.1 Linking metabolic activities to biomass production

Though methanogenesis rates are overall higher at 23 °C, the ratio of methane to biomass production is higher at the 4 °C than at 23 °C phenotype simulation (401 and 240, respectively), suggesting that while growth is slow, methanol reduction to methane is efficient. Interestingly, the opposite holds for cells from both temperatures with the highest methanol incorporation: here the methane to biomass production ra-

tio at 4 °C is about half of that at 23 °C (442 and 822, respectively). The highest ratio of methane to biomass production appears in the simulation for the 4 °C phenotype with the least nitrogen uptake: here 404.52 mmol gDW^{-1} h^{-1} of methane were produced but biomass production was only 0.00247 mmol gDW^{-1} h^{-1}. This indicates that while growth is limited by nitrogen, methane production is not, and even if cells do not grow and multiply, they may be able to metabolize methanol to produce both energy and methane.

Ratios of absolute fluxes through individual subsystems over the biomass (Figure 4.5) and methanogenesis (Figure 4.6) fluxes were calculated. There are no differences in coenzyme syntheses, methionine, histidine, glycine, serine, glutamate, glutamine, tyrosine, tryptophan, and phenylalanine metabolisms, or glycolysis and gluconeogenesis fluxes per biomass unit. Due to its very low biomass output, flux ratios for the minimal nitrogen phenotypes at 4 °C are always high for all other subsystems, and similarly increased for both temperatures' minimum carbon phenotypes as well as the minimum nitrogen cell phenotype at 23 °C. Additionally, for carbon limited phenotypes as well as the 23 °C mean cell phenotype, lipid cell wall metabolism flux ratios over biomass are small, suggesting that carbon is diverted from these subsystems and used elsewhere, potentially for growth. Similarly, in both carbon limited phenotypes, as well as the nitrogen limited phenotypes flux ratios of the central metabolism over biomass are higher than for other phenotypes, suggesting a shift from cellular growth to maintenance. In the 4 °C mean phenotype the metabolism/biomass ratio is two times higher than in the 23 °C. An increase in subsystem over biomass ratios, suggesting higher utilization and potentially upregulation of the corresponding genes, was identified for the methanogenesis subsystem in the 4 °C mean and both maximum carbon phenotypes, but interestingly not for the 23 °C mean phenotype. This suggests that at 23 °C phenotypes are not optimizing for methane production, though the growth rate is relatively high. Transport and exchange flux ratios are the highest in the 23 °C nitrogen minimum phenotype, and lowest in the carbon minimum, nitrogen maximum, and mean 23 °C phenotype.

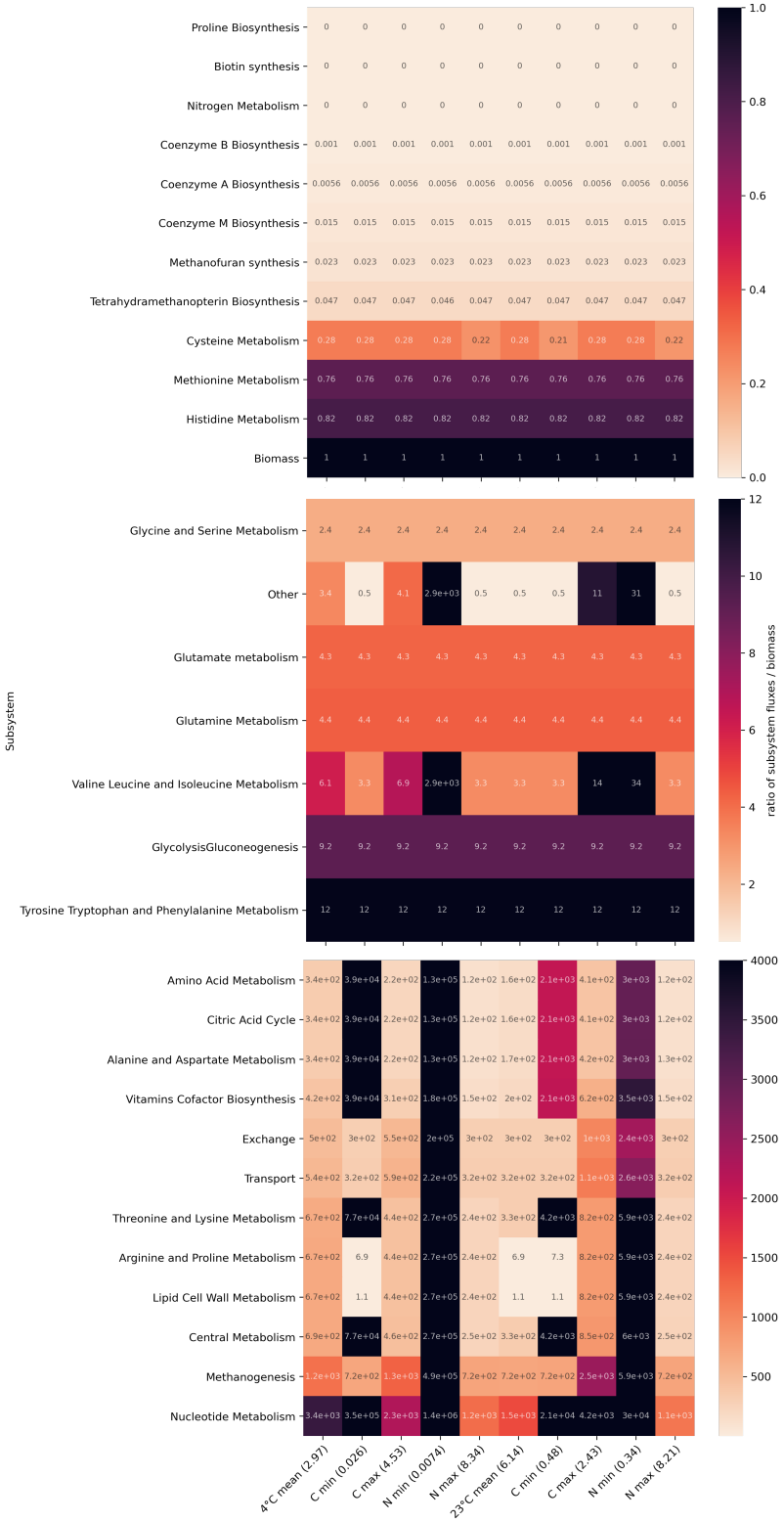

Figure 4.5 Heatmaps of subsystem absolute fluxes over the biomass flux through all subsystems. Grouped from small ratios (top) to large ratios (bottom). Numbers at labels indicate biomass fluxes. Phenotypes are based on mean carbon and nitrogen uptakes across all cells, minimum and maximum carbon assimilation rates with corresponding nitrogen values, and minimum and maximum nitrogen assimilation rates with corresponding carbon values for individual cells.

Figure 4.6 Heatmaps of subsystem absolute fluxes over methanogenesis fluxes through all subsystems. Grouped from small ratios (top) to large ratios (bottom). Numbers at labels indicate methanogenesis fluxes. Phenotypes are based on mean carbon and nitrogen uptakes across all cells, minimum and maximum carbon assimilation rates with corresponding nitrogen values, and minimum and maximum nitrogen assimilation rates with corresponding carbon values for individual cells.

4.3.3.2 Linking metabolic activities to methanogenesis

Subsystem over methanogenesis flux ratios are generally lower in both nitrogen minimum and the 23 °C maximum carbon phenotype, and the highest in the 4 °C minimum carbon phenotype. The mean temperature phenotypes differ mainly in the amino acid as well as CoM, CoA, CoB, MFR, and H4MPT over methanogenesis flux ratios, with higher ratios at 23 °C, and higher lipid cell wall metabolism over methanogenesis flux ratios at 4 °C, again suggesting that at 23 °C carbon is shifted towards methanogenesis rather than cell growth.

Another point that was to be verified through metabolic modeling based on the data in Chapter 3 was the use of CO_2 for biomass when growth and methanogenesis are slow, as has been shown by Yin et al. (2019). In an extensive early study of *M. barkeri* with radioisotopes of CO_2 and CH_3OH, Kenealy & Zeikus (1982) showed that when grown on H_2, CO_2, and CH_3OH, equal amounts of carbon dioxide and methanol are incorporated into cellular carbon (lipids, proteins, and nucleic acids). The authors also identified the fate of labeled carbon: in the case of methanol, half of the label was incorporated into the C-3 atom of alanine, and a quarter each into the C-1 and C-2 atoms. In the case of carbon dioxide, half of the label was incorporated into the C-1, 30% into the C-2, and 15 % into the C-3 atom of alanine.

4.3.3.3 Carbon substrates for methanogenesis

Here, the utilization of carbon dioxide for methanogenesis was verified when methanol was minimized, using formylmethanofuran dehydrogenase (Fmd, reaction ID: FMFD), methanol:coenzyme M methyltransferase (Mta, reaction ID: MCMMT), and methyl-H4SPT:coenzyme M methyltransferase (Mtr, reaction ID: MTSPCMMT) fluxes as proxies. To account for the differences in flux directionalities (uptake fluxes with negative signs and production fluxes with positive signs), absolute values were compared. Directionalities of relevant reactions are as seen in Figure 4.7. Fmd catalyzes the first step in methanogenesis from CO_2, and Mta catalyzes the first step in methanogenesis from CH_3OH. Mtr is the first reaction of methyl group oxidation to CO_2 for methylotrophs (Figure 4.7). Comparing these fluxes and the flux ratios with biomass production and methanol uptake reveals the simulated fate of methanol as

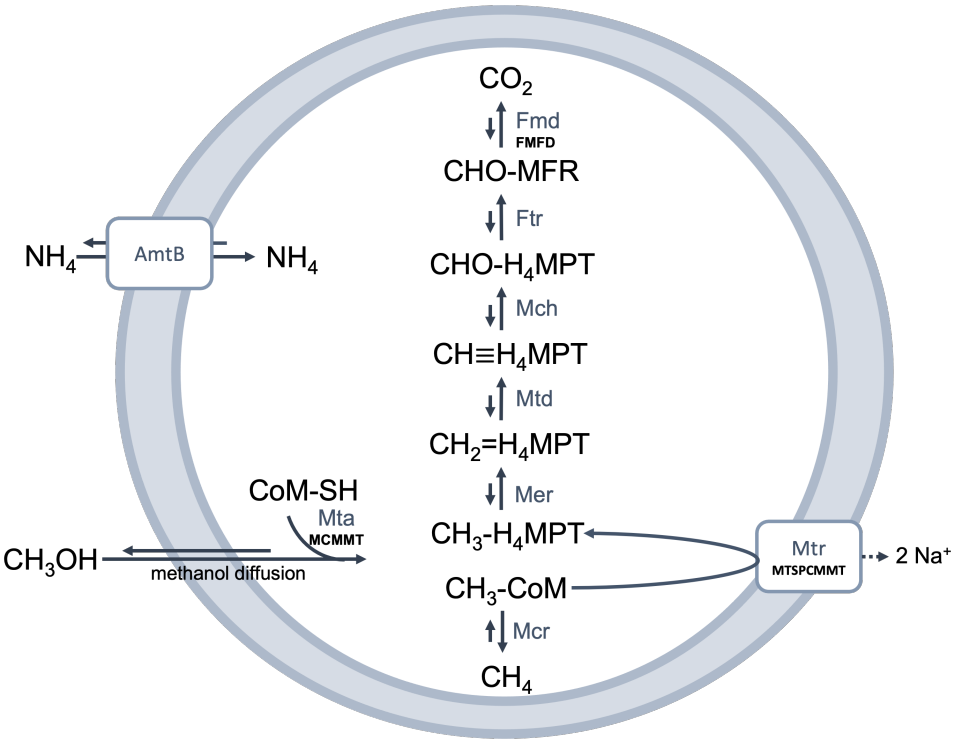

Figure 4.7 Schematic of reactions used for methylotrophic methanogenesis. Gene names are indicated in blue, reaction IDs in the model in bold. Adapted from Timmers et al. (2017).

.

well as potential sources for cellular carbon. It has previously been shown that the incubation temperature affects the isotopic fractionation of methylated compounds into biomass, lipids, and methane within species, and it has been proposed that similar observations can be made across species Summons et al. (1998).

The flux ratios of the methane exchange reaction over Fmd, Mta, and Mtr as well as the ratios of methanol uptake over Fmd, Mta, and Mtr were calculated for all flux solutions. In the case of Fmd, variations over the ten conditions are minimal (ranging from 2.44 to 2.47 for methane/Fmd and 3.65 to 3.73 for methanol/Fmd). Ratios are higher (more CO_2 being produced) in the maximum carbon uptake and minimum nitrogen uptake phenotypes. Methanol/Fmd ratios are minimally smaller for methanol limited cells in both temperature conditions, suggesting that relatively less CO_2 is produced from methanol when methanol is limited in the cell.

Mta to methanol uptake ratios are always 1, since Mta consumes all of the methanol being taken up by the cell, and methane production to Mta ratios are contrary to those of methane/Fmd: ratios are minimally smaller for methanol limited cells

in both temperature. The decrease in methane/Mta ratio indicates that less methanol is used for methane production, and that more methanol is available for cellular carbon when cells are not limited by methanol. Mta over biomass production ratios range from 0.000004039 in minimal nitrogen uptake at 4 °C to 0.002789 in the mean phenotype at 23 °C, and are lower in maximum carbon uptake phenotypes as well as in minimum nitrogen uptake phenotypes at both temperatures.

Flux ratios of Fmd/Mta are smaller in high carbon uptake phenotypes, suggesting that less methanol that is being taken up is oxidized to CO_2 and more is reduced to CH_4 when it is available.

For Mtr flux ratio variations are also minimal, but slightly smaller in methanol limited cells in both temperature conditions (ranging from 1.95 to 2.029 for methane/Mtr and 2.95 to 3.029 for methanol/Mtr). Additionally, Mtr over Fmd flux ratios are lower in minimum carbon cells. In all cases, the 23 °C mean cell simulation values follow those of the carbon limited cell simulations.

CO_2 reduction to formylmethanofuran being used more than the coenzyme-M methyltransferase indicates that more methane is produced from CO_2 than from CH_3OH and that a lack of methanol in methanogenesis can partly be compensated with by CO_2. In this case, methanol would be completely oxidized to CO_2, using the generated electrons for the reduction of CO_2 to methane. At the same time, if more carbon dioxide is used for methanogenesis, more methanol is available as a cellular carbon source.

To investigate the cell's anabolism however, metabolic modeling alone is not sufficient to clearly determine whether cellular carbon is assimilated from carbon dioxide or methanol, and further isotope incorporation studies with labels of both compounds similar to the approach by Kenealy & Zeikus (1982) are needed.

Flux solutions for all reactions in each phenotype simulation are provided as supplementary material.

Table 4.3
Calculated flux boundaries for the core metabolic model based on single cell carbon and nitrogen assimilation data for *M. burtonii*. Mean uptake values were calculated for both substrates, for carbon and nitrogen minima and maxima the corresponding carbon or nitrogen value was taken for the same cell. Model growth rates were calculated for the optimized flux solutions for corresponding methanol and ammonia fluxes.
*Methanol uptake rates had to be readjusted for biomass to be produced in carbon minimum sampling for both temperatures.

simulated phenotype	relative carbon assimilation rate	relative nitrogen assimilation rate	methanol uptake flux [mmol gDW^{-1} h^{-1}]	ammonia uptake flux [mmol gDW^{-1} h^{-1}]	computed growth rate [mmol gDW^{-1} h^{-1}]
***M. burtonii* 4 °C**					
mean both	0.0287	0.0153	595.00	12.00	0.988
carbon minimum	0.000149	0.0287	3.09*	22.52	1.828*
carbon maximum	0.139	0.0233	2881.71	18.28	1.505
nitrogen minimum	0.0295	0.0000379	611.59	0.03	0.00247
nitrogen maximum	0.0580	0.078	1202.44	61.19	2.772
***M. burtonii* 23 °C**					
mean both	0.0336	0.0315	659.69	24.71	2.0399
carbon minimum	0.000981	0.00251	20.34*	1.97	0.159*
carbon maximum	0.145	0.0125	3006.10	9.81	0.808
nitrogen minimum	0.0159	0.000173	329.63	1.36	0.112
nitrogen maximum	0.0475	0.819	984.76	642.55	2.728

4.4 Conclusion

The chemical reactions of life are slowed down at lower temperatures (Gillooly et al., 2001), but due to the complexity of organism's responses to not only temperature, but also other abiotic factors, the quantification of cellular responses from the whole metabolism level down to individual reactions are less intuitive than they might seem. Metabolic models open up a novel, efficient way to test growth responses to changing parameters, both in terms of medium composition (Marinos et al., 2020) and temperature (Li et al., 2021).

Previous studies on the effects of temperature on metabolic fluxes, using metabolic modeling approaches are limited to plants. (Williams et al., 2010b) integrated ^{13}C incorporation data and metabolic flux predictions to link metabolic models to in vivo fluxes of *Arabidopsis thaliana*. They found that during high temperatures, fluxes through the TCA cycle as well as that for phosphoenolpyruvate carboxylase are increased, and suggest the combined use of cellular uptake data and metabolic modeling to verify computational growth simulations. Li et al. (2021) established a temperature constrained GEM for yeast, incorporating heat capacity change, melting temperature, and optimal temperature as thermal parameters for each enzyme. The authors used the model to show that during heat stress, yeast requires more non growth associated maintenance energy, and that sterol and mitochondrial energy metabolisms are involved in thermotolerance.

Here, a metabolic core model for methylotrophic methanogenesis based on a genome scale reconstruction was established. The flux boundaries of the model were then adjusted according to growth media compositions used. Nitrogen and carbon uptake data for ammonia and methanol of cells grown at different temperatures were then incorporated into the model, and flux solutions satisfying their observed values generated.

It was shown that the observed mean growth phenotypes of cells at 23 °C have similar lipid cell wall metabolism fluxes as those cells taking up less methanol, and similar amino acid metabolism fluxes as those cells taking up more ammonia, while maintaing high methanogenesis and growth rates. The mean growth phenotype at 4 °C differs from the mean 23 °C mainly in the above fluxes, and growth is lower at 4 °C.

This study adds to our understanding of the causalities between growth temperature and metabolix fluxes, identified through metabolic modeling.

To fully understand the dynamics of methanogenesis and methanogenic growth at different temperatures, additional studies, especially those analyzing how much substrate is incorporated into biomass and how much labeled compounds is entering and leaving the cell without incorporation, are needed.

He et al. (2022) suggest the use of metabolic models to predict growth phenotypes of some of the novel, lesser known alkane physiologies that have been discovered in recent years and were briefly introduced in Chapter 2. This could be especially beneficial when trying to isolate new organisms: theoretical growth simulations with flux boundaries based on media design can give us an idea if growth is possible, and how it could be maximized. This approach of using constraint based modeling for growth media design has recently been suggested by Wang et al. (2021a).

When generating metabolic models, the opportunities for manual refinement for accuracy improvements are seemingly endless (Thiele & Palsson, 2010; Henry et al., 2010). Similarly, the approaches to optimize models for specific growth conditions of organisms through the incorporation of growth medium composition and known uptake dynamics are nearly unlimited, and would ultimately result in a metabolic model almost perfectly simulating observable growth.

CHAPTER FIVE
Conclusion and Outlook

Growth may be faster at higher temperatures, but optimal growth rates do not necessarily imply optimal growth conditions and sometimes induce cellular stress responses. Temperature is an important factor for the growth dynamics of all living things and organisms inhabiting *extreme* temperature environments adapt on various levels.

Their genomes vary in size, composition, function, and evolution, as shown in Chapter 2: high temperature genomes are smaller, are enriched in lysine, leucine, and isoleucine residues, transport related genes, and show an average net loss in genes when compared to genomes from cold adapted organisms. Low temperature genomes are bigger, are enriched in polar uncharged amino acid residues, additional structural and cell motility related genes, and show an average net gain in genes.

At the phenotype level, growth rate differences and a change in the degree of phenotypic heterogeneity are observed, as shown in Chapter 3: psychrotolerant species grow slower and present higher heterogeneity in carbon uptake than in nitrogen uptake. Thermotolerant species grow faster and have higher heterogeneity in nitrogen uptake than in carbon uptake. Spatial heterogeneity is observed in cold-grown cell aggregates, with higher substrate uptake rates in the outer cells compared to the center and again carbon uptake variation is higher than nitrogen uptake variation. Spatial heterogeneity is negligible in warmer-grown cell aggregates, where cells are more homogeneous throughout the aggregates and nitrogen uptake variations are higher than carbon uptake variations.

Chapter 4 presents a reduced core model for methylotrophic methanogenesis, with modified flux boundaries based on the growth medium used for species grown for this thesis. This model was used to simulate the metabolic fluxes for phenotypes observed through SIMS data.

The simulation for the phenotype with mean carbon and nitrogen assimilation rates at 23 °C was found to be overall similar to minimum carbon incorporation phenotypes of both temperatures, though methanogenesis fluxes and growth remained

high. Additionally, the 4 °C mean phenotype showed comparatively high methanogenesis rates for its slow growth.

5.1 Contextualization

5.1.1 Methanogen Habitats

Our knowledge of the environmental distribution of methanogens and alkane utilizing microorganisms has expanded greatly within the last decade. Many genomes come from metagenome assembled genomes, and their exact growth requirements are not known. Using the observed features of genomes at different growth temperatures, such as amino acid biases, their phylogenetic positioning within the archaeal tree, and the increased presence of some functions, could allow us to approximate temperature conditions for uncultured organisms.

5.1.2 Evolutionary History of an Ancient Group of Organisms

In terms of their evolutionary history, the computational part of this thesis suggests a hot origin of methanogenesis, with an expansion into colder habitats. This goes against the thermoreduction hypothesis, where an expansion of species into warmer habitats with a concurrent reduction of their genomes is proposed. Phylogenetic analyses of functional groups enriched in different temperature groups, such as structural proteins in psychrotolerant and metal ion transporters in thermotolerant species could be used to further elucidate on the evolutionary history within the methanogens.

5.1.3 Methanogens on Earth Today

Across species microbial growth, including that of methanogens, increases with temperature. Increasing global temperatures could increase the rates of methanogenesis in natural and artificial environments for some species, resulting in a positive feedback loop.

Using a metabolic modeling approach, the dynamics of methane production in different environments can be evaluated. Contributions of methanogens to specific environments using this approach have previously been done for gut microbial communities, and similarly an environmental model for soil or sediment microbial

communities could be established to quantify the contribution of microorganisms to methane cycling. In a further step, these systems can be used to simulate changes in environments that cause decreased methane production, and could be used to modify anthropogenically created systems in such a way that the total methane output decreases (such as through a change in livestock diets or changes or pretreatments of sewage digesters).

5.1.4 Life at its Limits

Microbial growth is limited by many factors, including temperature, pH, salinity, pressure, or radiation. Optimal growth is often defined as the condition in which growth is the fastest. Across life's growth temperatures, growth is faster at higher temperatures, and slower at lower temperatures across species, while within species a sharp decrease in growth is often observed above the optimal growth temperature.

Here it was shown that while growth at low temperatures is slower, pure cultures of methanogens at higher temperatures exhibit higher levels of single-cell nitrogen assimilation heterogeneity. An increase in phenotypic heterogeneity is associated with stressful or limiting growth, however the data presented here suggests that cell populations exhibit stress responses even at their optimal growth rates.

It has previously been shown that even at the fastest growth rates, some microorganisms express stress-response proteins. The observations made here, together with the previous findings of stress responses in faster growth suggest that fastest growth does not necessary imply optimal growth conditions for organisms and that factors other than growth rate should be considered to distinguish between optimal and stressful growth.

5.2 Outlook

Temperature adaptations at the genome and single-cell level were identified and the use of metabolic modeling to explain observed phenotypes was introduced. This theses included three distinct methodologies to characterize such adaptations, all coming with their own potential and flaws.

In Chapter 2 well-established methodologies were applied to methanogen

genome data. Though the methods themselves could be applied untroubled, the vast amount of available bioinformatics pipelines and terminologies makes many studies intuitively less comparable. The field of computational biology has rapdily expanded in the past decades, and only now standardizations are slowly emerging, through databases such as the GTDB. As even more genome data and analytical pipelines become available, greater emphasis needs to be put onto regulating terminologies and analytical parameters such as cutoff values. Additionally, many comparative studies identify proteins of unknown functions, which, in some cases, are unique to certain environmental conditions. However, comparatively little effort is given towards identifying the functions of these proteins, which may hold the keys to habitat adaptation.

In computational biology analyses, comparative genomic studies can be expanded across a greater diversity of organisms, further helping to clarify how environment, physiology, and evolution each contribute to genome content and evolution. In the case of methanogens, comparative analyses with more emphasis on ancestral reconstruction for different substrate groups can help elucidate on the evolutionary history of the metabolism. In terms of temperature, comparative studies could include all organisms with known extreme growth temperatures, to identify temperature-related genome signatures spanning across domains.

In Chapter 3 impacts of temperature on phenotypic heterogeneity were investigated for archaea. Here previously described methodologies were followed: there is a trade-off between spatial resolution and dilution effect of fixed cells. For filtered cells, the spatial resolution was still sufficient to identify individual cells, however for embedded aggregates, cells had to be grouped due to low resolution. To some extend, an increase in resolution may be accomplishable through refining nanoSIMS machine settings. However, in some cases and especially when analyzing aggregates, cell fixation by aldehydes, which chemically bond macromolecules together, may be inevitable to conserve the structural features of samples. Another factor to be considered in future analyses may be the use of multiple isotopes, such as labeled dinitrogen gas in addition to ammonia, or labeled carbon dioxide gas in addition to methanol. Then, the uptake dynamics of more substrates can be understood as in Kenealy & Zeikus (1982), and could also be used to further constrain metabolic models.

To identify the truly optimal growth conditions of any organism, different

combinations of growth temperatures, growth substrates, and other abiotic factors that may limit growth need to be explored. For the assessment of phenotypic responses to temperature stress, more proteomics studies focusing on growth differences with temperature, rather than substrate, will be needed. In combination with isotope probing experiments, these could help understand the efficiency of reactions and metabolic subsystems and the differences in cellular anabolism and catabolism across temperatures. Adding a temporal component to SIP-SIMS experiments would also be beneficial to understand how heterogeneity changes across time.

Chapter 4 introduces the incorporation of uptake data into metabolic models to understand subsystem flux differences in different phenotypes. Growth medium constraints on fluxes were incorporated based on substrate concentrations and the number of cells in each incubation vial. Additionally, depending on which limiting factor is to be investigated, the possibilities to refine flux boundaries and additional constraints, such as thermodynamics and enzyme kinetics for different temperatures, are seemingly endless. Here, folding and unfolding, turnover, and temperature dependent activity data for enzymes was not available. Instead carbon and nitrogen uptake rates were incorporated to identify fluxes that can explain observed phenotypes.

Metabolic modeling is a relatively unexplored field that makes use of rapidly expanding genome information. The optimizations of metabolic models for any given organism at any growth condition are seemingly endless. For yet uncultured organisms, metabolic models and computationally testing growth media compositions could aid in the isolation of fastidious organisms.

Further combining computational and experimental approaches will in the future help our understanding of growth dynamics in different environments on Earth today, stretching towards the limits of life known to us, and will also allow us to investigate and understand the dynamics of life throughout Earth's history.

REFERENCES

Ackermann, M. (2013). Microbial individuality in the natural environment. *ISME Journal*, (pp. 465–467).

Ackermann, M. (2015). REVIEWS A functional perspective on phenotypic heterogeneity in microorganisms. *Nature Publishing Group*, 13(8), 497–508.

Alcolombri, U., Pioli, R., Stocker, R., & Berry, D. (2022). Single-cell stable isotope probing in microbial ecology. *ISME Communications*, 2(1), 1–9.

Amend, J. P. & Shock, E. L. (2001). Energetics of overall metabolic reactions of thermophilic and hyperthermophilic Archaea and Bacteria. *FEMS microbiology reviews*, 25(2), 175–243.

Ando, N., Barquera, B., Bartlett, D. H., Boyd, E., Burnim, A. A., Byer, A. S., Colman, D., Gillilan, R. E., Gruebele, M., & Makhatadze, G. (2021). The molecular basis for life in extreme environments. *Annual review of biophysics*, 50(1).

Arshad, A., Speth, D. R., De Graaf, R. M., Op den Camp, H. J. M., Jetten, M. S. M., & Welte, C. U. (2015). A metagenomics-based metabolic model of nitrate-dependent anaerobic oxidation of methane by Methanoperedens-like archaea. *Frontiers in microbiology*, 6, 1423.

Balch, W. E. & Wolfe, R. S. (1979). Specificity and biological distribution of coenzyme M (2-mercaptoethanesulfonic acid). *Journal of bacteriology*, 137(1), 256–263.

Bapteste, É., Brochier, C., & Boucher, Y. (2005). Higher-level classification of the Archaea: evolution of methanogenesis and methanogens. *Archaea*, 1(5), 353–363.

Barajas, H. R., Romero, M. F., Martínez-Sánchez, S., & Alcaraz, L. D. (2019). Global genomic similarity and core genome sequence diversity of the Streptococcus genus as a toolkit to identify closely related bacterial species in complex environments. *PeerJ*, 2019(1), e6233.

Barker, H. A. (1936). Studies upon the methane-producing bacteria. *Archiv für Mikrobiologie*, 7(1), 420–438.

Benedict, M. N., Gonnerman, M. C., Metcalf, W. W., & Price, N. D. (2012). Genome-scale metabolic reconstruction and hypothesis testing in the methanogenic archaeon Methanosarcina acetivorans C2A. *Journal of bacteriology*, 194(4), 855–865.

Berghuis, B. A., Yu, B., Schulz, F., Blainey, P. C., Woyke, T., & Quake, S. R. (2019). Hydrogenotrophic methanogenesis in archaeal phylum Verstraetearchaeota reveals the shared ancestry of all methanogens. *PNAS*, 116(11), 5037–5044.

Berthelot, H., Duhamel, S., L'helguen, S., Maguer, J.-F., Wang, S., Cetinić, I., & Cassar, N. (2019). NanoSIMS single cell analyses reveal the contrasting nitrogen sources for small phytoplankton. *The ISME journal*, 13(3), 651–662.

Boetius, A., Ravenschlag, K., Schubert, C. J., Rickert, D., Widdel, F., Gieseke, A., Amann, R., Jørgensen, B. B., Witte, U., & Pfannkuche, O. (2000). A marine microbial consortium apparently mediating anaerobic oxidation of methane. *Nature*, 407(6804), 623–626.

Borrel, G., Adam, P. S., McKay, L. J., Chen, L.-X., Sierra-García, I. N., Sieber, C. M. K., Letourneur, Q., Ghozlane, A., Andersen, G. L., & Li, W.-J. (2019). Wide diversity of methane and short-chain alkane metabolisms in uncultured archaea. *Nature microbiology*, 4(4), 603–613.

Borrel, G., O'Toole, P. W., Harris, H. M. B., Peyret, P., Brugere, J.-F., & Gribaldo, S. (2013). Phylogenomic data support a seventh order of methylotrophic methanogens and provide insights into the evolution of methanogenesis. *Genome biology and evolution*, 5(10), 1769–1780.

Borton, M. A., Daly, R. A., O'Banion, B., Hoyt, D. W., Marcus, D. N., Welch, S., Hastings, S. S., Meulia, T., Wolfe, R. A., & Booker, A. E. (2018). Comparative genomics and physiology of the genus Methanohalophilus, a prevalent methanogen in hydraulically fractured shale. *Environmental microbiology*, 20(12), 4596–4611.

Boyd, E. S., Skidmore, M., Mitchell, A. C., Bakermans, C., & Peters, J. W. (2010). Methanogenesis in subglacial sediments. *Environmental microbiology reports*, 2, 685–692.

Brochier-Armanet, C., Forterre, P., & Gribaldo, S. (2011). Phylogeny and evolution of the Archaea: one hundred genomes later. *Current opinion in microbiology*, 14(3), 274–281.

Bryant, M. P. & Boone, D. R. (1987). Emended description of strain MST (DSM 800T), the type strain of Methanosarcina barkeri. *International Journal of Systematic and Evolutionary Microbiology*, 37(2), 169–170.

Burke, S. A., Lo, S. L., & Krzycki, J. A. (1998). Clustered genes encoding the methyltransferases of methanogenesis from monomethylamine. *Journal of bacteriology*, 180(13), 3432–3440.

Buswell, A. M. & Sollo, F. W. (1948). The Mechanism of the Methane Fermentation. *Journal of the American Chemical Society*, 70(5), 1778–1780.

Calabrese, F., Stryhanyuk, H., Moraru, C., Schlömann, M., Wick, L. Y., Richnow, H. H., Musat, F., & Musat, N. (2021). Metabolic history and metabolic fitness as drivers of anabolic heterogeneity in isogenic microbial populations. *Environmental Microbiology*, 23(11), 6764–6776.

Calabrese, F., Voloshynovska, I., Musat, F., Thullner, M., Schlömann, M., Richnow, H. H., Lambrecht, J., Müller, S., Wick, L. Y., & Musat, N. (2019). Quantitation and comparison of phenotypic heterogeneity among single cells of monoclonal microbial populations. *Frontiers in microbiology*, (pp. 2814).

Campanaro, S., Williams, T. J., Burg, D. W., De Francisci, D., Treu, L., Lauro, F. M., & Cavicchioli, R. (2011). Temperature-dependent global gene expression in the Antarctic archaeon Methanococcoides burtonii. *Environmental Microbiology*, 13(8), 2018–2038.

Catchpole, R. J. & Forterre, P. (2019). The evolution of reverse gyrase suggests a non-hyperthermophilic last universal common ancestor. *Molecular biology and evolution*, 36(12), 2737–2747.

Catling, D. C., Claire, M. W., & Zahnle, K. J. (2007). Anaerobic methanotrophy and the rise of atmospheric oxygen. *Philosophical Transactions of the Royal Society A: Mathematical, Physical and Engineering Sciences*, 365(1856), 1867–1888.

Catling, D. C., Zahnle, K. J., & McKay, C. P. (2001). Biogenic methane, hydrogen escape, and the irreversible oxidation of early earth. *Science*, 293(5531), 839–843.

Cavicchioli, R. (2002). Extremophiles and the search for extraterrestrial life. *Astrobiology*, 2(3), 281–292.

Cavicchioli, R., Amils, R., Wagner, D., & McGenity, T. (2011). Life and applications of extremophiles.

Cavicchioli, R., Ripple, W. J., Timmis, K. N., Azam, F., Bakken, L. R., Baylis, M., Behrenfeld, M. J., Boetius, A., Boyd, P. W., & Classen, A. T. (2019). Scientists' warning to humanity: microorganisms and climate change. *Nature Reviews Microbiology*, 17(9), 569–586.

Charlebois, R. L. & Doolittle, W. F. (2004). Computing prokaryotic gene ubiquity: Rescuing the core from extinction. *Genome Research*, 14(12), 2469–2477.

Chen, S.-C., Huang, H.-H., Lai, M.-C., Weng, C.-Y., Chiu, H.-H., Tang, S.-L., Rogozin, D. Y., & Degermendzhy, A. G. (2018). Methanolobus psychrotolerans sp. nov., a psychrotolerant methanoarchaeon isolated from a saline meromictic lake in Siberia. *International Journal of Systematic and Evolutionary Microbiology*, 68(4), 1378–1383.

Cheng, H., Schaeffer, R. D., Liao, Y., Kinch, L. N., Pei, J., Shi, S., Kim, B.-H., & Grishin, N. V. (2014). ECOD: an evolutionary classification of protein domains. *PLoS computational biology*, 10(12), e1003926.

Cheng, L., Qiu, T.-L., Yin, X.-B., Wu, X.-L., Hu, G.-Q., Deng, Y., & Zhang, H. (2007). Methermicoccus shengliensis gen. nov., sp. nov., a thermophilic, methylotrophic methanogen isolated from oil-production water, and proposal of Methermicoccaceae fam. nov. *International Journal of Systematic and Evolutionary Microbiology*, 57(12), 2964–2969.

Conrad, R. (2009). The global methane cycle: recent advances in understanding the microbial processes involved. *Environmental microbiology reports*, 1(5), 285–292.

Csűrös, M. (2010). Count: evolutionary analysis of phylogenetic profiles with parsimony and likelihood. *Bioinformatics*, 26(15), 1910–1912.

Csűrös, M. & Miklós, I. (2009). Streamlining and large ancestral genomes in Archaea inferred with a phylogenetic birth-and-death model. *Molecular biology and evolution*, 26(9), 2087–2095.

De Maayer, P., Anderson, D., Cary, C., & Cowan, D. A. (2014). Some like it cold: Understanding the survival strategies of psychrophiles.

De Martino, D., Mori, M., & Parisi, V. (2015). Uniform sampling of steady states in metabolic networks: heterogeneous scales and rounding. *PloS one*, 10(4), e0122670.

Dick, J. M. & Shock, E. L. (2011). Calculation of the relative chemical stabilities of proteins as a function of temperature and redox chemistry in a hot spring. *PLoS One*, 6(8), e22782.

Dick, J. M., Yu, M., & Tan, J. (2020). Uncovering chemical signatures of salinity gradients through compositional analysis of protein sequences. *Biogeosciences*, 17(23), 6145–6162.

Dill, K. A., Ghosh, K., & Schmit, J. D. (2011). Physical limits of cells and proteomes. *Proceedings of the National Academy of Sciences*, 108(44), 17876–17882.

Dombrowski, N., Williams, T. A., Sun, J., Woodcroft, B. J., Lee, J.-H., Minh, B. Q., Rinke, C., & Spang, A. (2020). Undinarchaeota illuminate DPANN phylogeny and the impact of gene transfer on archaeal evolution. *Nature communications*, 11(1), 1–15.

D'Souza, G. G. (2020). Phenotypic variation in spatially structured microbial communities: ecological origins and consequences. *Current Opinion in Biotechnology*, 62, 220–227.

Emms, D. M. & Kelly, S. (2015). OrthoFinder: solving fundamental biases in whole genome comparisons dramatically improves orthogroup inference accuracy. *Genome biology*, 16(1), 1–14.

Emms, D. M. & Kelly, S. (2017). STRIDE: species tree root inference from gene duplication events. *Molecular biology and evolution*, 34(12), 3267–3278.

Emms, D. M. & Kelly, S. (2018). STAG: Species tree inference from all genes. bioRxiv 267914.

Emms, D. M. & Kelly, S. (2019). OrthoFinder: phylogenetic orthology inference for comparative genomics. *Genome biology*, 20(1), 1–14.

Erdrich, P., Steuer, R., & Klamt, S. (2015). An algorithm for the reduction of genome-scale metabolic network models to meaningful core models. *BMC systems biology*, 9(1), 1–12.

Ermler, U., Grabarse, W., Shima, S., Goubeaud, M., & Thauer, R. K. (1997). Crystal structure of methyl-coenzyme M reductase: the key enzyme of biological methane formation. *Science*, 278(5342), 1457–1462.

Evans, P. N., Boyd, J. A., Leu, A. O., Woodcroft, B. J., Parks, D. H., Hugenholtz, P., & Tyson, G. W. (2019). An evolving view of methane metabolism in the Archaea. *Nature Reviews Microbiology*, 17(4), 219–232.

Evans, P. N., Parks, D. H., Chadwick, G. L., Robbins, S. J., Orphan, V. J., Golding, S. D., & Tyson, G. W. (2015). Methane metabolism in the archaeal phylum Bathyarchaeota revealed by genome-centric metagenomics. *Science*, 350(6259), 434–438.

Farias, S. T. & Bonato, M. C. (2003). Preferred amino acids and thermostability. *Genet Mol Res*, 2(4), 383–393.

Feist, A. M., Scholten, J. C. M., Palsson, B. Ø., Brockman, F. J., & Ideker, T. (2006). Modeling methanogenesis with a genome-scale metabolic reconstruction of Methanosarcina barkeri. *Molecular systems biology*, 2(1), 4–2006.

Feller, G. (2010). Protein stability and enzyme activity at extreme biological temperatures. *Journal of Physics: Condensed Matter*, 22(32), 323101.

Feller, G. (2018). Protein folding at extreme temperatures: Current issues. In *Seminars in Cell and Developmental Biology*, volume 84 (pp. 129–137).: Elsevier.

Ferry, J. G., Smith, P. H., & Wolfe, R. S. (1974). Methanospirillum, a new genus of methanogenic bacteria, and characterization of Methanospirillum hungatii sp. nov. *International Journal of Systematic and Evolutionary Microbiology*, 24(4), 465–469.

Fielding, E. R., Archer, D. B., de Macario, E. C., & Macario, A. J. L. (1988). Isolation and characterization of methanogenic bacteria from landfills. *Applied and environmental microbiology*, 54(3), 835–836.

Forterre, P. (1995). Thermoreduction, a hypothesis for the origin of prokaryotes. *Comptes rendus de l'Academie des sciences. Serie III, Sciences de la vie*, 318(4), 415–422.

Forterre, P. (2002). A hot story from comparative genomics: reverse gyrase is the only hyperthermophile-specific protein. *Trends in Genetics*, 18(5), 236–237.

Fournier, G. P. & Gogarten, J. P. (2008). Evolution of acetoclastic methanogenesis in Methanosarcina via horizontal gene transfer from cellulolytic Clostridia. *Journal of bacteriology*, 190(3), 1124–1127.

Franzmann, P. D., Liu, Y., Balkwill, D. L., Aldrich, H. C., De Macario, E. C., & Boone, D. R. (1997). Methanogenium frigidum sp. nov., a psychrophilic, H2-using methanogen from Ace Lake, Antarctica. *International Journal of Systematic and Evolutionary Microbiology*, 47(4), 1068–1072.

Franzmann, P. D., Springer, N., Ludwig, W., De Macario, E. C., & Rohde, M. (1992). A methanogenic archaeon from Ace Lake, Antarctica: Methanococcoides burtonii sp. nov. *Systematic and Applied Microbiology*, 15(4), 573–581.

Friedrich, M. W. (2005). Methyl-coenzyme M reductase genes: unique functional markers for methanogenic and anaerobic methane-oxidizing Archaea. *Methods in enzymology*, 397, 428–442.

Fuller, B. J. (2004). Cryoprotectants: the essential antifreezes to protect life in the frozen state. *CryoLetters*, 25(6), 375–388.

Galagan, J. E., Nusbaum, C., Roy, A., Endrizzi, M. G., Macdonald, P., FitzHugh, W., Calvo, S., Engels, R., Smirnov, S., & Atnoor, D. (2002). The genome of M. acetivorans reveals extensive metabolic and physiological diversity. *Genome research*, 12(4), 532–542.

Garcia, P. S., Gribaldo, S., & Borrel, G. (2022). Diversity and Evolution of Methane-Related Pathways in Archaea. *Annual Review of Microbiology*, 76.

Genovese, C. R., Lazar, N. A., & Nichols, T. (2002). Thresholding of statistical maps in functional neuroimaging using the false discovery rate. *Neuroimage*, 15(4), 870–878.

Gillooly, J. F., Brown, J. H., West, G. B., Savage, V. M., & Charnov, E. L. (2001). Effects of size and temperature on metabolic rate. *science*, 293(5538), 2248–2251.

Goldschmidt, F., Caduff, L., & Johnson, D. R. (2021). Causes and consequences of pattern diversification in a spatially self-organizing microbial community. *The ISME Journal*, 15(8), 2415–2426.

Gonnerman, M. C., Benedict, M. N., Feist, A. M., Metcalf, W. W., & Price, N. D. (2013). Genomically and biochemically accurate metabolic reconstruction of Methanosarcina barkeri Fusaro, iMG746. *Biotechnology journal*, 8(9), 1070–1079.

Goodchild, A., Saunders, N. F. W., Ertan, H., Raftery, M., Guilhaus, M., Curmi, P. M. G., & Cavicchioli, R. (2004). A proteomic determination of cold adaptation in the Antarctic archaeon, Methanococcoides burtonii. *Molecular microbiology*, 53(1), 309–321.

Goyal, N., Widiastuti, H., Karimi, I. A., & Zhou, Z. (2014). A genome-scale metabolic model of Methanococcus maripaludis S2 for CO 2 capture and conversion to methane. *Molecular BioSystems*, 10(5), 1043–1054.

Gromiha, M. M., Oobatake, M., & Sarai, A. (1999). Important amino acid properties for enhanced thermostability from mesophilic to thermophilic proteins. *Biophysical chemistry*, 82(1), 51–67.

Gu, C., Kim, G. B., Kim, W. J., Kim, H. U., & Lee, S. Y. (2019). Current status and applications of genome-scale metabolic models. *Genome biology*, 20(1), 1–18.

Gunsalus, R. P. & Wolfe, R. S. (1980). Methyl coenzyme M reductase from Methanobacterium thermoautotrophicum. Resolution and properties of the components. *Journal of Biological Chemistry*, 255(5), 1891–1895.

Gurobi Optimization, LLC (2022). Gurobi Optimizer Reference Manual.

Hallam, S. J., Putnam, N., Preston, C. M., Detter, J. C., Rokhsar, D., Richardson, P. M., & DeLong, E. F. (2004). Reverse methanogenesis: testing the hypothesis with environmental genomics. *Science*, 305(5689), 1457–1462.

Hamilton, J. J., Calixto Contreras, M., & Reed, J. L. (2015). Thermodynamics and H2 transfer in a methanogenic, syntrophic community. *PLoS computational biology*, 11(7), e1004364.

Hanson, R. S. & Hanson, T. E. (1996). Methanotrophic bacteria. *Microbiological reviews*, 60(2), 439–471.

Haroon, M. F., Hu, S., Shi, Y., Imelfort, M., Keller, J., Hugenholtz, P., Yuan, Z., & Tyson, G. W. (2013). Anaerobic oxidation of methane coupled to nitrate reduction in a novel archaeal lineage. *Nature*, 500(7464), 567–570.

He, B., Cai, C., McCubbin, T., Muriel, J. C., Sonnenschein, N., Hu, S., Yuan, Z., & Marcellin, E. (2022). A Genome-Scale Metabolic Model of Methanoperedens nitroreducens: Assessing Bioenergetics and Thermodynamic Feasibility. *Metabolites*, 12(4), 314.

Heirendt, L., Arreckx, S., Pfau, T., Mendoza, S. N., Richelle, A., Heinken, A., Haraldsdóttir, H. S., Wachowiak, J., Keating, S. M., & Vlasov, V. (2019). Creation and analysis of biochemical constraint-based models using the COBRA Toolbox v. 3.0. *Nature protocols*, 14(3), 639–702.

Henry, C. S., DeJongh, M., Best, A. A., Frybarger, P. M., Linsay, B., & Stevens, R. L. (2010). High-throughput generation, optimization and analysis of genome-scale metabolic models. *Nature biotechnology*, 28(9), 977–982.

Hermelink, A., Brauer, A., Lasch, P., & Naumann, D. (2009). Phenotypic heterogeneity within microbial populations at the single-cell level investigated by confocal Raman microspectroscopy. *Analyst*, 134(6), 1149–1153.

Hildenbrand, C., Stock, T., Lange, C., Rother, M., & Soppa, J. (2011). Genome copy numbers and gene conversion in methanogenic archaea. *Journal of bacteriology*, 193(3), 734–743.

Hoehler, T., Losey, N. A., Gunsalus, R. P., & McInerney, M. J. (2010). *Environmental constraints that limit methanogenesis*. Technical report, Univ. of Oklahoma, Norman, OK.

Hoehler, T. M., Alperin, M. J., Albert, D. B., & Martens, C. S. (1994). Field and laboratory studies of methane oxidation in an anoxic marine sediment: Evidence for a methanogen-sulfate reducer consortium. *Global biogeochemical cycles*, 8(4), 451–463.

Hua, Z.-S., Wang, Y.-L., Evans, P. N., Qu, Y.-N., Goh, K. M., Rao, Y.-Z., Qi, Y.-L., Li, Y.-X., Huang, M.-J., & Jiao, J.-Y. (2019). Insights into the ecological roles and evolution of methyl-coenzyme M reductase-containing hot spring Archaea. *Nature communications*, 10(1), 1–11.

Huerta-Cepas, J., Forslund, K., Coelho, L. P., Szklarczyk, D., Jensen, L. J., von Mering, C., & Bork, P. (2017). Fast Genome-Wide Functional Annotation through Orthology Assignment by eggNOG-Mapper. *Molecular Biology and Evolution*, 34(8), 2115–2122.

Hungate, R. E. (1950). The anaerobic mesophilic cellulolytic bacteria. *Bacteriological reviews*, 14(1), 1–49.

Jablonka, E., Oborny, B., Molnar, I., Kisdi, E., Hofbauer, J., & Czaran, T. (1995). The adaptive advantage of phenotypic memory in changing environments. *Philosophical Transactions of the Royal Society of London. Series B: Biological Sciences*, 350(1332), 133–141.

Jackson, R. B., Saunois, M., Bousquet, P., Canadell, J. G., Poulter, B., Stavert, A. R., Bergamaschi, P., Niwa, Y., Segers, A., & Tsuruta, A. (2020). Increasing anthropogenic methane emissions arise equally from agricultural and fossil fuel sources. *Environmental Research Letters*, 15(7), 71002.

Jeanthon, C., L'Haridon, S., Reysenbach, A.-L., Corre, E., Vernet, M., Messner, P., Sleytr, U. B., & Prieur, D. (1999). Methanococcus vulcanius sp. nov., a novel hyperthermophilic methanogen isolated from East Pacific Rise, and identification of Methanococcus sp. DSM 4213Tas Methanococcus fervens sp. nov. *International Journal of Systematic and Evolutionary Microbiology*, 49(2), 583–589.

Jebbar, M., Hickman-Lewis, K., Cavalazzi, B., Taubner, R.-S., Rittmann, S. K.-M., & Antunes, A. (2020). Microbial diversity and biosignatures: an icy moons perspective. *Space Science Reviews*, 216(1), 1–47.

Jiang, B., Parshina, S. N., van Doesburg, W., Lomans, B. P., & Stams, A. J. (2005). Methanomethylovorans thermophila sp. nov., a thermophilic, methylotrophic methanogen from an anaerobic reactor fed with methanol. *International Journal of Systematic and Evolutionary Microbiology*, 55(6), 2465–2470.

Jin, Q., Wu, Q., Shapiro, B. M., & McKernan, S. E. (2022). Limited Mechanistic Link Between the Monod Equation and Methanogen Growth: a Perspective from Metabolic Modeling. *Microbiology Spectrum*, 10(2), e02259–21.

Jones, W. J., Nagle Jr, D. P., & Whitman, W. B. (1987). Methanogens and the diversity of archaebacteria. *Microbiological Reviews*, 51(1), 135–177.

Jones, W. J., Stugard, C. E., & Jannasch, H. W. (1989). Comparison of thermophilic methanogens from submarine hydrothermal vents. *Archives of Microbiology*, 151(4), 314–318.

Kanehisa, M., Araki, M., Goto, S., Hattori, M., Hirakawa, M., Itoh, M., Katayama, T., Kawashima, S., Okuda, S., & Tokimatsu, T. (2007). KEGG for linking genomes to life and the environment. *Nucleic acids research*, 36(1), D480–D484.

Kaster, A.-K., Goenrich, M., Seedorf, H., Liesegang, H., Wollherr, A., Gottschalk, G., & Thauer, R. K. (2011). More than 200 genes required for methane formation from H2 and CO2 and energy conservation are present in Methanothermobacter marburgensis and Methanothermobacter thermautotrophicus. *Archaea*, 2011.

Kellermann, M. Y., Wegener, G., Elvert, M., Yoshinaga, M. Y., Lin, Y.-S., Holler, T., Mollar, X. P., Knittel, K., & Hinrichs, K.-U. (2012). Autotrophy as a predominant mode of carbon fixation in anaerobic methane-oxidizing microbial communities. *Proceedings of the National Academy of Sciences*, 109(47), 19321–19326.

Kendrick, M. G. & Kral, T. A. (2006). Survival of methanogens during desiccation: implications for life on Mars. *Astrobiology*, 6(4), 546–551.

Kenealy, W. R. & Zeikus, J. G. (1982). One-carbon metabolism in methanogens: evidence for synthesis of a two-carbon cellular intermediate and unification of catabolism and anabolism in Methanosarcina barkeri. *Journal of bacteriology*, 151(2), 932–941.

Kessler, P. S. & Leigh, J. A. (1999). Genetics of nitrogen regulation in Methanococcus maripaludis. *Genetics*, 152(4), 1343–1351.

Kim, J. H., Kang, H. J., Yu, B. J., Kim, S. C., & Lee, P. C. (2015). Planococcus faecalis sp. nov., a carotenoid-producing species isolated from stools of Antarctic penguins. *International Journal of Systematic and Evolutionary Microbiology*, 65(10), 3373–3378.

Kiviet, D. J., Nghe, P., Walker, N., Boulineau, S., Sunderlikova, V., & Tans, S. J. (2014). Stochasticity of metabolism and growth at the single-cell level. *Nature*, 514(7522), 376–379.

Klipcan, L., Safro, I., Temkin, B., & Safro, M. (2006). Optimal growth temperature of prokaryotes correlates with class II amino acid composition. *FEBS letters*, 580(6), 1672–1676.

Kopf, S. H., McGlynn, S. E., Green-Saxena, A., Guan, Y., Newman, D. K., & Orphan, V. J. (2015). Heavy water and 15 N labelling with N ano SIMS analysis reveals growth rate-dependent metabolic heterogeneity in chemostats. *Environmental microbiology*, 17(7), 2542–2556.

Kotelnikova, S., Macario, A. J. L., & Pedersen, K. (1998). Methanobacterium subterraneum sp. nov., a new alkaliphilic, eurythermic and halotolerant methanogen isolated from deep granitic groundwater. *International journal of systematic and evolutionary microbiology*, 48(2), 357–367.

Kral, T. A., Brink, K. M., Miller, S. L., & Mckay, C. P. (1998). Hydrogen consumption by methanogens on the early Earth. *Origins of Life and Evolution of the Biosphere*, 28(3), 311–319.

Kuhn, E. (2012). Toward understanding life under subzero conditions: the significance of exploring psychrophilic "cold-shock" proteins. *Astrobiology*, 12(11), 1078–1086.

Kurr, M., Huber, R., König, H., Jannasch, H. W., Fricke, H., Trincone, A., Kristjansson, J. K., & Stetter, K. O. (1991). Methanopyrus kandleri, gen. and sp. nov. represents a novel group of hyperthermophilic methanogens, growing at 110 C. *Archives of Microbiology*, 156(4), 239–247.

Kurth, J. M., den Camp, H. J. M. O., & Welte, C. U. (2020). Several ways one goal—methanogenesis from unconventional substrates. *Applied Microbiology and Biotechnology*, 104(16), 6839–6854.

Lange, M., Macario, A. J. L., Ahring, B. K., & Conway de Macario, E. (1997). Heat-shock response in Methanosarcina mazei S-6. *Current microbiology*, 35(2), 116–121.

Laso-Pérez, R., Wegener, G., Knittel, K., Widdel, F., Harding, K. J., Krukenberg, V., Meier, D. V., Richter, M., Tegetmeyer, H. E., & Riedel, D. (2016). Thermophilic archaea activate butane via alkyl-coenzyme M formation. *Nature*, 539(7629), 396–401.

Lechner, M., Findeiß, S., Steiner, L., Marz, M., Stadler, P. F., & Prohaska, S. J. (2011). Proteinortho: detection of (co-) orthologs in large-scale analysis. *BMC bioinformatics*, 12(1), 124.

Leigh, J. A., Albers, S.-V., Atomi, H., & Allers, T. (2011). Model organisms for genetics in the domain Archaea: methanogens, halophiles, Thermococcales and Sulfolobales. *FEMS microbiology reviews*, 35(4), 577–608.

Leigh, J. A., Rinehart Jr, K. L., & Wolfe, R. S. (1984). Structure of methanofuran, the carbon dioxide reduction factor of Methanobacterium thermoautotrophicum. *Journal of the American Chemical Society*, 106(12), 3636–3640.

Lepock, J. R., Frey, H. E., & Inniss, W. E. (1990). Thermal analysis of bacteria by differential scanning calorimetry: relationship of protein denaturation in situ to maximum growth temperature. *Biochimica et Biophysica Acta (BBA)-Molecular Cell Research*, 1055(1), 19–26.

Lepot, K. (2020). Signatures of early microbial life from the Archean (4 to 2.5 Ga) eon. *Earth-Science Reviews*, (pp. 103296).

Letunic, I. & Bork, P. (2021). Interactive Tree Of Life (iTOL) v5: an online tool for phylogenetic tree display and annotation. *Nucleic acids research*, 49(W1), W293–W296.

Li, G., Hu, Y., Zrimec, J., Luo, H., Wang, H., Zelezniak, A., Ji, B., & Nielsen, J. (2021). Bayesian genome scale modelling identifies thermal determinants of yeast metabolism. *Nature communications*, 12(1), 1–12.

Li, L., Li, Q., Rohlin, L., Kim, U., Salmon, K., Rejtar, T., Gunsalus, R. P., Karger, B. L., & Ferry, J. G. (2007). Quantitative Proteomic and Microarray Analysis of the Archaeon Methanosarcina acetivorans Grown with Acetate versus Methanol. *Journal of proteome research*, 6(2), 759–771.

Li, Q., Li, L., Rejtar, T., Lessner, D. J., Karger, B. L., & Ferry, J. G. (2006). Electron transport in the pathway of acetate conversion to methane in the marine archaeon Methanosarcina acetivorans. *Journal of Bacteriology*, 188(2), 702–710.

Liu, Y. & Whitman, W. B. (2008). Metabolic, phylogenetic, and ecological diversity of the methanogenic archaea. *Annals of the New York Academy of Sciences*, 1125, 171–189.

Lobo, A. L. & Zinder, S. H. (1988). Diazotrophy and nitrogenase activity in the archaebacterium Methanosarcina barkeri 227. *Applied and environmental microbiology*, 54(7), 1656–1661.

Lovley, D. R., Greening, R. C., & Ferry, J. G. (1984). Rapidly growing rumen methanogenic organism that synthesizes coenzyme M and has a high affinity for formate. *Applied and Environmental Microbiology*, 48(1), 81–87.

Lu, H., Li, F., Sánchez, B. J., Zhu, Z., Li, G., Domenzain, I., Marcišauskas, S., Anton, P. M., Lappa, D., & Lieven, C. (2019). A consensus S. cerevisiae metabolic model Yeast8 and its ecosystem for comprehensively probing cellular metabolism. *Nature communications*, 10(1), 1–13.

Lyu, Z., Shao, N., Akinyemi, T., & Whitman, W. B. (2018). Methanogenesis. *Current Biology*, 28(13), R727–R732.

Mah, R. A. & Kuhn, D. A. (1984). Transfer of the type species of the genus Methanococcus to the genus Methanosarcina, naming it Methanosarcina mazei (Barker 1936) comb. nov. et emend. and conservation of the genus Methanococcus (approved lists 1980) with Methanococcus vannielii (approved lists 1980) as the type species. Request for an opinion. *International Journal of Systematic Bacteriology*, 34(2), 263–265.

Majerník, A. I., Lundgren, M., McDermott, P., Bernander, R., & Chong, J. P. J. (2005). DNA content and nucleoid distribution in Methanothermobacter thermautotrophicus. *Journal of bacteriology*, 187(5), 1856–1858.

Malandrin, L., Huber, H., & Bernander, R. (1999). Nucleoid structure and partition in Methanococcus jannaschii: an archaeon with multiple copies of the chromosome. *Genetics*, 152(4), 1315–1323.

Marinos, G., Kaleta, C., & Waschina, S. (2020). Defining the nutritional input for genome-scale metabolic models: A roadmap. *PloS one*, 15(8), e0236890.

Martijn, J., Schön, M. E., Lind, A. E., Vosseberg, J., Williams, T. A., Spang, A., & Ettema, T. J. G. (2020). Hikarchaeia demonstrate an intermediate stage in the methanogen-to-halophile transition. *Nature communications*, 11(1), 1–14.

Martinez-Gutierrez, C. A. & Aylward, F. O. (2021). Phylogenetic signal, congruence, and uncertainty across bacteria and archaea. *Molecular biology and evolution*, 38(12), 5514–5527.

McGenity, T. J. & Sorokin, D. Y. (2010). Methanogens and methanogenesis in hypersaline environments. In *Handbook of hydrocarbon and lipid microbiology* (pp. 665–680). Springer Berlin.

McKay, L. J., Dlakić, M., Fields, M. W., Delmont, T. O., Eren, A. M., Jay, Z. J., Klingelsmith, K. B., Rusch, D. B., & Inskeep, W. P. (2019). Co-occurring genomic capacity for anaerobic methane and dissimilatory sulfur metabolisms discovered in the Korarchaeota. *Nature Microbiology*, 4(4), 614–622.

Medina-Chávez, N. O. & Travisano, M. (2021). Archaeal Communities: The Microbial Phylogenomic Frontier. *Frontiers in Genetics*, (pp. 693193).

Mehta, M. P. & Baross, J. A. (2006). Nitrogen fixation at 92 C by a hydrothermal vent archaeon. *Science*, 314(5806), 1783–1786.

Mendler, K., Chen, H., Parks, D. H., Lobb, B., Hug, L. A., & Doxey, A. C. (2019). AnnoTree: visualization and exploration of a functionally annotated microbial tree of life. *Nucleic acids research*, 47(9), 4442–4448.

Metpally, R. P. R. & Reddy, B. V. B. (2009). Comparative proteome analysis of psychrophilic versus mesophilic bacterial species: Insights into the molecular basis of cold adaptation of proteins. *BMC genomics*, 10(1), 1–10.

Meyer, N. R., Fortney, J. L., & Dekas, A. E. (2021). NanoSIMS sample preparation decreases isotope enrichment: magnitude, variability and implications for single-cell rates of microbial activity. *Environmental Microbiology*, 23(1), 81–98.

Michał, B., Gagat, P., Jabłoński, S., Chilimoniuk, J., Gaworski, M., Mackiewicz, P., & Marcin, Ł. (2018). PhyMet2: a database and toolkit for phylogenetic and metabolic analyses of methanogens. *Environmental microbiology reports*, 10(3), 378–382.

Mickol, R. L. & Kral, T. A. (2017). Low Pressure Tolerance by Methanogens in an Aqueous Environment : Implications for Subsurface Life on Mars. *Origins of Life and Evolution of Biospheres*, (pp. 511–532).

Morozova, D. & Wagner, D. (2007). Stress response of methanogenic archaea from Siberian permafrost compared with methanogens from nonpermafrost habitats. *FEMS Microbiology Ecology*, 61, 16–25.

Musat, N., Foster, R., Vagner, T., Adam, B., & Kuypers, M. M. M. (2012). Detecting metabolic activities in single cells, with emphasis on nanoSIMS. *FEMS microbiology reviews*, 36(2), 486–511.

Musat, N., Stryhanyuk, H., Bombach, P., Adrian, L., Audinot, J.-N., & Richnow, H. H. (2014). The effect of FISH and CARD-FISH on the isotopic composition of 13C-and 15N-labeled Pseudomonas putida cells measured by nanoSIMS. *Systematic and Applied Microbiology*, 37(4), 267–276.

Nazem-Bokaee, H., Gopalakrishnan, S., Ferry, J. G., Wood, T. K., & Maranas, C. D. (2016). Assessing methanotrophy and carbon fixation for biofuel production by Methanosarcina acetivorans. *Microbial cell factories*, 15(1), 1–13.

Nedwell, D. B. (1999). Effect of low temperature on microbial growth: lowered affinity for substrates limits growth at low temperature. *FEMS microbiology ecology*, 30(2), 101–111.

Nguyen, J., Fernandez, V., Pontrelli, S., Sauer, U., Ackermann, M., & Stocker, R. (2021). A distinct growth physiology enhances bacterial growth under rapid nutrient fluctuations. *Nature Communications*, 12(1), 1–12.

Ni, S. & Boone, D. R. (1998). Extremophilic methanogenic archaea and their adaptation mechanisms. *Extremophiles: Microbial Life in Extreme Environments.*, (pp. 211–232).

Nichols, D. S., Miller, M. R., Davies, N. W., Goodchild, A., Raftery, M., & Cavicchioli, R. (2004). Cold adaptation in the Antarctic archaeon Methanococcoides burtonii involves membrane lipid unsaturation. *Journal of Bacteriology*, 186(24), 8508–8515.

Nishizawa, M., Miyazaki, J., Makabe, A., Koba, K., & Takai, K. (2014). Physiological and isotopic characteristics of nitrogen fixation by hyperthermophilic methanogens: key insights into nitrogen anabolism of the microbial communities in Archean hydrothermal systems. *Geochimica et Cosmochimica Acta*, 138, 117–135.

Olson, S. L., Reinhard, C. T., & Lyons, T. W. (2016). Limited role for methane in the mid-Proterozoic greenhouse. *Proceedings of the National Academy of Sciences of the United States of America*, 113(41), 11447–11452.

Olson, S. L., Schwieterman, E. W., Reinhard, C. T., & Lyons, T. W. (2018). Earth: Atmospheric evolution of a habitable planet. *arXiv preprint arXiv:1803.05967*.

Orth, J. D., Fleming, R. M. T., & Palsson, B. Ø. (2010). Reconstruction and use of microbial metabolic networks: the core Escherichia coli metabolic model as an educational guide. *EcoSal plus*, 4(1).

Österlund, T., Nookaew, I., & Nielsen, J. (2012). Fifteen years of large scale metabolic modeling of yeast: developments and impacts. *Biotechnology advances*, 30(5), 979–988.

Parks, D. H., Chuvochina, M., Rinke, C., Mussig, A. J., Chaumeil, P.-A., & Hugenholtz, P. (2022). GTDB: an ongoing census of bacterial and archaeal diversity through a phylogenetically consistent, rank normalized and complete genome-based taxonomy. *Nucleic acids research*, 50(D1), D785–D794.

Paul, S., Bag, S. K., Das, S., Harvill, E. T., & Dutta, C. (2008). Molecular signature of hypersaline adaptation: insights from genome and proteome composition of halophilic prokaryotes. *Genome biology*, 9(4), 1–19.

Perfumo, A., Elsaesser, A., Littmann, S., Foster, R. A., Kuypers, M. M. M., Cockell, C. S., & Kminek, G. (2014). Epifluorescence, SEM, TEM and nanoSIMS image analysis of the cold phenotype of Clostridium psychrophilum at subzero temperatures. *FEMS Microbiology Ecology*, 90(3), 869–882.

Peterson, J. R., Thor, S., Kohler, L., Kohler, P. R. A., Metcalf, W. W., & Luthey-Schulten, Z. (2016). Genome-wide gene expression and RNA half-life measurements allow predictions of regulation and metabolic behavior in Methanosarcina acetivorans. *BMC genomics*, 17(1), 1–23.

Pett-Ridge, J. & Weber, P. K. (2012). NanoSIP: NanoSIMS applications for microbial biology. In *Microbial Systems Biology* (pp. 375–408). Springer.

Poehlein, A., Schneider, D., Soh, M., Daniel, R., & Seedorf, H. (2018). Comparative genomic analysis of members of the genera Methanosphaera and Methanobrevibacter reveals distinct clades with specific potential metabolic functions. *Archaea*, 2018.

Polerecky, L., Adam, B., Milucka, J., Musat, N., Vagner, T., & Kuypers, M. M. M. (2012). Look@ NanoSIMS–a tool for the analysis of nanoSIMS data in environmental microbiology. *Environmental microbiology*, 14(4), 1009–1023.

Privalov, P. L. (1990). Cold denaturation of protein. *Critical reviews in biochemistry and molecular biology*, 25(4), 281–306.

Prondzinsky, P., Toyoda, S., & McGlynn, S. E. (2022). The methanogen core and pangenome: conservation and variability across biology's growth temperature extremes. *DNA Research*.

Quek, L.-E., Dietmair, S., Hanscho, M., Martínez, V. S., Borth, N., & Nielsen, L. K. (2014). Reducing Recon 2 for steady-state flux analysis of HEK cell culture. *Journal of biotechnology*, 184, 172–178.

Raghoebarsing, A. A., Pol, A., Van de Pas-Schoonen, K. T., Smolders, A. J. P., Ettwig, K. F., Rijpstra, W. I. C., Schouten, S., Damsté, J. S. S., Op den Camp, H. J. M., & Jetten, M. S. M. (2006). A microbial consortium couples anaerobic methane oxidation to denitrification. *Nature*, 440(7086), 918–921.

Reeburgh, W. S. (2007). Oceanic methane biogeochemistry. *Chemical reviews*, 107(2), 486–513.

Reed, J. L. & Palsson, B. Ø. (2003). Thirteen years of building constraint-based in silico models of Escherichia coli. *Journal of bacteriology*, 185(9), 2692–2699.

Reid, I. N., Sparks, W. B., Lubow, S., McGrath, M., Livio, M., Valenti, J., Sowers, K. R., Shukla, H. D., MacAuley, S., & Miller, T. (2006). Terrestrial models for extraterrestrial life: methanogens and halophiles at Martian temperatures. *International Journal of Astrobiology*, 5(2), 89–97.

Rohlin, L. & Gunsalus, R. P. (2010). Carbon-dependent control of electron transfer and central carbon pathway genes for methane biosynthesis in the Archaean, Methanosarcina acetivorans strain C2A. *BMC microbiology*, 10(1), 1–15.

Rosentreter, J. A., Borges, A. V., Deemer, B. R., Holgerson, M. A., Liu, S., Song, C., Melack, J., Raymond, P. A., Duarte, C. M., & Allen, G. H. (2021). Half of global methane emissions come from highly variable aquatic ecosystem sources. *Nature Geoscience*, 14(4), 225–230.

Rothman, D. H., Fournier, G. P., French, K. L., Alm, E. J., Boyle, E. A., Cao, C., & Summons, R. E. (2014). Methanogenic burst in the end-Permian carbon cycle. *Proceedings of the National Academy of Sciences*, 111(15), 5462–5467.

Rothschild, L. J. & Mancinelli, R. L. (2001). Life in extreme environments. *Nature*, 409(6823), 1092–1101.

Sánchez, B. J., Zhang, C., Nilsson, A., Lahtvee, P., Kerkhoven, E. J., & Nielsen, J. (2017). Improving the phenotype predictions of a yeast genome-scale metabolic model by incorporating enzymatic constraints. *Molecular systems biology*, 13(8), 935.

Satish Kumar, V., Ferry, J. G., & Maranas, C. D. (2011). Metabolic reconstruction of the archaeon methanogen Methanosarcina Acetivorans. *BMC systems biology*, 5(1), 1–10.

Sato, Y., Okano, K., Kimura, H., & Honda, K. (2020). TEMPURA: Database of Growth TEMPeratures of Usual and RAre Prokaryotes. *Microbes and environments*, 35(3), ME20074.

Saunders, N. F. W., Thomas, T., Curmi, P. M. G., Mattick, J. S., Kuczek, E., Slade, R., Davis, J., Franzmann, P. D., Boone, D., & Rusterholtz, K. (2003). Mechanisms of thermal adaptation revealed from the genomes of the Antarctic Archaea Methanogenium frigidum and Methanococcoides burtonii. *Genome research*, 13(7), 1580–1588.

Sauterey, B., Charnay, B., Affholder, A., Mazevet, S., & Ferrière, R. (2020). Co-evolution of primitive methane-cycling ecosystems and early Earth's atmosphere and climate. *Nature communications*, 11(1), 1–12.

Sawle, L. & Ghosh, K. (2011). How do thermophilic proteins and proteomes withstand high temperature? *Biophysical journal*, 101(1), 217–227.

Scheller, S., Yu, H., Chadwick, G. L., McGlynn, S. E., & Orphan, V. J. (2016). Artificial electron acceptors decouple archaeal methane oxidation from sulfate reduction. *Science*, 351(6274), 703–707.

Scherer, P., Lippert, H., & Wolff, G. (1983). Composition of the major elements and trace elements of 10 methanogenic bacteria determined by inductively coupled plasma emission spectrometry. *Biological trace element research*, 5(3), 149–163.

Schnellen, C. (1947). *Onderzoekingen over de methaangisting*. PhD thesis, TU Delft.

Schreiber, F., Littmann, S., Lavik, G., Escrig, S., Meibom, A., Kuypers, M. M. M., & Ackermann, M. (2016). Phenotypic heterogeneity driven by nutrient limitation promotes growth in fl uctuating environments. *Nature Microbiology*, 1(May), 1–7.

Schröder, C., Burkhardt, C., & Antranikian, G. (2020). What we learn from extremophiles. *ChemTexts*, 6(1), 1–6.

Schwartzman, J. A., Ebrahimi, A., Chadwick, G., Sato, Y., Roller, B. R. K., Orphan, V. J., & Cordero, O. X. (2022). Bacterial growth in multicellular aggregates leads to the emergence of complex life cycles. *Current Biology*, 32(14), 3059–3069.

Seabold, S. & Perktold, J. (2010). Statsmodels: Econometric and statistical modeling with python. In *Proceedings of the 9th Python in Science Conference*, volume 57 (pp. 10–25080).: Austin, TX.

Shao, N., Fan, Y., Chou, C.-W., Yavari, S., Williams, R. V., Amster, I. J., Brown, S. M., Drake, I. J., Duin, E. C., & Whitman, W. B. (2022). Expression of divergent methyl/alkyl coenzyme M reductases from uncultured archaea. *Communications biology*, 5(1), 1–11.

Sheik, A. R., Muller, E. E. L., Audinot, J.-N., Lebrun, L. A., Grysan, P., Guignard, C., & Wilmes, P. (2016). In situ phenotypic heterogeneity among single cells of the filamentous bacterium Candidatus Microthrix parvicella. *The ISME journal*, 10(5), 1274–1279.

Shoaie, S., Karlsson, F., Mardinoglu, A., Nookaew, I., Bordel, S., & Nielsen, J. (2013). Understanding the interactions between bacteria in the human gut through metabolic modeling. *Scientific reports*, 3(1), 1–10.

Smith, P. H. & Hungate, R. E. (1958). Isolation and characterization of Methanobacterium ruminantium n. sp. *Journal of Bacteriology*, 75(6), 713–718.

Söllinger, A. & Ulrich, T. (2019). Methylotrophic methanogens everywhere—physiology and ecology of novel players in global methane cycling. *Biochemical Society Transactions*, 47(6), 1895–1907.

Soppa, J. (2014). Polyploidy in archaea and bacteria: about desiccation resistance, giant cell size, long-term survival, enforcement by a eukaryotic host and additional aspects. *Microbial Physiology*, 24(5-6), 409–419.

Sorokin, D. Y., Abbas, B., Merkel, A. Y., Rijpstra, W. I. C., Damsté, J. S. S., Sukhacheva, M. V., & van Loosdrecht, M. C. M. (2015). Methanosalsum natronophilum sp. nov., and Methanocalculus alkaliphilus sp. nov., haloalkaliphilic methanogens from hypersaline soda lakes. *International journal of systematic and evolutionary microbiology*, 65(Pt_10), 3739–3745.

Sowers, K. R., Baron, S. F., & Ferry, J. G. (1984). Methanosarcina acetivorans sp. nov., an Acetotrophic Methane-Producing Bacterium Isolated from Marine Sediments. *Applied and Environmental Microbiology*, 47(5).

Stadtman, T. C. & Barker, H. A. (1949). Studies on the methane fermentation; tracer experiments on the mechanism of methane formation. *Archives of biochemistry*, 21(2), 256–64.

Stephenson, M. & Stickland, L. H. (1933). The bacterial formation of methane by the reduction of one-carbon compounds by molecular hydrogen. *Biochemical Journal*, 27(5), 1517–1527.

Storey, K. B. & Storey, J. M. (1991). Biochemistry of cryoprotectants. In *Insects at low temperature* (pp. 64–93). Springer.

Striednig, B. & Hilbi, H. (2022). Bacterial quorum sensing and phenotypic heterogeneity: how the collective shapes the individual. *Trends in Microbiology*, 30(4), 379–389.

Stryhanyuk, H., Calabrese, F., Kümmel, S., & Musat, F. (2018). Calculation of Single Cell Assimilation Rates From SIP-NanoSIMS-Derived Isotope Ratios : A Comprehensive Approach. *Frontiers in microbiology*, 9(October), 1–15.

Suhre, K. & Claverie, J.-M. (2003). Genomic correlates of hyperthermostability, an update. *Journal of Biological Chemistry*, 278(19), 17198–17202.

Summons, R. E., Franzmann, P. D., & Nichols, P. D. (1998). Carbon isotopic fractionation associated with methylotrophic methanogenesis. *Organic Geochemistry*, 28(7-8), 465–475.

Takai, K., Nakamura, K., Toki, T., Tsunogai, U., Miyazaki, M., Miyazaki, J., Hirayama, H., Nakagawa, S., Nunoura, T., & Horikoshi, K. (2008). Cell proliferation at 122 C and isotopically heavy CH4 production by a hyperthermophilic methanogen under high-pressure cultivation. *Proceedings of the National Academy of Sciences*, 105(31), 10949–10954.

Takhaveev, V. & Heinemann, M. (2018). Metabolic heterogeneity in clonal microbial populations. *Current opinion in microbiology*, 45, 30–38.

Tamura, T. (2018). Grid-based computational methods for the design of constraint-based parsimonious chemical reaction networks to simulate metabolite production: GridProd. *BMC bioinformatics*, 19(1), 1–9.

Taubner, R.-S., Pappenreiter, P., Zwicker, J., Smrzka, D., Pruckner, C., Kolar, P., Bernacchi, S., Seifert, A. H., Krajete, A., & Bach, W. (2018). Biological methane production under putative Enceladus-like conditions. *Nature communications*, 9(1), 1–11.

Taubner, R.-S., Schleper, C., Firneis, M. G., & Rittmann, S. K.-M. (2015). Assessing the ecophysiology of methanogens in the context of recent astrobiological and planetological studies. *Life*, 5(4), 1652–1686.

Thauer, R. K. (1998). Biochemistry of methanogenesis: a tribute to Marjory Stephenson: 1998 Marjory Stephenson prize lecture. *Microbiology*, 144(9), 2377–2406.

Thiele, I. & Palsson, B. Ø. (2010). A protocol for generating a high-quality genome-scale metabolic reconstruction. *Nature protocols*, 5(1), 93–121.

Thomas, C. M., Taib, N., Gribaldo, S., & Borrel, G. (2021). Comparative genomic analysis of Methanimicrococcus blatticola provides insights into host adaptation in archaea and the evolution of methanogenesis. *ISME Communications*, 1(1), 1–11.

Thor, S., Peterson, J. R., & Luthey-Schulten, Z. (2017). Genome-scale metabolic modeling of archaea lends insight into diversity of metabolic function. *Archaea*, 2017.

Timmers, P. H. A., Welte, C. U., Koehorst, J. J., Plugge, C. M., Jetten, M. S. M., & Stams, A. J. M. (2017). Reverse methanogenesis and respiration in methanotrophic archaea. *Archaea*, 2017.

Torres-Alvarado, R., Ramírez-Vives, F., Fernández, F. J., & Barriga-Sosa, I. (2005). Methanogenesis and methane oxidation in wetlands: implications in the global carbon cycle. *Hidrobiológica*, 15(3), 327–349.

Trent, J. D., Gabrielsen, M., Jensen, B., Neuhard, J., & Olsen, J. (1994). Acquired thermotolerance and heat shock proteins in thermophiles from the three phylogenetic domains. *Journal of bacteriology*, 176(19), 6148–6152.

Tsoka, S., Simon, D., & Ouzounis, C. A. (2004). Automated metabolic reconstruction for Methanococcus jannaschii. *Archaea*, 1(4), 223–229.

Ueno, Y., Yamada, K., Yoshida, N., Maruyama, S., & Isozaki, Y. (2006). Evidence from fluid inclusions for microbial methanogenesis in the early Archaean era. *Nature*, 440(7083), 516–519.

Van Beelen, P., Stassen, A. P. M., Bosch, J. W. G., Vogels, G. D., Guijt, W., & Haasnot, C. A. G. (1984). Elucidation of the structure of methanopterin, a coenzyme from Methanobacterium thermoautotrophicum, using two-dimensional nuclear-magnetic-resonance techniques. *European journal of biochemistry*, 138(3), 563–571.

Van de Peer, Y., Mizrachi, E., & Marchal, K. (2017). The evolutionary significance of polyploidy. *Nature Reviews Genetics*, 18(7), 411–424.

Van De Vossenberg, J. L. C. M., Driessen, A. J. M., & Konings, W. N. (1998). The essence of being extremophilic: the role of the unique archaeal membrane lipids. *Extremophiles*, 2(3), 163–170.

Vanwonterghem, I., Evans, P. N., Parks, D. H., Jensen, P. D., Woodcroft, B. J., Hugenholtz, P., & Tyson, G. W. (2016). Methylotrophic methanogenesis discovered in the archaeal phylum Verstraetearchaeota. *Nature microbiology*, 1(12), 1–9.

Virtanen, P., Gommers, R., Oliphant, T. E., Haberland, M., Reddy, T., Cournapeau, D., Burovski, E., Peterson, P., Weckesser, W., Bright, J., van der Walt, S. J., Brett, M., Wilson, J., Millman, K. J., Mayorov, N., Nelson, A. R. J., Jones, E., Kern, R., Larson, E., Carey, C. J., Polat, İ., Feng, Y., Moore, E. W., VanderPlas, J., Laxalde, D., Perktold, J., Cimrman, R., Henriksen, I., Quintero, E. A., Harris, C. R., Archibald, A. M., Ribeiro, A. H., Pedregosa, F., van Mulbregt,

P., & SciPy 1.0 Contributors (2020). SciPy 1.0: Fundamental Algorithms for Scientific Computing in Python. *Nature Methods*, 17, 261–272.

Vishnivetskaya, T. A., Buongiorno, J., Bird, J., Krivushin, K., Spirina, E. V., Oshurkova, V., Shcherbakova, A., Wilson, G., Lloyd, K. G., & Rivkina, E. M. (2018). Methanogens in the Antarctic Dry Valley permafrost. *FEMS Microbiology Ecology*, 94(June), 1–14.

Vlassis, N., Pacheco, M. P., & Sauter, T. (2014). Fast reconstruction of compact context-specific metabolic network models. *PLoS computational biology*, 10(1), e1003424.

Vo, C. H., Goyal, N., Karimi, I. A., & Kraft, M. (2020). First Observation of an Acetate Switch in a Methanogenic Autotroph (Methanococcus maripaludis S2). *Microbiology insights*, 13, 1178636120945300.

Wagner, D. & Liebner, S. (2010). Methanogenesis in Arctic permafrost habitats. In *Handbook of hydrocarbon and lipid microbiology* (pp. 655–666). Springer Berlin.

Wang, F., Wang, J., Jian, H., Zhang, B., Li, S., Wang, F., Zeng, X., Gao, L., Bartlett, D. H., & Yu, J. (2008). Environmental adaptation: genomic analysis of the piezotolerant and psychrotolerant deep-sea iron reducing bacterium Shewanella piezotolerans WP3. *PLoS one*, 3(4), e1937.

Wang, H., Byrne, J. M., Liu, P., Liu, J., Dong, X., & Lu, Y. (2020). Redox cycling of Fe (II) and Fe (III) in magnetite accelerates aceticlastic methanogenesis by Methanosarcina mazei. *Environmental Microbiology Reports*, 12(1), 97–109.

Wang, H., Robinson, J. L., Kocabas, P., Gustafsson, J., Anton, M., Cholley, P.-E., Huang, S., Gobom, J., Svensson, T., & Uhlen, M. (2021a). Genome-scale metabolic network reconstruction of model animals as a platform for translational research. *Proceedings of the National Academy of Sciences*, 118(30), e2102344118.

Wang, Q., Cen, Z., & Zhao, J. (2015). The survival mechanisms of thermophiles at high temperatures: an angle of omics. *Physiology*, 30(2), 97–106.

Wang, Y., Wegener, G., Williams, T. A., Xie, R., Hou, J., Tian, C., Zhang, Y., Wang, F., & Xiao, X. (2021b). A methylotrophic origin of methanogenesis and early divergence of anaerobic multicarbon alkane metabolism. *Science advances*, 7(27).

Ward, D. M., Brassell, S. C., & Eglinton, G. (1985). Archaebacterial lipids in hot-spring microbial mats. *Nature*, 318(6047), 656–659.

Ward, O. P. & Moo-Young, M. (1988). Thermostable enzymes. *Biotechnology advances*, 6(1), 39–69.

Williams, T. A., Szöllősi, G. J., Spang, A., Foster, P. G., Heaps, S. E., Boussau, B., Ettema, T. J. G., & Embley, T. M. (2017). Integrative modeling of gene and genome evolution roots the archaeal tree of life. *Proceedings of the National Academy of Sciences*, 114(23), E4602–E4611.

Williams, T. C. R., Poolman, M. G., Howden, A. J. M., Schwarzlander, M., Fell, D. A., Ratcliffe, R. G., & Sweetlove, L. J. (2010a). A genome-scale metabolic model accurately predicts fluxes in central carbon metabolism under stress conditions. *Plant physiology*, 154(1), 311–323.

Williams, T. J., Burg, D. W., Raftery, M. J., Poljak, A., Guilhaus, M., Pilak, O., & Cavicchioli, R. (2010b). Global proteomic analysis of the insoluble, soluble, and supernatant fractions of the psychrophilic archaeon Methanococcoides burtonii part I: the effect of growth temperature. *Journal of proteome research*, 9(2), 640–652.

Williams, T. J., Lauro, F. M., Ertan, H., Burg, D. W., Poljak, A., Raftery, M. J., & Cavicchioli, R. (2011). Defining the response of a microorganism to temperatures that span its complete growth temperature range (2 °C to 28 °C) using multiplex quantitative proteomics. *Environmental Microbiology*, 13(8), 2186–2203.

Woese, C. R. (1977). A comment on methanogenic bacteria and the primitive ecology. *Journal of molecular evolution*, 9(4), 369–371.

Woese, C. R. (1987). Bacterial evolution. *Microbiological reviews*, 51(2), 221–271.

Woese, C. R., Magrum, L. J., & Fox, G. E. (1978). Archaebacteria. *Journal of molecular evolution*, 11(3), 245–252.

Wolfe, J. M. & Fournier, G. P. (2018). Horizontal gene transfer constrains the timing of methanogen evolution. *Nature ecology and evolution*, 2(5), 897–903.

Wolfe, R. S. (1993). An Historical Overview of Methanogenesis. In *Methanogenesis* (pp. 1–32). Springer, Boston, MA.

Wolfe, R. S. & McBride, B. C. (1971). New coenzyme of methyl transfer, coenzyme M. *Biochemistry*, 10(12), 2317–2324.

Wolin, M. J., Wolin, E. A., & Wolfe, R. S. (1964). The cobalamin product of the conversion of methylcobalamin to CH4 by extracts of Methanobacillusomelianskii. *Biochemical and biophysical research communications*, 15(5), 420–423.

Wood, J. M., Wolin, M. J., & Wolfe, R. S. (1966). Formation of methane from methyl factor B and methyl factor III by cell-free extracts of Methanobacillus omelianskii. *Biochemistry*, 5(7), 2381–2384.

Wu, Y., Zaiden, N., & Cao, B. (2018). The Core- and Pan-Genomic Analyses of the Genus Comamonas: From Environmental Adaptation to Potential Virulence. *Frontiers in Microbiology*, 9(DEC), 3096.

Yang, L.-L., Tang, S.-K., Huang, Y., & Zhi, X.-Y. (2015). Low temperature adaptation is not the opposite process of high temperature adaptation in terms of changes in amino acid composition. *Genome biology and evolution*, 7(12), 3426–3433.

Yin, X., Wu, W., Maeke, M., Richter-Heitmann, T., Kulkarni, A. C., Oni, O. E., Wendt, J., Elvert, M., & Friedrich, M. W. (2019). CO2 conversion to methane and biomass in obligate methylotrophic methanogens in marine sediments. *The ISME journal*, 13(8), 2107–2119.

Zamboni, N. & Sauer, U. (2009). Novel biological insights through metabolomics and 13C-flux analysis. *Current opinion in microbiology*, 12(5), 553–558.

Zeikus, J. G. (1979). Thermophilic bacteria: ecology, physiology and technology. *Enzyme and Microbial Technology*, 1(4), 243–252.

Zimmermann, M., Escrig, S., Hübschmann, T., Kirf, M., Bran, A., Inglis, R. F., Musat, Nicolina, Müller, S., Meiborn, A., Ackermann, M., & Schreiber, F. (2015). Phenotypic heterogeneity in metabolic traits among single cells of a rare bacterial species in its natural environment quantified with a combination of flow cell sorting and NanoSIMS. *Frontiers in Microbiology*, 6(April), 1–11.

Zimmermann, M., Escrig, S., Lavik, G., Kuypers, M. M. M., & Meibom, A. (2018). Substrate and electron donor limitation induce phenotypic heterogeneity in different metabolic activities in a green sulphur bacterium. *Environmental microbiology reports*, 10, 179–183.

APPENDICES

APPENDIX A
Chapter 2: Genome Comparison

Parts of this chapter are accepted for publication in DNA Research (Prondzinsky et al., 2022). The accepted version is provided as Supplementary File 1.

Large data tables are provided as a separate excel file. This file "SupplementaryTables.xlsx" contains the following sheets:

- Supplementary Table 1: Database of mcrABG containing archaea with checkM score $\geq$ 90, including genome information, environments, temperatures and substrates where possible.
- Supplementary Table 2: Orthogroups for analysis including 255 mcrABG containing organisms (methanogens, methylotrophs and other alkane utilizers).
- Supplementary Table 3: Substrate specific functions for acetoclastic, methylotrophic and hydrogenotrophic methanogens.

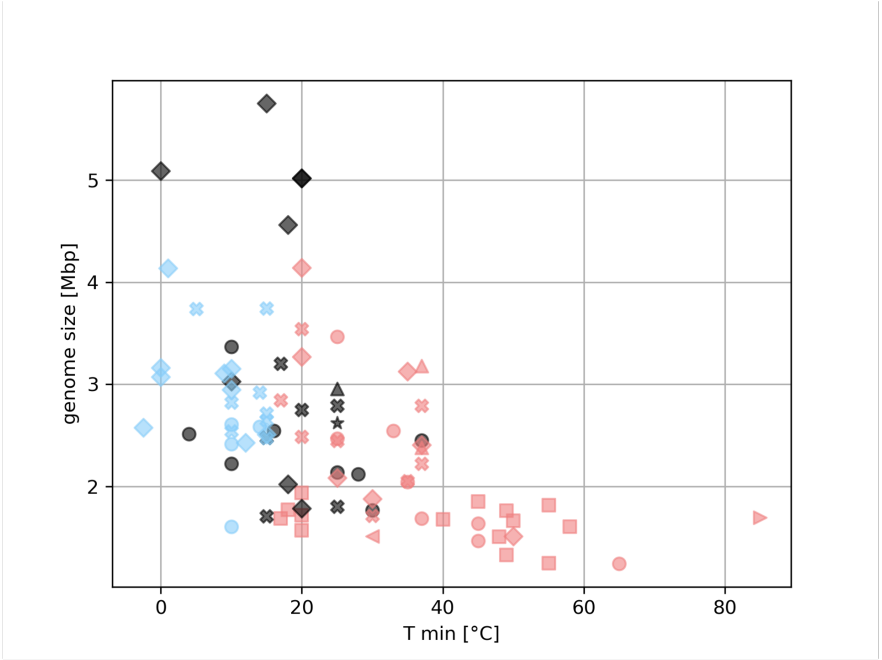

(a) Genome size with minimum growth temperature.

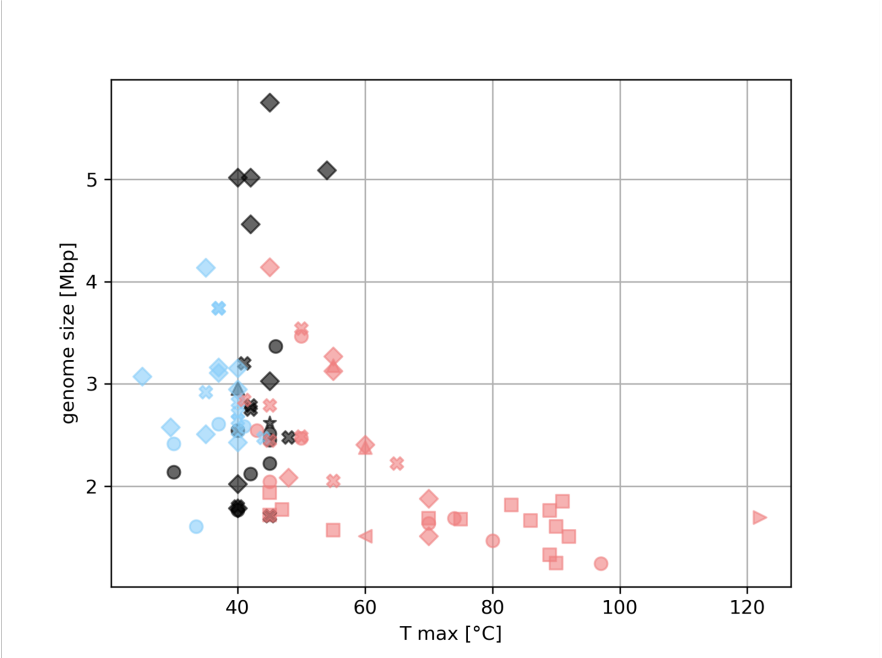

(b) Genome size with maximum growth temperature.

Figure A.1 Genome size ranges at (a) minimum and (b) maxium growth temperatures.

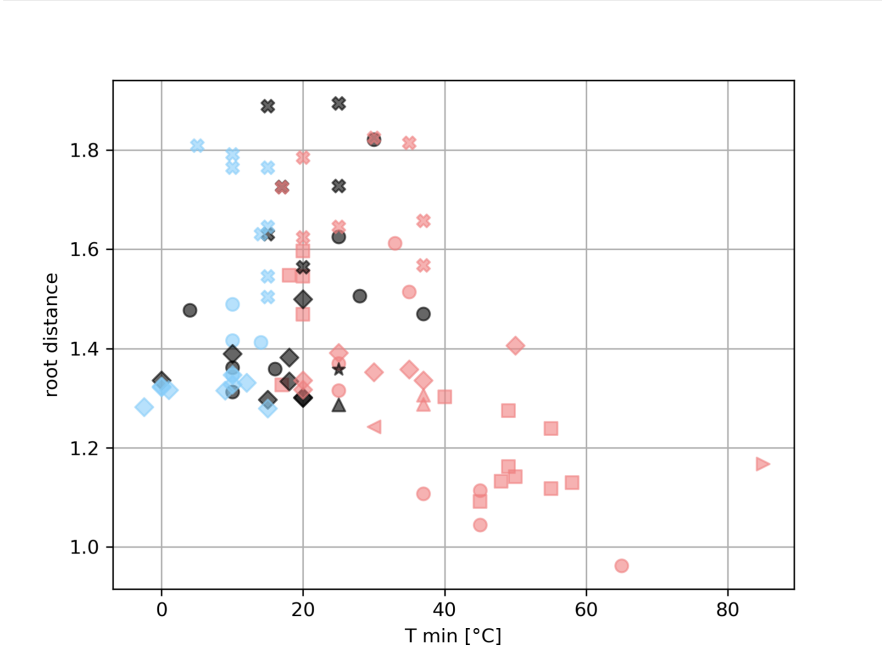

(a) Distance to the archaeal root with minimum growth temperature.

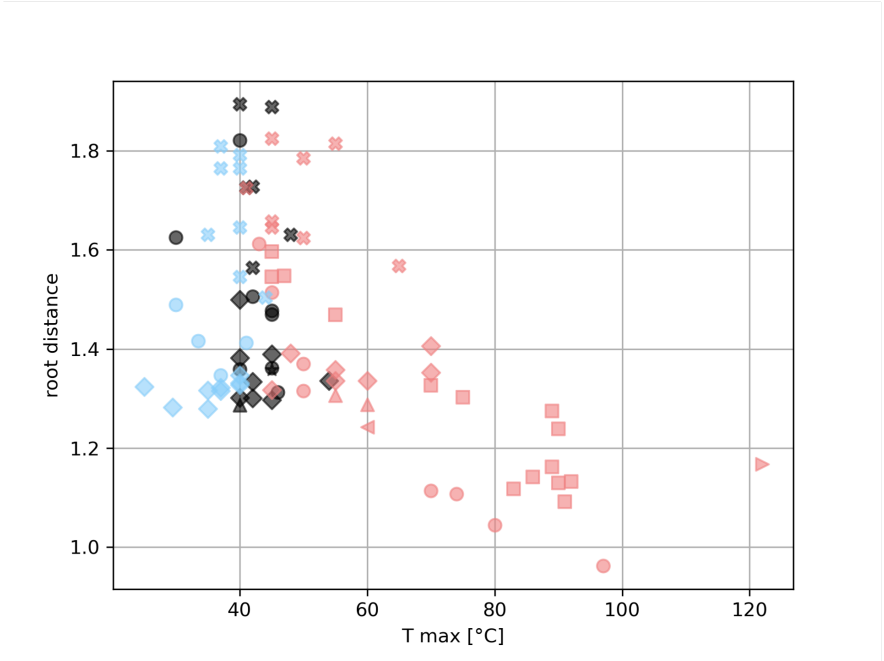

(b) Distance to the archaeal root with maximum growth temperature.

Figure A.2 Branch length to the root of the archaeal species tree with (a) minimum and (b) maxium growth temperatures.

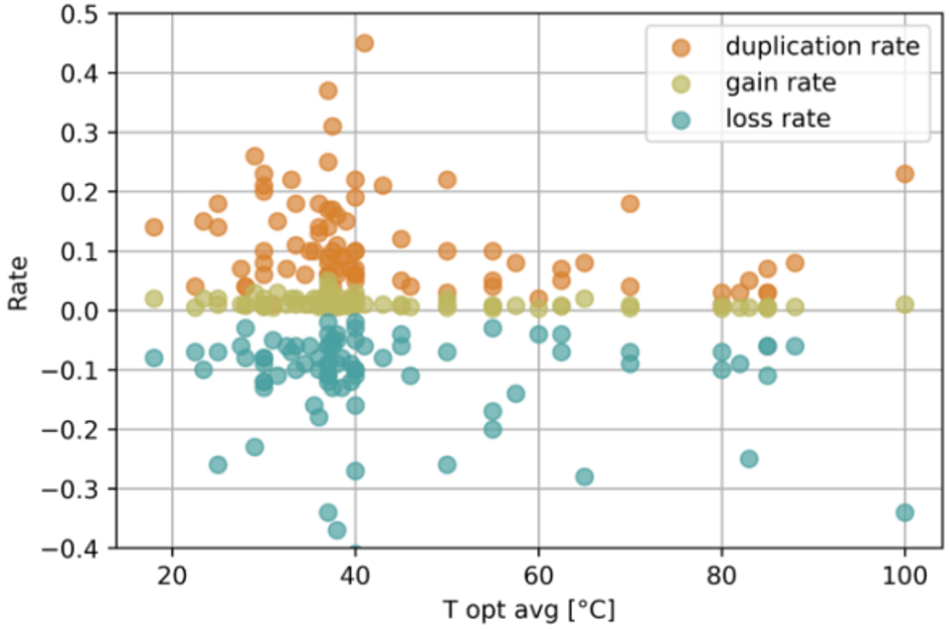

Figure A.3 Gene duplication, gain and loss rates with optimal growth temperature.

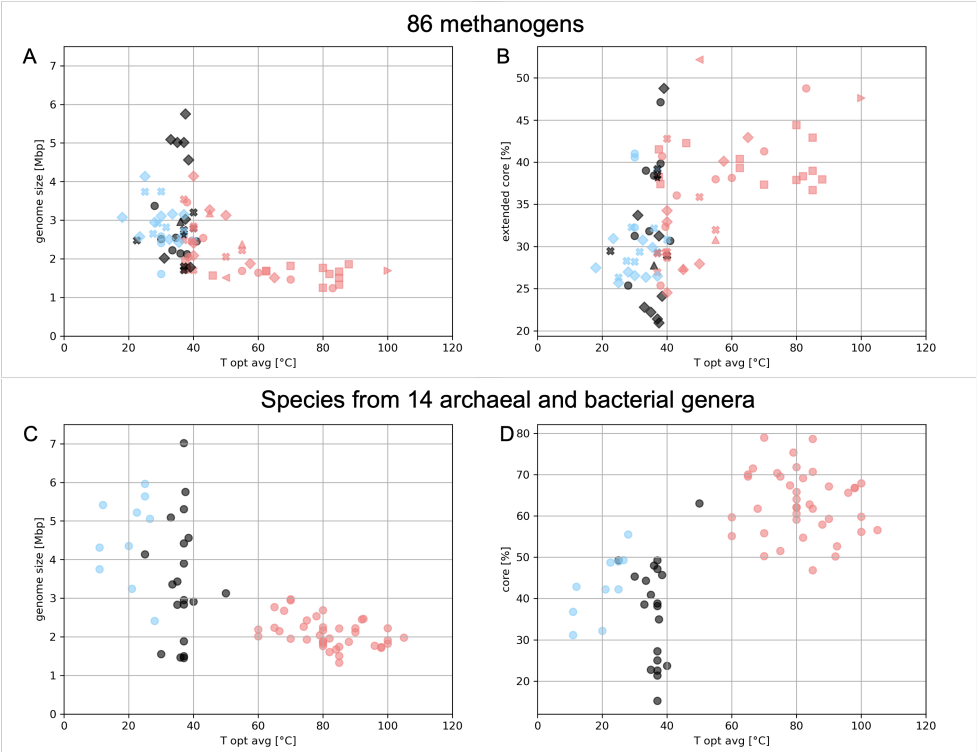

Figure A.4 Genome sizes and core fractions with optimal growth temperatures for all methanogens in the analysis (top panels) and 70 prokaryotic species from 14 different genera (bottom panels).

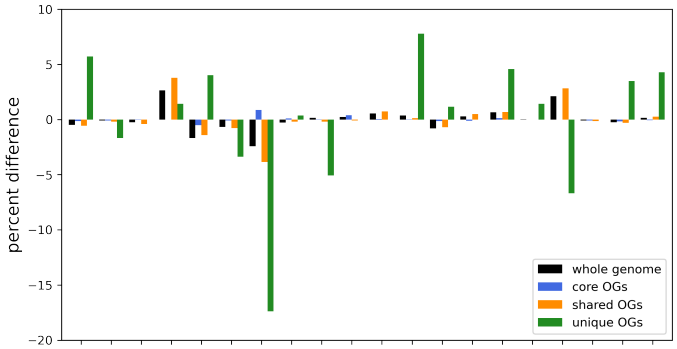

(a) Psychrotolerant vs. Thermotolerant

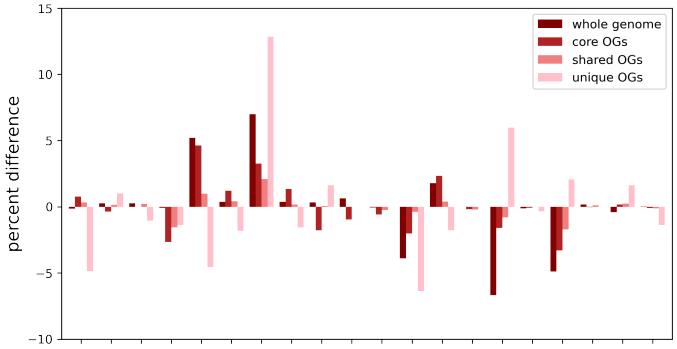

(b) Thermotolerant vs. All

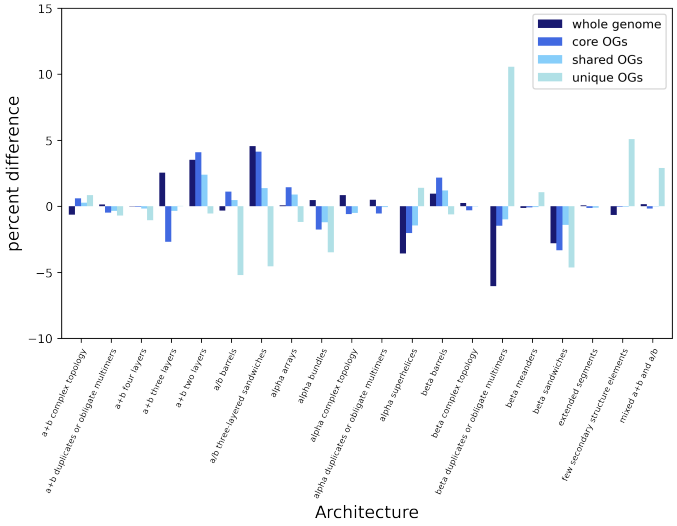

(c) Psychrotolerant vs. All

Figure A.5 Architecture biases throughout the gene groupings. In (a) positive percentages show a relative enrichment in psychrotolerant organisms and negative percentages show a relative enrichment in thermotolerant organisms. In (b) and (c) positive percentages indicate the respective temperature group has a higher abundance of the architecture when compared to the mean of all organisms, negative percentages indicate the respective temperature groups has less abundance of the architecture when compared to the mean.

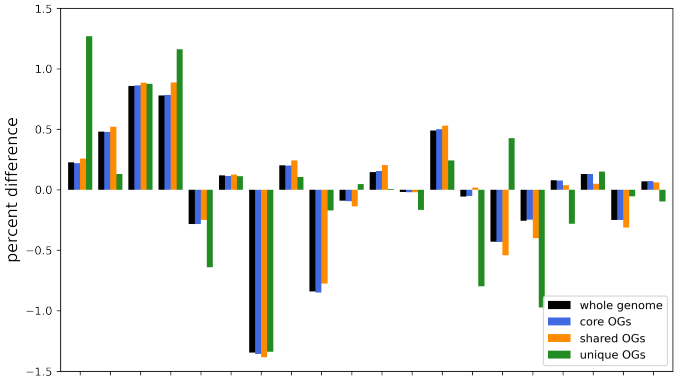

(a) Psychrotolerant vs. Thermotolerant

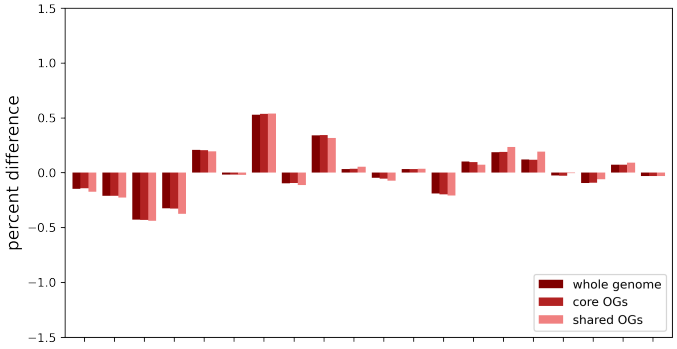

(b) Thermotolerant vs. All

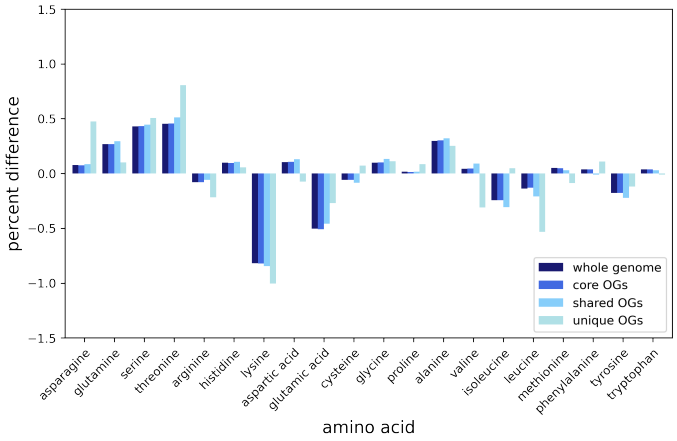

(c) Psychrotolerant vs. All

Figure A.6 Amino acid biases throughout the gene groupings. In (a) positive percentages show a relative enrichment in psychrotolerant organisms and negative percentages show a relative enrichment in thermotolerant organisms. In (b) and (c) positive percentages indicate the respective temperature group has a higher abundance of the amino acid when compared to the mean of all organisms, negative percentages indicate the respective temperature groups has less abundance of the amino acid when compared to the mean.

APPENDIX B
Chapter 3: Phenotypic Heterogeneity

B.1 Media Details

Trace element solution composition used in modified DSMZ 141-c and NBRC 1433 media:

Table B.1
Modified Wolin's trace element solution (based on DSMZ141 medium)

component	per L
Nitrilotriacetic acid	1.50 g
$MgSO_4$ x 7 H_2O	3.00 g
$MnSO_4$ x H_2O	0.50 g
NaCl	1.00 g
$FeSO_4$x 7 H_2O	0.10 g
$CoSO_4$ x 7 H_2O	0.18 g
$CaCl_2CaCl2$ x 2 H_2O	0.10 g
$ZnSO_4$ x 7 H_2O	0.18 g
$CuSO_4$ x 5 H_2O	0.01 g
$KAl(SO_4)_2$ x 12 H_2O	0.02 g
H_3BO_3	0.01 g
Na_2MoO_4 x 2 H_2O	0.01 g
$NiCl_2$ x 6 H_2O	0.03 g
Na_2SeO_3x 5 H_2O	0.30 mg
Na_2WO_4 x 2 H_2O	0.40 mg
Distilled water	1000 ml

Table B.2
Wolin's vitamin solution (based on DSMZ141 medium)

component	per L
Biotin	2.00 mg
Folic acid	2.00 mg
Pyridoxine-HCl	10.00 mg
Thiamine HCl	5.00 mg
Riboflavin	5.00 mg
Nicotinic acid	5.00 mg
Ca-D-pantothenate	5.00 mg
Vitamin B12	0.10 mg
p-Aminobenzoic acid	5.00 mg
(+-)-alpha-Lipoic acid	5.00 mg
Distilled water	1000 ml

B.2 Additional NanoSIMS Data

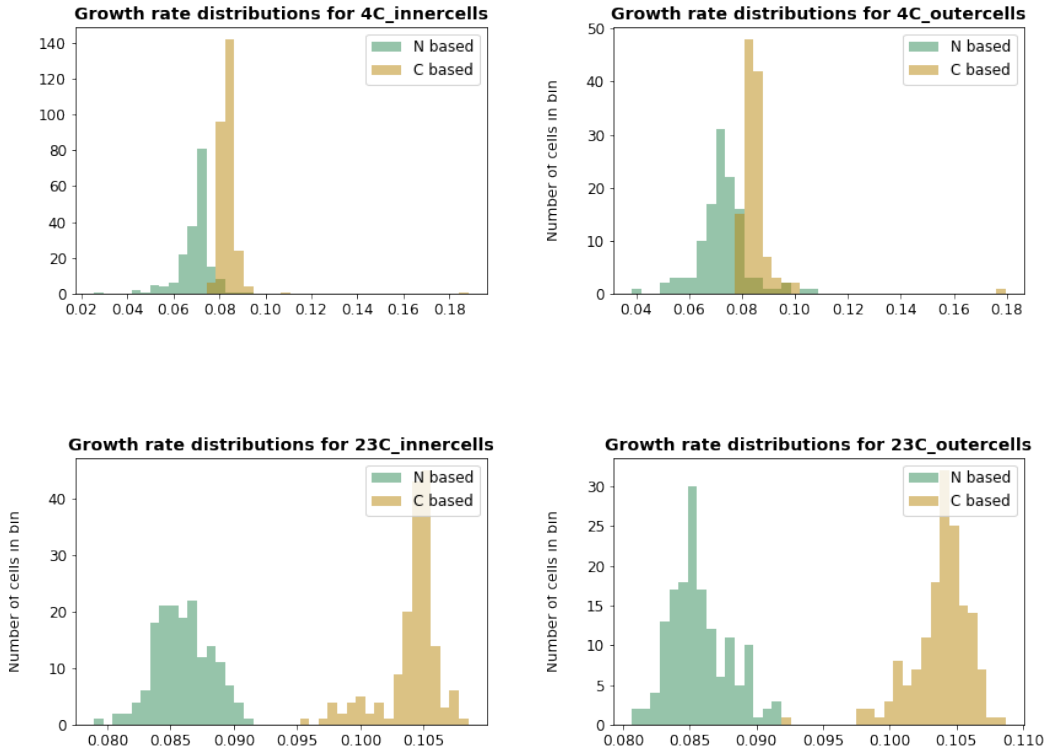

Figure B.1 SIMS data based doubling time distributions for *M. burtonii* aggregates. Top row: 4 °C inner (left) and outer (right) cells. Bottom row: 23 °C inner (left) and outer (right) cells.

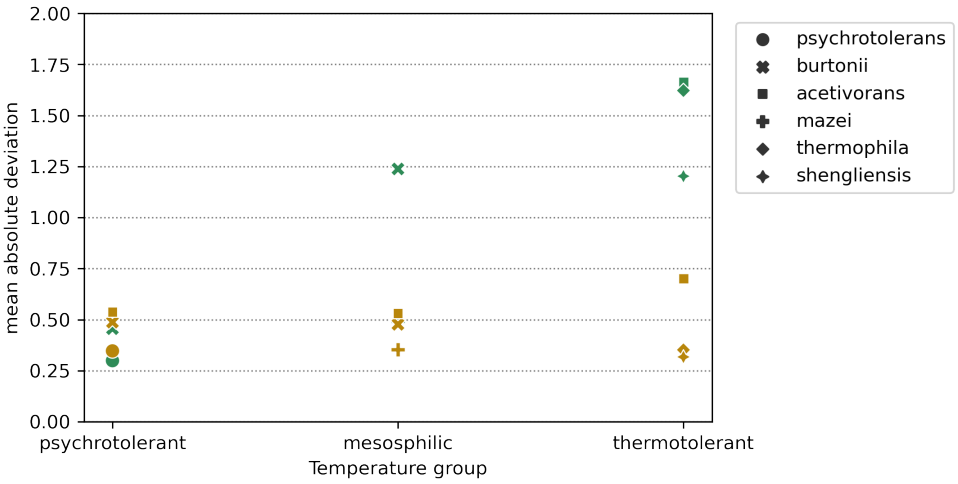

Figure B.2 Mean absolute deviations of relative nitrogen (green) and carbon (yellow) assimilation rates for single cell data of filtered cells. Increasing carbon assimilation variation with decreasing temperature, increasing nitrogen assimilation variation with increasing temperature.

APPENDIX C
Chapter 4: Metabolic Modeling

In addition to the Supplementary Figures below, the model files for (1) the GEM iST807 from Peterson et al. (2016) and (2) the generated methylotrophic core model are provided as iST807.mat and methylotroph_core_iST807.mat as separate files. Flux simulation solutions and an overview of the metabolic subsystems after Peterson et al. (2016) are provided as "metabolic_models_supplementary.xlsx" which contains the following sheets:

- modeled_conditions: an overview of simulation parameters for integrating SIMS data, and simulated doubling times.
- SIMS_phenotypes_fluxes: flux solutions for all reactions when solving the methylotroph core model for different single cell phenotypes.
- optimization_fluxes: flux solutions for all reactions when optimizing the methylotroph core model for biomass output, methanol uptake, ammonia uptake, and methane production.
- iST807_reactions: all reactions of the genome scale metabolic with gene names, stoichiometries and the metabolic subsystems they belong to.

C.1 Additional flux analysis outputs

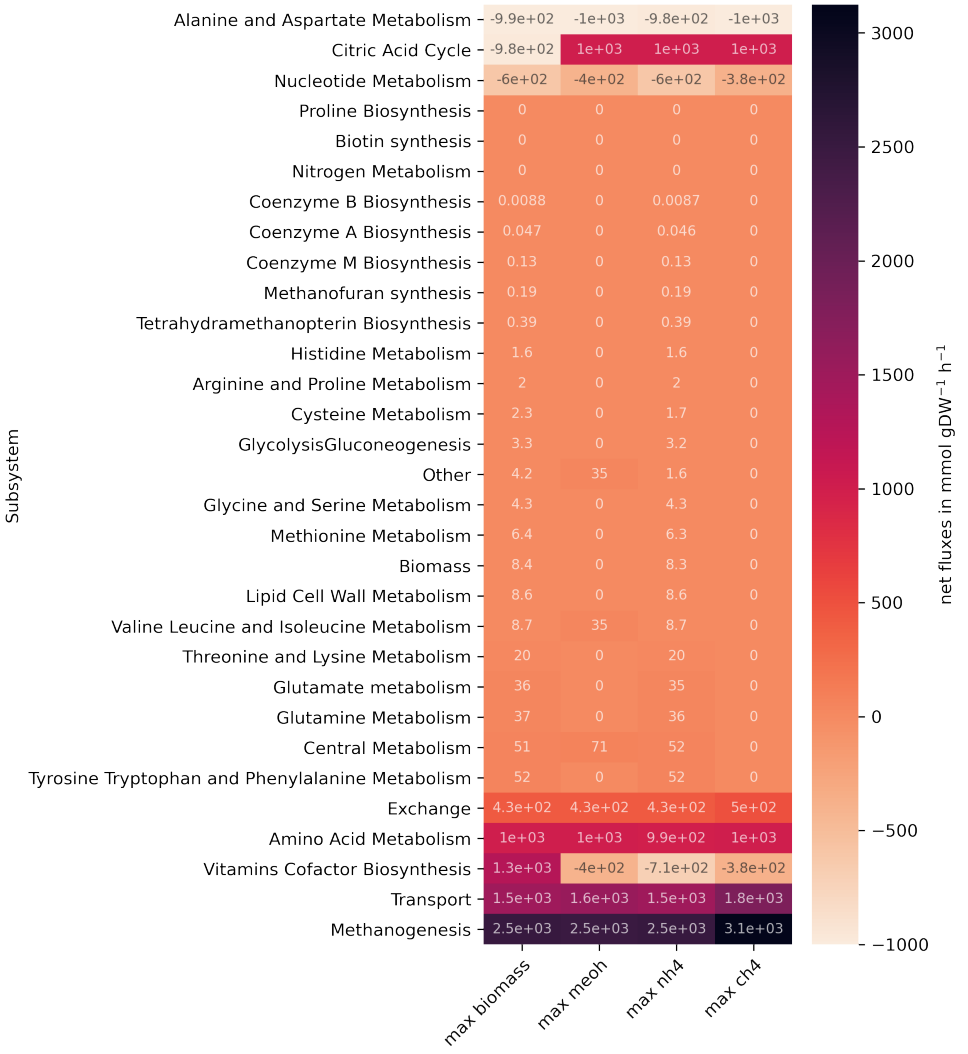

Figure C.1 Heatmaps for net fluxes through all subsystems for optimizations of biomass output, methanol consumption, ammonia consumption, and methane production. Grouped by flux magnitudes from small fluxes (top) to large fluxes (bottom).

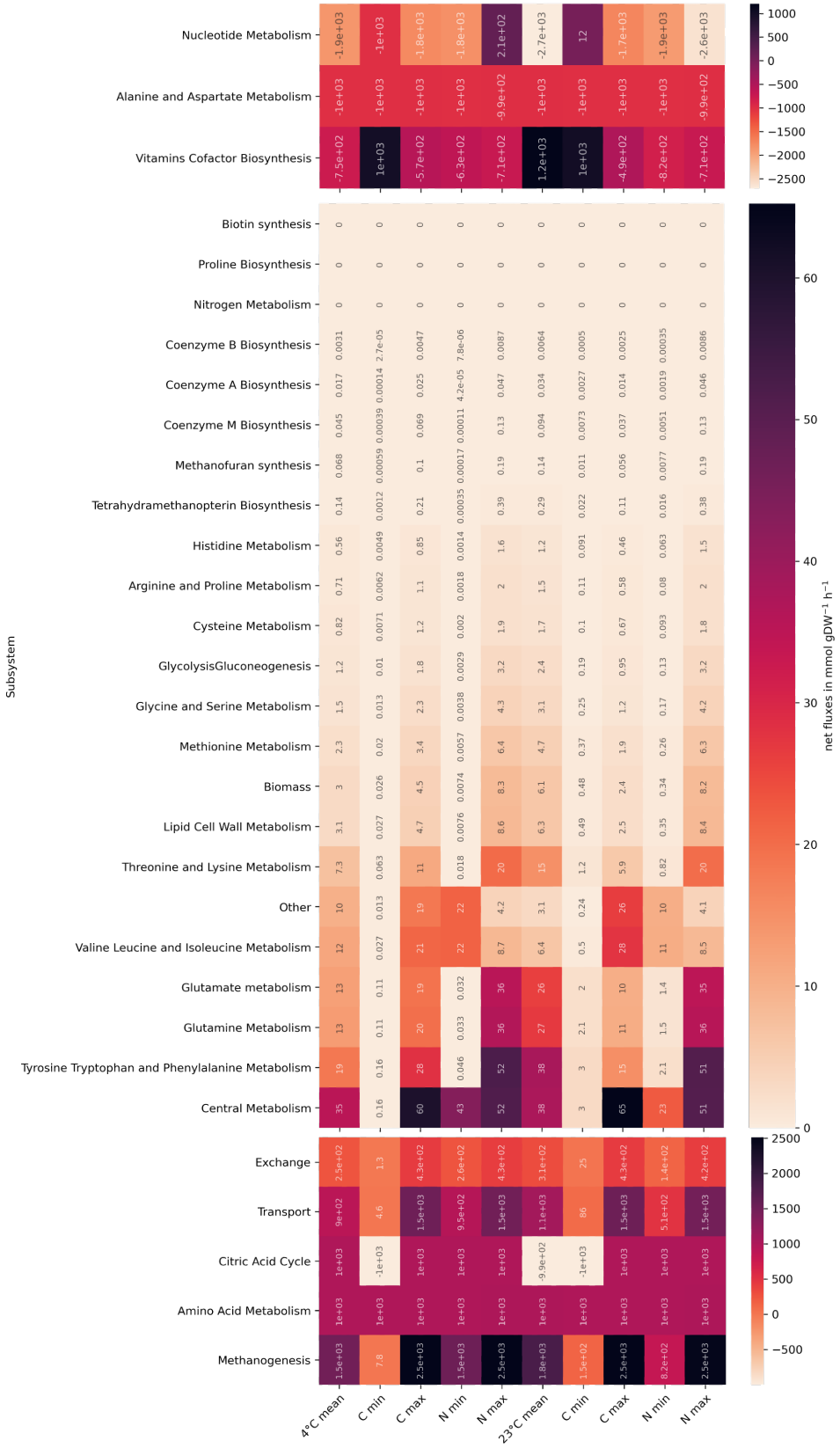

Figure C.2 Heatmaps for net fluxes through all subsystems, grouped by flux magnitudes from small fluxes (top) to large fluxes (bottom).

APPENDIX D
Code

Code written for genome data analyses in Chapter 2 was written in python. JupyterNotebooks for Orthofinder output analyses, amino acid counts, eggnog mapper output analyses, ECOD mappings, TEMPURA analyses, and general plotting of genome features are available through github upon reasonable request.

Code written for NanoSIMS data analyses in Chapter 3 was written in python. The JupyterNotebook for MATLAB generated ion count and ratio outputs is available through github upon reasonable request.

In Chapter 4, flux analyses were done using functions from the Cobratoolbox in MATLAB, and data visualized using python. The MATLAB script used for flux analyses, as well as the JupyterNotebook for visualization are available through github upon reasonable request.